Heat Transfer Through Roofs of Low Cost Brazilian Houses

by

Roberto Lamberts

Submitted in accordance with the requirements
for the degree of
Doctor of Philosophy

Department of Civil Engineering
The University of Leeds

March 1988

ABSTRACT

Summer discomfort in low cost houses is a major problem throughout Brazil. The thermal performance of typical roofs and the effect the heat transfer has on the thermal environment in the house were studied. Ways of improving the performance of typical roofs were developed and tested. These were painting the roof white, ventilating the attic, insulating the ceiling and using a low emissivity material in the attic.

A mathematical model was developed which calculated natural ventilation flow rates in attics.

Steady state heat transfer models were also developed to simulate the thermal performance of typical roofs. The thermal models differed on the number of surfaces considered, the heat removed by ventilation, the roof's natural convection coefficient and ventilation air speed. Results from simulations were compared with observations on a test roof built in the laboratory. Based on this comparison, an unsteady state model for whole house simulation was developed using finite differences. The model was used to predict the expected effective thermal resistance of a ventilated attic for different improvements to the roof thermal performance.

Analysis showed that the use of a low emissivity material in the attic was the best single improvement for reducing ceiling heat flux; attic ventilation was the least effective. Improvements in the thermal performance of the roof substantially reduced the underside ceiling surface temperature which lowered the room air temperature.

Effective thermal resistance data for ventilated attics are suggested. This is appropriate for designing naturally ventilated houses.

TABLE OF CONTENTS

LIST OF TABLES AND ILLUSTRATIVE MATERIAL

ACKNOWLEDGEMENTS

Space limitations prevent me from mentioning everyone who contributed to this thesis.

I would like to give special thanks to the following persons and institutions:

- Dr. D. Fitzgerald and Dr. W. Houghton Evans, for the supervision and encouragement during this research work;
- Dr. J. Tinker, for the help during the use of the hot-plate apparatus and the meticulous and much appreciated comments on the draft thesis;
- Mr. J. Higgins, Mr. G. Kemp and the technical staff involved in building the test roof, for the friendliness and constant help.
- Mr. G Broadhead, for constant and useful discussions about instrumentation;
- My wife, Helena Piccoli Romanowski, for the support, constant help and all the rest so necessary for the completion of this work;
- Dr Rosemary Creasey for carefully reformatting the text and typing the equations;
- Coordenacao de Aperfeicoamento de Pessoal de Nivel Superior (CAPES) for financial support throughout this work;
- Committee of Vice Chancellors and Principals of the Universities of the United Kingdom, for the ORS-Award during 1984 and 1985.

NOMENCLATURE

Symbol		Unit
c	specific heat capacity,	J/kg K
	cloud cover factor (0- clear sky, 1- overcast)	—
chf	ceiling heat flux	W/m^2
C_v	ventilation heat transfer conductance	W/K
E_{bi}	emissive power of surface i if it were black	W/m^2
ER	effective thermal resistance of a ventilated attic	m^2K/W
F_{ij}	fraction of the radiation leaving surface i which is intercepted by surface j (view factor)	—
g_{re}	ground reflectance	—
Gr	Grashof number	—
h_c	natural convection heat transfer coefficient	W/m^2 K
h_f	forced convection heat transfer coefficient	W/m^2 K
h_r	radiation heat transfer coefficient	W/m^2 K
h_{wind}	convection heat transfer coefficient due to wind	W/m^2 K
I	total (direct + diffuse) irradiance on horizontal surface	W/m^2
I_b	direct (beam) solar irradiance on horizontal surface	W/m^2
I_{bt}	direct (beam) solar irradiance on sloping surface	W/m^2
I_c	estimated clear sky irradiance on horizontal surface	W/m^2
I_d	diffuse (sky) irradiance on horizontal surface	W/m^2
I_{dt}	diffuse (sky) irradiance on sloping surface	W/m^2
I_{gt}	ground reflected irradiance on sloping surface	W/m^2
I_{le}	longwave radiation emitted by a surface	W/m^2
I_{ls}	atmospheric (sky) long wave radiation	W/m^2
I_{lt}	total (sky + ground) longwave radiation on sloping surface	W/m^2
I_t	total (direct + diffuse + ground reflected) irradiance on sloping surface	W/m^2
J_i	radiosity of surface i	W/m^2
l	length, thickness	m
L	characteristic length	m

Symbol		Unit
Nu	Nusselt number	—
Pr	Prandtl number	—
q	total heat transfer	W
R	thermal resistance	m^2 K/W
Re	Reynolds number	—
S	area	m^2
T	absolute temperature	K
t	temperature	°C
t_{dp}	dew point temperature	°C
V	air volume flow rate	m^3/s
v	air speed	m/s
α	solar absorptivity	—
β	slope of a surface	degrees
ϵ	emissivity	—
ϵ_s	clear sky emissivity	—
ϵ_{so}	partially overcast emissivity	—
ρ	air density	kg/m^3
σ	Stefan Bolzmann constant = 5.67 10^{-8}	$W/m^2 K^4$
θ	angle between the beam radiation on the surface and its normal	degrees
θ_z	angle between the beam radiation on the surface and zenith	degrees
λ	thermal conductivity	W/m K

Subscripts

rt	upper-side of roof
r	under-side of roof
ci	under-side of ceiling
co	upper-side of ceiling
a	inside air
o	outside air

CHAPTER 1 INTRODUCTION

One of the major functions of a building is to provide a comfortable internal environment. A clear understanding of the climatic variables and their influence on the heat transfer through the building envelope is necessary to allow economic constraints and human thermal comfort demands to be combined to produce a sound building design.

1.1 BRAZIL AND ITS CLIMATES

Brazil is a vast country covering 8.5 million square kilometres (35 times the size of U.K.), ranging from latitude 5° N to 34° S. Its population is about 120 million (1980). The larger cities are Greater Sao Paulo (15 million, 1985) and Greater Rio de Janeiro (9.5 million, 1982).

The climate is divided into three main zones (Sodha et al., 1986). All three have a common summer that is warm and humid (mean temperature 20-30 °C, mean vapour pressure over 2 kPa), but differ in the type of winter. In the North and Amazon basin, the winter is warm and humid; south of latitude 15 °S, it is temperate (mean temperature 10-20 °C); and, in a relatively narrow stretch of land between these two zones, winter is warm and dry (mean vapour pressure under 2 kPa).

The design data for ten big cities (latitude varying from 1° S to 30° S) is given by ASHRAE (1985). The summer design dry bulb temperature (frequency level of 2.5% *) varies from 29 °C to 33 °C and the wet bulb from 23 to 26 °C. One of these cities, Porto Alegre (latitude 30° S) has a design dry bulb temperature of 33 °C and a design wet bulb temperature of 24 °C. It is therefore a city very representative of the whole country as far as summer design is concerned. Over the country, winter design temperatures vary from 3 to 22 °C and Porto Alegre has a design temperature of 4 °C.

The present work concentrates on the design of roofs for low cost houses in Porto Alegre. Due to the climatic similarities of summer over the whole country, the summer design solutions apply

* frequency level of 2.5%, represents temperatures that have been equalled or exceeded by 2.5% of the total hours during the months of December through March.

throughout Brazil. Winter design solutions are not relevant to the other climatic regions.

1.2 PORTO ALEGRE AND ITS CLIMATE

Porto Alegre is the capital of the State of Rio Grande do Sul and has 1.1 million inhabitants (1980). It is on the banks of a large river (Rio Guaiba), about 100 km from the Atlantic Ocean and close to a very large lagoon (Lagoa dos Patos). The climate is humid subtropical, and a detailed description can be found in Sattler (1986). The annual average air temperature is 19.5 °C with recorded extremes of 40.7 °C and -1.9 °C. Normal annual average relative humidity is 76 %. Normal annual total number of bright sunshine hours is 2450 hours.

Typical hourly summer and winter design day data covering dry bulb temperature, relative humidity, global solar radiation and wind (Sattler 1986) are given in tables 1.1 and 1.2.

Indoor comfort during summer depends largely on the protection from radiant heat and there being some air movement. Occupants should be protected from solar radiation transmitted through the windows or from overheated internal surfaces. Air movement passing over the body should be encouraged to increase evaporative cooling.

Winter comfort depends on direct use of solar radiation and limiting the ventilation.

1.3 THE HOUSING PROBLEMS

The fast industrialization of Brazil over the last few decades has led to mass migration to the cities. In 1940, 69% of the population was living in the countryside, by 1980 the pattern reversed and 68% were living in urban areas (Azevedo and Andrade 1981). This, allied to the population growth, caused a shortage of urban housing, an increase in rents and market speculation.

Part of the housing demand is being supplied by governmental policies and the rest by self construction and favelas (slums).

The governmental provision of low cost housing from 1946 to 1964 was through the Fundaçao Casa Popular (Foundation for Low Cost

Table 1.1 Typical hourly summer design data, 2.5% level *, for Porto Alegre, Rio Grande do Sul, Brazil (30° 02'S, 51° 13'W) according to Sattler (1986).

Time (LMT)	Dry Bulb Temperature (°C)	Relative Humidity (%)	Global Solar Radiation (W/m^2)	Wind Speed (m/s)
1	24.1	89	0	1.7
2	23.8	91	0	1.3
3	23.5	93	0	1.1
4	23.2	94	0	1.0
5	23.0	95	0	0.8
6	22.9	91	24	1.0
7	24.1	79	146	0.9
8	26.1	67	321	1.7
9	28.0	60	495	2.8
10	29.2	56	633	3.1
11	30.4	51	779	3.1
12	31.5	48	834	3.1
13	32.4	45	858	2.9
14	33.2	44	782	3.0
15	33.5	43	664	3.1
16	33.5	43	505	2.6
17	33.3	46	318	1.9
18	32.0	61	141	2.8
19	29.6	73	21	3.0
20	27.7	78	0	3.1
21	27.0	81	0	3.6
22	26.3	83	0	3.4
23	26.0	86	0	2.6
24	24.8	89	0	1.9
mean	27.9	70	272	2.3

* representing a day with daily average temperature only exceeded by 2.5% of the total number of hot days during five years.

Table 1.2 Typical hourly winter design data, 2.5% level *, for Porto Alegre, Rio Grande do Sul, Brazil (30° 02'S, 51° 13'W) according to Sattler (1986).

Time (LMT)	Dry Bulb Temperature (°C)	Relative Humidity (%)	Global Solar Radiation (W/m^2)	Wind Speed (m/s)
1	7.5	80	0	2.7
2	7.0	81	0	2.7
3	6.5	86	0	3.0
4	6.2	88	0	3.0
5	5.9	88	0	3.0
6	5.6	89	0	2.9
7	5.4	89	4	2.7
8	6.2	87	86	2.9
9	7.4	78	218	2.8
10	8.7	70	331	3.5
11	9.9	63	431	3.7
12	11.0	57	483	3.9
13	11.9	54	482	4.3
14	12.4	54	426	4.1
15	12.6	53	330	4.2
16	12.4	54	212	4.3
17	11.9	59	82	3.7
18	11.0	66	4	2.9
19	10.1	73	0	2.7
20	9.7	75	0	2.9
21	9.2	79	0	2.6
22	8.8	82	0	2.5
23	8.4	86	0	2.2
24	8.0	89	0	1.8
mean	8.9	74	129	3.1

* representing a day with daily average temperature only exceeding 2.5% of the total number of cold days during five years.

Housing) and its outcome was very modest (17000 houses) (Azevedo and Andrade 1981).

In 1964, after the military coup, the Banco Nacional de Habitaçao BNH (National Bank for Housing) was created. It operated until the beginning of 1987 when it was dissolved. The municipal agents of the BNH for the low income population were the Cohabs. They were supposed to meet the demand of people earning from one to five monthly minimal wages (mmw, equivalent to £33 in May 1987) but due to insolvency problems, they tended to concentrate on those earning five mmw. In 1980, 79 % of the working population were earning less than three mmw (Maricato 1983) and therefore had no access to BNH financing schemes.

The output of the Cohabs for the period 1965 to 1980 was about one million houses, three quarters of those being in the last five years (Azevedo and Andrade, 1981). From 1976, the Cohabs substantially increased their output and the Cohab of the State of Sao Paulo, for example, built a housing development for 150,000 inhabitants (Itaquera I, II and III), equivalent to a medium sized town (Maricato 1983). Although these numbers might seem large, the demand was much larger.

The estimated demand for low cost houses of the population earning up to three mmw, for the period 1986 to 1990 is about one million houses per year (Fundaçao Joao Pinheiro, 1984). This gives an idea of the ineffectiveness of the governmental policies. The result has been a tremendous increase in the 'informal' housing market (Azevedo and Andrade 1981). In the city of Rio de Janeiro, for example, the population doubled between 1950 and 1980. During the same period, its slum population increased tenfold, reaching an astonishing level of two million, one in every four inhabitants in 1980 (Maricato 1983).

At present, Brazil is in a political and economic crisis. With the recent dissolution of the BNH it is difficult to predict future policies. The data presented here indicates that it is not a minor change in governmental policies that will solve or ease Brazil's housing problem.

1.4 TYPICAL LOW COST HOUSES

Most of the houses built by the Cohab of the State of Rio Grande do Sul have two or three bedrooms (31 m^2 or 36 m^2).

The materials used in their construction are

-Pitched roof: corrugated asbestos cement sheets, clay tiles or corrugated galvanized steel;

-Ceiling: 25mm wood waste board, 10mm plaster board or 10mm pine timber;

-Walls: bricks plastered and rendered (140mm), solid concrete (partition walls = 90mm, external walls = 110mm) or hollow concrete blocks (partition walls = 90mm, external walls = 140mm).

New materials and construction techniques are frequently tested to reduce cost. No thermal performance specifications are set by the Cohabs. The building contractors therefore, conscious only of cost, are providing houses with poor environmental qualities.

Aroztegui (1981) describes a Cohab new development near Porto Alegre. Sixty five per cent of the 2584 houses built, had two bedrooms and followed the standard plan shown in figure 1.1. He studied the thermal behaviour of those houses in summer, built with three different types of wall construction and different orientations. The internal air temperatures recorded in the houses sometimes differed by more than 2 K. In general, the houses which had the better thermal performance, showed a peak internal air temperature slightly under the peak external air temperature. Other houses of lower thermal performance had peak internal air temperatures higher than that of the external air. Surface temperatures of the ceiling were recorded to be 4 K higher than the peak outside air temperature. In some houses thin metal doors were used that were painted dark brown. The recorded internal surface temperature of those doors was 7 K above the air temperature.

In an attempt to develop some performance specifications for low cost houses, BNH commissioned the Instituto de Pesquisas Tecnologicas do Estado de Sao Paulo (IPT, Technological Research Institute for the State of Sao Paulo) to develop performance standards for the different regions of Brazil. In 1982 the preliminary results were presented to the technical community for discussion. Whether or not they have been adopted is not known. However, there is a considerable lack of understanding of the thermal

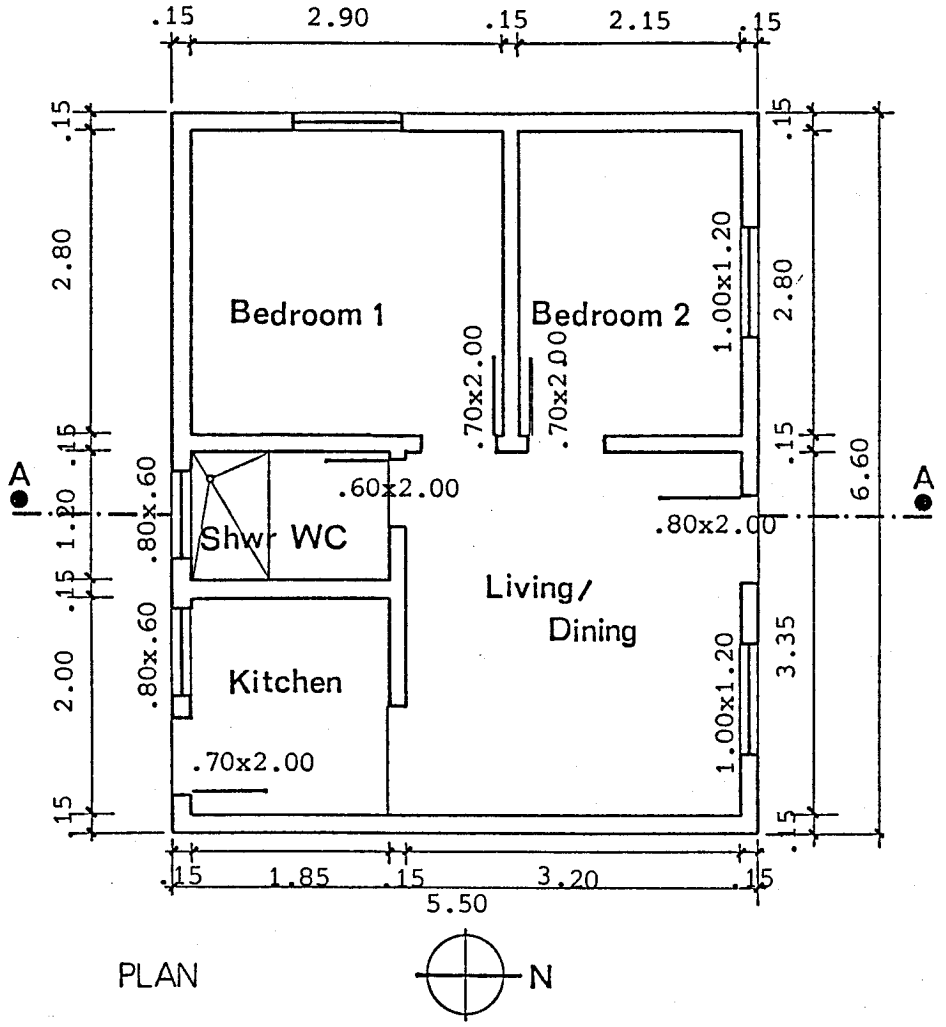

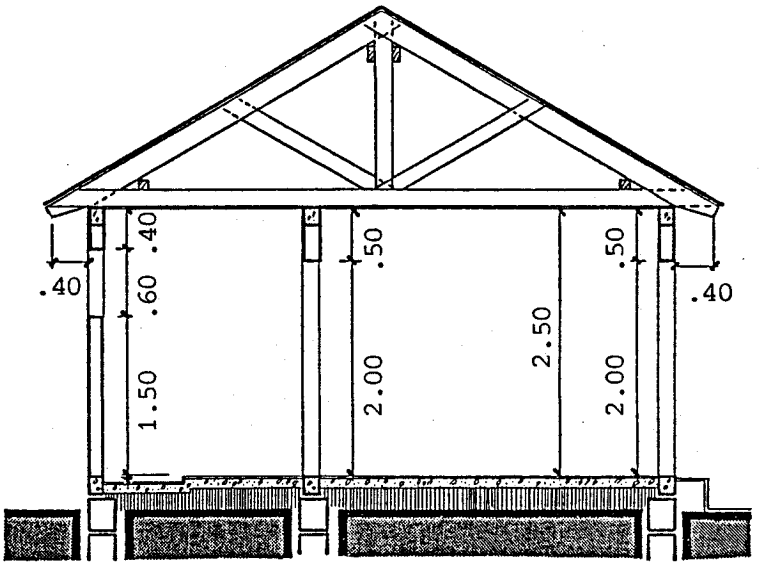

SECTION AA

Figure 1.1 Plan and section of a typical low cost house built by COHAB in the State of Rio Grande do Sul (RS 15-I.2-36) (all values in metres).

behaviour of local building materials and components. It is very important to study the thermal performance of each component and its contribution to the behaviour of the whole house in order to maximize its performance within the cost limitations. This is further stressed by the need to build one million low cost houses per year.

1.5 ROOF THERMAL PERFORMANCE

The roof is the building component most exposed to the external climate. Corrugated asbestos cement sheets, corrugated metal sheets or clay tiles are the most common roofing materials. When used by themselves they allow excessive heat flow into the house. To reduce summer heat gains and winter heat losses a ceiling is needed.

During summer, solar radiation is absorbed by the outside of the roof. Part of the heat is conducted through the roof to the attic space. It is then transfered by radiation and convection to the ceiling below. Of the heat received on the top of the ceiling, part is re-radiated or convected back to the attic and part is conducted into the living quarters of the house.

Excessive ceiling heat flux can cause indoor overheating and a high ceiling surface temperature. Good roof design should minimize this. Thermal comfort in hot environments depends partly on radiative cooling of the body. The thermal discomfort caused by radiation from warm ceilings is felt at much lower radiant temperature asymmetries than from warm walls, cool walls or cool ceilings by persons in thermal neutrality (Fanger 1986). It is expected to be worse for persons exposed to air temperatures above the comfort limits.

During winter, solar and internal gains tend to keep the inside air temperature higher than outside. The roof is responsible for major losses. This mainly occurs during clear sky nights, when radiative cooling causes the external roof surface temperature to drop below external air temperature.

Winter discomfort in south Brazil is not a great problem. It can however be reduced by designing windows to admit solar radiation.

Summer is the main time for concern, especially in low cost houses. When trying to establish a performance standard one is faced with the question: how much heat flux through the ceiling can be

permitted before it affects the life and work of the inhabitants? Social pressures increase when one rationalizes that higher costs can limit the number of people having access to a house.

Heat transfer through a ventilated cavity such as a roof is a complex phenomenon. Typical values of the thermal resistance of ventilated air spaces are given in table A3.3 of the CIBSE guide (1986), but neither the direction of the heat flow nor the ventilation flow rate are indicated. ASHRAE (1985) provides a table (table 4, p. 23.13) listing effective resistance of ventilated attics based on work by Joy (1958). This table shows that ventilation greatly increases the effective thermal resistance of ventilated attics. This contradicts the general conclusion of the 'Summer Attic and Whole-House Ventilation Workshop' (NBS 1979), which concluded that attic ventilation has no effect on energy consumption and comfort in buildings with insulated attics. It further reflects how poorly the transfer of heat through a ventilated cavity is understood. Joy used an insulated attic ventilated by openings high in the gables; this is not typical in Brazil and so direct application of ASHRAE data is not appropriate. Design data relevant to the local reality is crucial before thermal performance standards for roofs can be enforced.

1.6 PRESENT WORK

The aim of this work is to study the thermal performance of roofs typically found in low cost Brazilian houses and to monitor the effect these have on the internal environment.

Emphasis is given to heat gain through roofs because of the major importance of summer discomfort in Brazil. No attempt is made to stipulate performance standards as these will change with the economic situation of the country.

Ways of improving summer performance have been studied. These were

- painting the external surface of the roof white,
- use of low emissivity material in the attic,
- attic ventilation,
- ceiling insulation.

Natural ventilation flow rates of attics with different opening configurations were calculated using a mathematical model specially developed to simulate typical roofs.

Mathematical heat transfer modelling was chosen as the major approach to the thermal performance study. Several steady state models were developed combining different ways of modelling the radiation heat transfer (number of surfaces), treatment of attic ventilation, natural convection heat transfer coefficient under the roof and ventilation air speed.

A test roof was built inside a laboratory. Steady state heat flow observations were carried out under a wide range of conditions. These observations were compared with the results from the mathematical models. The model that best simulated the observed data was used as a basis for the development of an unsteady state model capable of simulating a whole house.

The unsteady state model was used to simulate the thermal conditions of the low cost house described previously under typical summer and winter weather conditions of Porto Alegre. The effects that the improvements to the roof have upon the thermal environment in the living quarters were analysed. The effective thermal resistance of the whole attic is calculated from the simulations to provide designers with a simple parameter representing the attic thermal performance.

CHAPTER 2 LITERATURE SURVEY AND THEORY DEVELOPMENT

2.1 RESEARCH ON THE THERMAL PERFORMANCE OF ROOFS: HISTORICAL BACKGROUND

Research in the U.K. into heat transfer through roofs has been carried out mainly by the Building Research Establishment and was concerned with winter heat losses. Early works include Beckett's (1935) on an equipment to measure air to air conductances of roofs in the BRS (Building Research Station) and Pratt and Daws's (1958) on U-value measurements for factory roofs in the BRS roof laboratory. Comparing these latter measurements with theoretical calculations, Loudon (1963) found good agreement. Anderson (1980), faced with a discrepancy between U-values for glass-fibre insulated ceilings measured in a hot box and those calculated using the CIBSE guidelines carried out laboratory measurements. Results showed the conductance of the glass-fibre to be dependent on the air speed at its upper surface. Later, Anderson and Ward (1981) measured roof heat losses in-situ. The thermal performance of the insulation was not affected by air speeds up to 0.1 m/s at its upper surface. The field observations showed that attic air speeds rarely exceeded 0.1 m/s. They obtained good agreement between measured thermal resistance and estimated according to CIBSE. Sabuja (1986) argued that the CIBSE guidelines for heat loss calculation underestimate the heat losses when attic insulation is at roof level. The main source of error is in ignoring gable losses and attic ventilation.

In the U.S.A. a major work on summer and winter heat transfer through roofs was done by Joy (1958). Experimental work was carried out in the laboratory under steady state conditions and a mathematical model developed. Results showed good agreement. Mumaw (1980) reported on the design and construction of a large calibrated hot box (metering chamber 4.3m x 6m) for testing horizontal building elements. Rucker and Mumaw (1981) discuss the calibration of this hot box and the necessity of redesigning it as a guarded hot box before final calibration is possible. Wilkes (1982) describes tests with an attic over this guarded hot box and compares these with mathematical simulations.

In Brazil, the IPT in Sao Paulo has done research on heat transfer through roofs for an asbestos cement manufacturer, and

measurements were taken in houses specially built for the project (IPT 1979, Valentin 1981, Kiyohara 1984). Lamberts (1983) developed a test rig for comparing different roof solutions with a standard roof exposed to the external climate. Two roofs were placed over a chamber with very high thermal capacity (semi buried) with almost constant air temperature. The standard roof had a slope of 30° and was covered with clay tiles. The configuration of the other roof was capable of being altered. Temperature differences across the two ceilings were compared. Roofs tested at different times could be approximately compared by reference to the standard roof. Using the same rig, Oliveira (1984) performed some measurements with asbestos cement sheets. The performance of the standard roof was altered by the effect of time on the tiles. This made comparisons with the results of Lamberts (1983) difficult to make.

Field observations to obtain design data for different roof configurations are often impracticable. It means building several roofs side by side which is expensive. Also, it may take a long time for extreme or typical weather conditions to occur. On the other hand, laboratory observations are difficult to organize due to the large scale of the roof element and problems associated with simulating the heat transfer at the external surface of the roof. Mathematical models can play an important role in overcoming this problem.

2.2 HEAT TRANSFER AT THE EXTERNAL ROOF SURFACE

The following section summarizes the literature on the heat transfer occuring at the external surface of the roof and discusses the theory involved in the mathematical simulation of it from climatic data.

2.2.1 Shortwave radiation

In hot countries, the solar irradiation absorbed by the building envelope has a great influence on the internal thermal environment of a building without air conditioning, and on the cooling load of one with air conditioning (Reagan and Acklam 1979, Cross 1984). Substantial reductions of the absorbed solar irradiation can be obtained by shading or white painting. The solar absorptivity of some common roofing materials is given in Appendix 2.

Van Straaten (1967) measured the outside surface temperatures of galvanized steel roofs with different colours in South Africa. A black roof reached 70 °C, while a white one, only 44 °C. Givoni (1962) observed reductions of 3.5 K on ceiling temperatures when a red cement tile roof was whitewashed. Reagan and Acklam (1979) estimated a reduction on the roof heat gain of 50% by the use of a light colour in south west U.S.A.. Whiteley and Gardiner (1981) discussed the importance of solar reflective paints for roofs and indicated that reducing the absorptivity usually means a gain in durability. Whitewashing a clay tile roof reduced the ceiling heat flux by 66% (Lamberts 1983).

The importance of roof absorptivity on the heat gain depends on the roof's thermal resistance. It is more pronounced when the thermal resistance is low, and so is very relevant in low cost housing. Periodic maintenance will be necessary but, as the walls are generally also painted, it is not an additional problem. Groups of buildings using white roof and walls may give rise to discomfort from the external luminous environment and the combined use of vegetation is recommended. Vegetation also creates a beneficial microclimate. Shading of buildings by trees is discussed by Sattler et al. (1987).

Solar irradiation data are available from many Brazilian meteorological stations. Generally records are made of hourly values of the total solar irradiation on a horizontal surface (W/m^2). For building use, an estimation of values on slopes is needed. The total solar irradiance on the horizontal surface (I) consists of diffuse (I_d) and beam (I_b) irradiances. According to Stauter and Klein (1979), as reported by Duffie and Beckman (1980), the diffuse component is found from the relationship between total solar irradiance and the estimated clear sky value (I_c):

$$\frac{I_d}{I} \begin{cases} = 1.00-0.1\left(\frac{I}{I_c}\right) & \text{for } 0 \leq \left(\frac{I}{I_c}\right) < 0.48 \\ = 1.11+0.0396\left(\frac{I}{I_c}\right)-0.789\left(\frac{I}{I_c}\right)^2 & \text{for } 0.48 \leq \left(\frac{I}{I_c}\right) < 1.10 \\ = 0.20 & \text{for } 1.10 \leq \left(\frac{I}{I_c}\right) \end{cases} \qquad (2.1)$$

And the beam irradiance is given by

$$I_b = I - I_d \tag{2.2}$$

The total solar irradiance on a sloping surface (I_t) is given by

$$I_t = I_{bt} + I_{gt} + I_{dt} \tag{2.3}$$

where

I_{bt} - beam radiation on the sloping surface, W/m^2
I_{gt} - ground reflected radiation to the sloping surface, W/m^2
I_{dt} - diffuse radiation on the sloping surface, W/m^2

The beam term on the sloping surface is

$$I_{bt} = I_b \cos\theta/\cos\theta_z \tag{2.4}$$

where

θ - angle between the beam irradiance on the surface and the normal to the surface
θ_z - angle between the beam irradiance on the surface and the zenith

The ground reflected term is

$$I_{gt} = I\ g_{re}\ 0.5(1-\cos\beta) \tag{2.5}$$

where

g_{re} - ground reflectance
β - slope of the surface

For the diffuse term, an anisotropic distribution is assumed and Klucher's model (Klucher 1979) applied.

$$I_{dt} = 0.5\ I_d\ (1+\cos\beta)\ (1 + F \sin^3(\beta/2))(1 + F \cos^2\theta\ \sin^3\theta_z) \tag{2.6}$$

where F, the modulating factor, is

$$F = 1 - \left(\frac{I_d}{I}\right)^2$$

Note that in the absence of any direct radiation, the modulating factor becomes zero and all the radiation is treated as isotropic.

2.2.2 Longwave radiation

The importance of longwave radiation on heat transmission through roofs has been pointed out by Loudon (1963) and by Hoglund et al. (1967).

The external surface of a roof emits longwave radiation (I_{le}) according to the Stefan Boltzmann Law.

$$I_{le} = \epsilon \sigma T^4 \qquad (2.7)$$

where
ϵ - emissivity of the surface
σ - Stefan-Boltzmann constant, $5.67\ 10^{-8}$ W/m^2 K^4
T - absolute surface temperature, K

This radiation tends to be counterbalanced by the atmospheric radiation due to re-emission of longwave radiation (infrared radiation - IR) by water vapour, carbon dioxide, ozone and other asymmetric molecules in the atmosphere. At ground level, only radiation from water vapour and carbon dioxide are relevant, the former being the more important (Bliss 1961).

Water vapour is transparent in the wave band 8.5-13 μm, and the re-emission of radiation decreases in this range, known as the 'Atmospheric Window' (Cole 1976a,b). The use of selective surface coatings with high emissivity in this wave band is the base of many studies of radiative cooling (Boldrin et al. 1978, Berdahl and Martin 1978, Higgs and Hand 1978).

The variation in the intensity of atmospheric radiation is mainly attributed to the amount of cloud and the direction of incidence. The effect of clouds, as they are opaque to IR radiation, is to close the 'Atmospheric Window'. When the sky is completely overcast, the atmospheric radiation approximates to that of a black body at air temperature (Parmelee and Aubele 1952). The intensity of the atmospheric radiation also depends on the direction of incidence: the greater the angle, the smaller the intensity (Kneubuhl et al. 1981), so that a horizontal surface loses more heat than a sloping one.

During an overcast day the radiation emitted by the surface of a roof is counterbalanced by atmospheric radiation, but when the sky is clear the roof can lose a lot of heat by this mechanism. In hot climates the use of low emissivity materials on the upper surface of roofs, such as galvanized sheet metal is not recommended as it inhibits radiative losses. Painting the upper surface white will eliminate this problem, while preserving the low emissivity in the attic that is desirable.

Longwave sky radiation is not measured by Brazilian meteorological stations and a theoretical estimation is necessary.

Cole (1976a) reviewed methods of estimating longwave radiation and later (Cole 1976b) presented data from measurements on a school in Sussex. Cole's method is very similar to that of Unsworth and Monteith (1975), both correlating sky radiation with air temperature. As water vapour strongly influences sky radiation, air humidity should be taken into account for a more universal correlation. Research at the Lawrence Berkeley Laboratory (Martin and Berdahl 1984a,b, Berdahl and Fromberg 1982, Berdahl and Martin 1984) studying six sites in the U.S.A. has produced a correlation between sky emissivity (ϵ_s) and dew-point temperature (t_{dp}, in °C).

$$\epsilon_s = 0.711 + 0.56(t_{dp}/100) + 0.73(t_{dp}/100)^2 \qquad (2.8)$$

When the sky is overcast the height of the clouds is included in this relationship. As such accuracy is not necessary here, an interpolation between clear sky emissivity and the black body emissivity for an overcast sky is used. Using a cloud cover factor (c) defined as zero for a clear sky and unity for an overcast sky, the partially overcast sky emissivity is

$$\epsilon_{so} = (1-c)\ \epsilon_s + c \qquad (2.9)$$

The sky radiation is then

$$I_{ls} = \epsilon_{so}\ \sigma\ T_a^4 \qquad (2.10)$$

where

T_a - absolute air temperature, K

Longwave radiation reaching a sloping surface can be divided into atmospheric radiation and ground radiation. The ground radiation emitted from grassy ground is similar to that from a black body at air temperature (Cole 1976a). Therefore, to calculate the total longwave radiation (ground + sky) reaching a sloping surface, a weighted average emissivity based on the view factors was used:

$$\epsilon_{slo} = \epsilon_{so}\ 0.5(1+\cos\beta) + 0.5(1-\cos\beta) \qquad (2.11)$$

The longwave radiation on a sloping surface is then

$$I_{lt} = \epsilon_{slo}\ \sigma\ T_a^4 \qquad (2.12)$$

2.2.3 Convection

Convection on the outside of a roof is affected by the air flow around the building caused by the wind. Ito et al. (1972) reported measurements of convection heat transfer on the exterior of a six floor building in Tokio, and Sharples (1984) on an eighteen floor building in Sheffield. They correlated the wind speed 10 metres high, with surface wind speed and this with the surface convective heat transfer coefficient. There is considerable disagreement between their results (Sharples 1984). Further research is needed to make the standardization of these coefficients possible. In the present work, the convection coefficient suggested by the IHVE Guide (1970) was adopted

$$h_{wind} = 5.8 + 4.1\ v\ (W/m^2K) \qquad (2.13)$$

where

v - wind speed at house height, m/s.

2.2.4 Evaporation

Roofs of clay tiles and asbestos cement sheets can absorb water in their pores. Asbestos cement sheet is very thin and so its maximum water absorptance is low (2.4 kg/m^2 for 6mm sheets). Clay tiles can absorb as much as 7.5 kg/m^2 and this is very important in damping large variations in energy input to the roof.

During clear nights, radiative cooling occurs and the roof's surface temperature drops below air temperature, causing

condensation in humid climates. This condensation is absorbed by the tiles and next morning is evaporated by the absorbed solar radiation. Lamberts (1983) made observations on a clay tile roof in South Brazil. A water loss of 1.7 kg/m^2 was measured during a day, when the total solar radiation was 20.9 MJ/m^2. Assuming the latent heat of vaporization for water at 30 °C as 2.4 MJ/kg (Incropera and De Witt 1981), the energy needed for this evaporation is 4.1 MJ/m^2. Thus, some 20% of the solar radiation incident has been used to evaporate the moisture in the tiles. The absorption of summer rains has a similar effect. A study in North-east Brazil by Cheema (1978), with water dripping on clay tiles, showed a reduction of 2 K of the internal air temperature of a house during the day.

Nayakm et al. (1982) calculated the heat flux through flat roofs in the hot/dry climate of North India and concluded that evaporative cooling systems are very effective in reducing roof heat flux.

Vahid (1982) analysed theoretically the effect of rainfall on the thermal behaviour of a house. He estimated that seven hours of rain can cause a reduction of about 2 K in the room air temperature and a little more in the attic air temperature.

Bogle et al. (1984) carried out a laboratory study on the influence of surface wetness on the thermal performance of a brick wall. They identified two drying phases. In the first, water evaporates directly from the wall surface (similar to pond evaporation) lasting five to ten hours. In the second, water diffuses from within the body of the brick and this can persist up to 40 h. They reported significant increases in heat losses a few hours after the wetting.

Evaporative cooling is very important in reducing summer heat gains, and it is thought to be the main reason for clay tile roofs having a better thermal performance than asbestos cement ones. During winter evaporative cooling is clearly disadvantageous.

2.3 HEAT TRANSFER THROUGH THE ROOF

The heat transfer through a roof (tiles, air gap and ceiling) is discussed together with the mathematical foundation necessary for the simulations.

2.3.1 Longwave radiation

Heat transfer by longwave radiation from the roof to the ceiling is the main form of heat transfer in an attic. The use of low emissivity surfaces in the attic is then very effective in increasing its thermal resistance. Appendix 2 gives the emissivity of common building materials.

Aluminium foil is a cheap and effective low emissivity material. There is however, much controversy in the literature about the effect that time has on its thermal performance.

Wilkes et al. (1940) listed several examples of foil retaining its low emissivity for up to ten years after installation. The emissivity of foil installed on the underside of a roof in 1933 did not change much over a five year period. The value obtained in 1938 was 0.054 as compared with 0.045 for the new foil. Aluminium foil exposed to salt spray under the roof of a boat house for two years had its emissivity increased to 0.1. They also mention that aluminium foil is affected by alkalis and contact with plaster should be avoided. For prolonged exposures to moisture, a transparent lacquer coating applied by the manufacturer is advisable.

Lund and Lander (1961) measured the emissivity of aluminium foil installed over the ceiling in four houses. Measurements were made annually for three years. The increase in emissivity was attributed to dust accumulation. This was shown to be dependent on attic ventilation, length of exposure time and neighbourhood of the house. The two extremes were (a) house near dusty open country, attic with eaves ventilation, starting emissivity 0.022, final emissivity 0.432 and (b) house in a town without attic ventilation, starting emissivity 0.022, final emissivity 0.207.

Lotz (1964) studied dust accumulation on aluminium foil placed over the ceiling in four houses. For a ventilated attic the coverage rate was about 29% of the area per year and 7% for an unventilated attic. He also worked on heat transfer through a scale model of a roof/ceiling combination. With dust free aluminium foil the ceiling heat flow was 18% of that without foil. A dust cover of 10% of ceiling area increased it to 44%. At a dust cover of 90% the ceiling heat flux approached that of the attic without aluminium foil. He suggested that a better place to put the aluminium foil is on the under side of the roof , but contact with any moist material should be kept to a minimum to avoid corrosion.

Placing aluminium foil under a clay tile roof reduced the ceiling heat flux by 86% and, when associated with whitewashing the outside of the roof, by 96% (Lamberts 1983). Aluminium foil under an old asbestos cement roof reduced the ceiling heat flux by 77% (Oliveira 1984).

Summer heat flux through attics with radiation barriers in hot box tests and in the field was measured by Fairey (1982). In some tests, a single layer of aluminium foil (150mm above the ceiling) performed better than 150mm glass-fibre batts.

Yarbrough (1983) assessed reflective insulation and concluded that the ageing effects on the thermal performance of aluminium foil are not yet well understood and that ways should be sought by which foil emissivity can be maintained or improved.

For the calculation of the radiation exchange inside the attic, all surfaces are considered to be isothermal and to have uniform radiosity and irradiation (radiosity is the rate of heat flow leaving the surface, emission plus reflection, and irradiation is the radiation incident from all directions). The surface behaviour is assumed to be opaque, diffuse-grey and the medium within the enclosure is taken to be non-participating.

The mathematical formulation used in this study to determine the net radiation heat transfer rate at each surface was that suggested by Incropera and De Witt (1981). This is summarized below.

The net rate at which radiation leaves a surface is

$$q_i = (E_{bi} - J_i)\ \epsilon_i\ S_i/(1-\epsilon_i) \qquad (2.14)$$

where

i - surface concerned
E_{bi} - emissive power if it were black, W/m^2
J - radiosity, W/m^2
S - area, m^2

Considering an enclosure of n surfaces, the irradiation of surface i can be evaluated from the radiosities of all the surfaces in the enclosure and the view factor between them (F_{ij})

$$q_i = \sum_{j=1}^{j=n} S_i\ F_{ij}\ (J_i - J_j) \qquad (2.15)$$

Combining equations 2.14 and 2.15

$$(E_{bi}-J_i)\ \epsilon_i\ S_i\ /(1-\epsilon_i) = \sum_{j=1}^{j=n} (J_i-J_j)\ S_i\ F_{ij} \qquad (2.16)$$

This equation has to be solved for all n surfaces and thus becomes a system of n linear algebraic equations with radiosities as unknowns

$$a_{i1}\ J_1 + \ldots + a_{in}\ J_n = C_i \qquad (2.17)$$

for i=1 to i=n

For plane surfaces, the configuration factor from a surface to itself is zero and then, for i=j

$$a_{ij} = 1+\epsilon_i/(1-\epsilon_i)$$

for $i \neq j$

$$a_{ij} = -F_{ij}$$

and

$$C_i = \epsilon_i^2\ \sigma\ T_i^4\ /\ (1-\epsilon_i)$$

Radiosity is obtained by solving this system of equations, and can then be used in (2.14) to determine the net radiation heat transfer rate at each surface.

2.3.2 Convection

Convection is responsible for the energy transfer between the attic surfaces and the attic air moving over them. The air motion can be caused by buoyancy, external forces such as wind or, as it is more common, by a combination of those two forces. When the speed of the air is not important convection is 'natural' and when speed becomes important it is 'forced'. In both cases, convection can still be divided into 'laminar' - when the fluid motion is highly ordered, and it is possible to identify streamlines along which particles move - and 'turbulent' - when fluid motion is irregular and has velocity fluctuations.

Natural convective heat transfer coefficients may be found from

$$Nu = C\ (Gr\ Pr)^{n} \qquad (2.18)$$

where

Nu - Nusselt number
C - constant dependent on orientation, geometry and type of flow
Gr - Grashof number
Pr - Prandtl number
n - 1/3 for turbulent flow and 1/4 for laminar flow.

Most empirical relationships for natural convection heat transfer found in the literature are based on a two part correlation: one for laminar and other for turbulent flow (see McAdams 1958, ASHRAE 1985, CIBSE 1986). Alamdari and Hammond (1983) pointed out that the use of this two part correlation in dynamic heat transfer models can lead to numerical instability because of the sudden change in the exponent. To overcome this, they developed a correlation valid for laminar and turbulent flows for vertical surfaces and horizontal surfaces with heat flowing upward. For horizontal surfaces, with heat flowing downwards, turbulent flow is not expected due to thermal stratification, and an exponent of 1/5 is considered to be more appropriate. Table 2.1 summarizes the natural convection heat transfer coefficients adopted.

Table 2.1 Natural convection heat transfer coefficients (Alamdary and Hammond 1983).

Heat Flow Direction	Heat Transfer Coefficient (W/m^2 K)
	$h_c=[\{1.5(\Delta t/L)^{0.25}\}^6 + \{1.23\Delta t^{0.33}\}^6]^{1/6}$
	$h_c=0.6(\Delta t/L^2)^{0.2}$
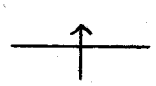	$h_c=[\{1.4(\Delta t/L)^{0.25}\}^6 + \{1.63\Delta t^{0.33}\}^6]^{1/6}$

Δt- temperature difference between air and surface, K
L - characteristic length of surface, m

The characteristic length to be used in the formulae for laminar convection heat transfer in vertical walls is the height. For rectangular horizontal surfaces there is some divergence in the literature. Kreith (1973) and CIBSE suggested the mean between the two dimensions. Incropera and De Witt (1981) used the area divided by the perimeter and Alamdari and Hammond (1983) proposed the hydraulic diameter (four times the area divided by the perimeter). Since in a ventilated attic, the air is generally moving due to an external force (wind), the dimension parallel to the air flow path was adopted.

Forced convection heat transfer coefficients are based on Reynolds (Re) and Prandtl (Pr) numbers and the CIBSE Guide (1986) gives the following equation for turbulent flow over flat plates:

$$Nu = 0.037\ Re^{0.8}\ Pr^{0.33} \tag{2.19}$$

Using air properties at 20 °C, the forced convection heat transfer coefficient (h_f) becomes

$$h_f = 6.14\ v^{0.8}\ L^{-0.2} \quad (W/m^2K) \tag{2.20}$$

where

v - air speed, m/s
L - characteristic length, m

When natural and forced convection occur simultaneously, McAdams (1958) recommends that both values be calculated and the larger used.

Natural convection is expected to predominate inside a naturally ventilated attic but forced convection is possible under very high rates of ventilation.

2.3.3 Conduction

Conduction is the transport of energy within a body due to a temperature gradient. The physical mechanism is random molecular activity. For a one-dimensional flow the heat transfer by conduction can be represented as

$$q_c/S = \Delta t\ \lambda/l \qquad (2.21)$$

where

λ - thermal conductivity of the material, W/m K
l - thickness, m
S - area, m^2
Δt - temperature difference between the two surfaces, K

The thermal conductivity will vary with density and moisture content of the material. Conduction in roofs will occur through the tiles and ceiling. The thermal transmittance of most roofing sheets and tiles is very high, mainly because of thickness. Conduction through a ceiling is quite variable because of the different materials that can be used.

Wilkes and Rucker (1983) report on the thermal performance of residential attic insulation. Comparing measurements and simulations, they found that the temperature dependence of the thermal conductivity of the materials and the effect of installed thickness and density on the thermal conductivity should be included in the simulations. This is important mainly for highly insulated ceilings.

2.3.4 Attic Ventilation

There is much controversy about the effect of attic ventilation on ceiling heat flux.

Mukhtar (1978) compared internal air temperatures of houses with or without ventilation of the attic and/or the living quarters. Ventilation of the attic caused a reduction of 0.5 K on the maximum internal temperature in a house without room ventilation. No difference was found when the room was ventilated.

In Brazil, work by IPT (1979) showed extra ventilation of a clay tile roof to be disadvantageous due to the reduction in the thermal inertia of the system. Valentin (1981), from the same

institution, showed the ventilation of an asbestos cement roof to improve the internal environment of a house. Still at IPT, measurements on flat asbestos cement roofs (Kiyohara et al. 1984) showed reductions of 40% on the ceiling heat flux at peak time by incorporating 300mm ventilation slots (full height of air cavity).

Givoni (1962) in Israel, reported only slight reductions (0.5 K) of ceiling temperature with very high ventilation in roofs with cement tiles and plaster ceiling, but van Straaten (1957) studying roofs of galvanized steel and asbestos cement ceilings in South Africa, obtained large reductions (3.5 K) in ceiling temperature. He also claimed ceiling heat flux reductions of 30%, but there are some doubts about this figure as his heat flux meters were not calibrated. Givoni (1962), discussing these results, concluded that the cooling effect of the attic ventilation is more pronounced in thin roofs with reduced thermal capacity and increased air tightness.

The 'Summer Attic and Whole-House Ventilation Workshop' (NBS 1979) reached the general conclusion that forced attic ventilation is of little value. It should be mentioned, however, that all papers reported houses having ceiling insulation.

Attic ventilation is important to avoid winter condensation. McQuiston et al. (1984), developing new effective thermal resistances for ventilated attics in the U.S.A., concluded that low ventilation rates sufficient for moisture removal should be used.

Ventilation of the attic causes heat to be exchanged between the attic air (T_{at}) and the external air (T_o). This heat transfer is proportional to the temperature difference and the ventilation flow rate. It can be expressed by

$$q_v = \rho \; c \; V \; (T_{at}-T_o) \qquad (2.22)$$

where

ρ - air density, kg/m^3
c - specific heat capacity of the air, J/kg K
V - air volume flow rate, m^3/s

Considering a perfect mixture of input air and attic air, air leaving the roof has the temperature of the attic air. This

assumption in practice is violated when there is stratification. For the sake of simplicity the assumption is normally used when formulating the heat balance.

It is useful to define a ventilation heat transfer conductance for use in the mathematical models. From equation 2.22 the conductance (C_v) will be

$$C_v = \rho \; c \; V \qquad (2.23)$$

Most of the research undertaken in attic ventilation relates to the avoidance of condensation in cold climates. A state of the art review of research into attic condensation was presented by Burch and Harrje (1985). The main moisture input to the attic comes from the living space, and they concluded that convective transfer of water vapour into the attic often transports more moisture than diffusive transfer through the ceiling. Special precautions like sealing cracks around pipes and flues that pass through a ceiling, should be taken to minimize this.

2.4 CEILING TEMPERATURES AND COMFORT

Radiation exchange between people and surroundings is important for thermal comfort.

Chrenko (1953) describes experiments made at BRE (U.K.) into the discomfort caused by heated ceilings. People were subjected to a constant air temperature while the ceiling temperature was increased. He suggested that the elevation of mean radiant temperature of the room at head-level, due to the heated ceiling, should not exceed 2K. He predicts that at this limit 20% will feel uncomfortable.

Koenigsberger and Lynn (1965), reviewing the literature on this subject, concluded that only a very small rise of ceiling temperature should be accepted in the warm and humid tropics and suggested a maximum acceptable increase in ceiling temperature above the room air of 4.5K.

Ahmad (1974) reviewed the influence of ceiling height upon comfort. He concluded that it is the ceiling heat flux and not its height that is the decisive factor.

Mukhtar (1978) investigated the thermal performance of roofs in northern Sudan and stressed the importance of ceiling surface temperature on thermal comfort.

Fanger et al. (1980) also studied the comfort limits for heated ceilings. They examined subjects in thermal neutrality and suggest a maximum radiant temperature asymmetry of 4K (similar to 2K elevation on mean radiant temperature) as a design criterion. They predicted only 5% feeling uncomfortable for this asymmetry. The high levels of discomfort found by Chrenko (1953) are attributed to the air temperature being kept constant for all experiments and therefore subjects not being in thermal neutrality.

Fanger (1986) indicated that the discomfort caused by asymmetric radiation from a warm ceiling is felt at much lower radiant temperature asymmetries than from warm walls, cool walls or cool ceilings.

A better understanding of the physiological reactions of the human body under high ambient temperatures and humidity to overhead long wave radiation is needed.

2.5 EFFECTIVE RESISTANCE OF VENTILATED ATTICS

Thermal resistances of non ventilated air spaces are given by Robinson et al. (1954) and Anderson (1981). The thermal resistance of an air space under steady state heat transfer can be calculated, if the heat flux and temperature difference are known. When the air space is ventilated, the 'effective' thermal resistance may be calculated. This value summarizes the complex phenomena involved in the heat transfer. Fairey (1982) discussed the difficulty in determining a resistance value for the radiant barriers used in attics. This is due to its interdependence with the remaining components of the roof. Yarbrough (1983) showed the thermal resistance of a reflective system to decrease as the temperature difference across it increased. This is caused by the non-linearity of the heat transfer by radiation and demonstrates the importance of the effective resistances (ER) for handbook heat transfer calculations.

Joy (1958) was the first to calculate ER's for attics in the steady state. He suggested that the ER be calculated by dividing the temperature difference from roof top to room air by the ceiling

heat flux and then subtracting the total ceiling resistance (including both surface resistances).

So Joy's ER's are

$$ER = \frac{T_{rt} - T_a}{chf} - (R_{su}+R_c+R_{si}) \qquad (2.24)$$

where

T_{rt} - surface temperature of the upper-side of roof, K
T_a - room air temperature, K
chf - ceiling heat flux, W/m^2
R_{su} - surface resistance above ceiling, m^2K/W
R_{si} - surface resistance under ceiling, m^2K/W
R_c - ceiling thermal resistance, m^2K/W

The values calculated by Joy are the basis of those used by ASHRAE (1985) for design heat transmission coefficients.

McQuiston et al. (1984) calculated the ER under unsteady state conditions in a slightly different way. They used the temperature difference between the inside roof surface and room air and did not include the upper ceiling surface resistance in the subtracted term. Values from midday to midnight were averaged. Thus, according to them, ER's are

$$ER = \frac{T_r - T_a}{chf} - (R_c+R_{si}) \qquad (2.25)$$

where

T_r - surface temperature of the under-side of the roof, K

ER values obtained this way are much lower than the ones obtained according to Joy (1958): 30 to 40% for no ventilation and 40 to 75% for high ventilation.

In both studies, it is assumed that the heat is flowing from the ceiling surface to the room air. However, part of the heat flux is by radiation to other room surfaces. It seems more appropriate therefore, to calculate ER's based on temperature difference from the inside roof surface to the under-side of the ceiling surface and using only the ceiling resistance as the

subtracting term. The effective resistance in this work will then be calculated by

$$ER = \frac{T_r - T_{ci}}{chf} - R_c \qquad (2.26)$$

where

T_{ci} - surface temperature of the upper-side of the ceiling, K

2.6 MATHEMATICAL MODELS FOR HEAT TRANSFER

The mathematical models found in the literature range from simple steady state models to complex dynamic models which perform simulations from hour to hour.

Joy (1958) developed a steady state model to compare with his experimental results. The heat transfer coefficients were assumed to be independent of temperature difference. Heat transfer through the gable was not included. Results from the model compared well with experimental.

Peavy (1979) produced a dynamic model based on Joy's mathematical analysis. The heat transfer coefficients varied with temperature difference. Heat transfer through the gables was not included. The model agreed well with summer field data from a house in Houston, Texas (U.S.A).

Wilkes (1981) reviewed six models that have been used to predict the thermal performance of ventilated attics, including the two above. He concluded that although Peavy's model does not contain all the desirable features, it is the most sophisticated of the six and should be the one used as basis for further developments.

Wilkes (1982) expanded Peavy's model to include seven surfaces (two roofs, two gables, two eave walls and the ceiling). Each surface is represented by conduction transfer functions. A complete radiation exchange analysis of the enclosure was carried out, assuming opaque grey diffuse isothermal surfaces. The outside climatic variables are represented by the sol-air temperature. Two versions of the model were studied: well mixed attic air and attic air temperature increasing along the flow path. The latter predicted the ceiling heat flux as measured in a guarded hot box, to within

± 10%. The limitations of this model for the present application are the sol-air representation of the external climate and its validation for an insulated attic with eaves to ridge ventilation.

2.7 MODELLING AND ENHANCING ATTIC VENTILATION

Ventilation causes heat and moisture removal from the attic space. Attic ventilation flow rate modelling is necessary for realistic calculations of heat transfer through the roof when the ventilation flow rate is not measured.

Natural ventilation is caused by pressure gradients originating from wind forces and/or thermal forces. When the wind blows over a building it will be decelerated and deflected. The deceleration causes positive pressure on the windward side. The deflection causes flow separation, developing zones of suction (negative pressure). The pressure distribution on the roof varies with its slope. Negative pressures are experienced on both faces of roofs sloping less than 30° (Liddament 1986). For steeper slopes, positive pressure are experienced on the windward face.

Thermal forces are created by differences in air temperature and hence air density between the interior and exterior of a building. A further force able to contribute to the ventilation of a building is that caused by wind pressure fluctuations due to turbulence. This is particularly relevant in single sided configurations. Most studies do not include wind turbulence (Liddament 1986).

Two kinds of openings can promote attic ventilation: infiltration openings, like cracks and permeability through materials, or purposely provided openings, like slots and air bricks. The development of mathematical models for predicting ventilation flow rates through these openings has been widely reported (Liddament and Allen 1983).

An important requirement for modelling ventilation is the knowledge of wind pressure coefficients on the building envelope. Wind pressure varies with the degree of shelter provided by surrounding buildings. Wiren (1984), studied buildings within a group of similar buildings in a wind tunnel. When the distance between houses was equal to two houses lengths, the pressure difference across a house (windward to leeward) generated by frontal wind was

60% of the pressure difference recorded for an isolated house. When the spacing was reduced to one house length, the pressure difference further decreased to one third of that for an exposed house.

The introduction of architectural features can severely modify the wind pressures exerted on building by trapping the wind. Ashley (1984) indicated an increase in pressure difference between the windward and leeward facade of 25% by extended eaves and end walls.

Attic ventilation is generally associated with the use of ridge ventilators which take advantage of the stack effect. The difference in height between ridge and eaves is small in low pitched roofs and so is the stack effect. However, the ridge of this type of roof is generally subjected to suction, and the combined effect tends to enhance ventilation. Adequate protection of the ridge openings against wind driven rain should be provided.

Fairey and Bettencourt (1981) devised a ridge ventilator for augmenting wind and stack driven natural ventilation. The device is complemented by opposing low pressure back draft dampers to induce a one way air flow and can be used for attic or whole house ventilation.

Schubert and Kennedy (1981) tested various ventilator caps, in a wind tunnel, to determine their effect on natural ventilation. Some caps increased the flow rate of the uncapped ventilator stack in over 50% for wind tunnel speeds of 4 m/s.

Special care should be taken when positioning natural ventilation stack openings. Gids (1984) mentioned the importance of considering the local wind environment to avoid flow reversal caused by the descending wake of tall buildings.

Kronvall (1985), studying the ventilation strategies for Swedish attics, presented a method for calculating ventilation flow rates. Comparing eave slots with different ventilators (150mm x 150mm and 250mm x 250mm), he concluded that the most effective way of ventilating the attic is by eave slots. This was the only theoretical model for calculating attic ventilation found in the literature. A more elaborated model was desired for the present study and its development is described in the next chapter.

CHAPTER 3 MODELLING ATTIC VENTILATION FLOW RATES

3.1 INTRODUCTION

The quantification of ventilation flow rates of typical Brazilian roofs with various opening configurations and degrees of exposure was needed for realistic calculations of the heat transfer through attics. Roofs are normally built without specially designed openings. Clay tiled roofs provide some attic ventilation even without specially provided openings due to their air permeability. Asbestos cement roofs are more airtight and the space between the tile corrugation and the purlin at eaves level can be left open if ventilation is desired. This allows only wind driven ventilation. To use stack effect, a ridge opening can be incorporated but careful protection from wind driven rain is important. If ventilation provided in the ways described above is not sufficient, an easy way of increasing it, if there is wind, is to incorporate a slot at the eaves. There should be no problem of wind driven rain ingressing the attic space with the protection provided by the extended eaves normally used (0.4m, figure 1.1)

Attic ventilation depends on several factors:

- dimension and location of ventilation openings,
- local wind speed,
- shelter provided by surrounding buildings,
- length to width ratio of the building,
- slope of the roof,
- difference between attic and external air temperature,
- air permeability of the roof cover.

A model capable of estimating attic ventilation considering the above variables was developed, based on the Air Infiltration and Ventilation Centre guide (Liddament 1986).

3.2 THE MODEL

The model consists of a single-zone with nine flow paths: three ventilation paths (two eave slots and one ridge slot) and six infiltration paths (two in each side of the roof and one in each

gable). Ventilation paths are purposely provided openings and infiltration paths are cracks or air permeable materials. The network is shown in figure 3.1.

A mass flow balance is given by

$$\sum_{i=1}^{i=9} \rho_i . Q_i = 0 \quad \text{kg/s} \tag{3.1}$$

where

ρ_i - density of air flowing through path i, kg/m^3
Q_i - air flow rate, m^3/s

The power law of the flow equation is

$$Q_i = k_i \, |p_i - p_{int}|^{n_i} \tag{3.2}$$

where

k_i - flow coefficient of path i, m^3/s at 1 Pa
p_i - air flow pressures, Pa
p_{int} - internal attic pressure, Pa
n_i - flow exponent of path i

Combining equation 3.2 and 3.1, when the internal/external air temperature difference is less than 20 K, the mass flow balance becomes

$$\sum_{i=1}^{i=9} k_i . |p_i - p_{int}|^{n_i} . ((p_i - p_{int})/|p_i - p_{int}|) = 0 \tag{3.3}$$

Wind pressure and stack pressure were calculated according to the AIVC Guide (Liddament 1986). The flow path characteristics (k and n values) given in the same guide were also used.

The model was used on a house of plan dimensions 6 m x 7 m under the conditions described below.

- Kinds of roof: (1) asbestos cement with a slope of 20° and (2) clay tiled with a slope of 30°.
- Roof ventilation openings:

(1) Asbestos cement: a) eave tile corrugation - space between tile corrugation and purlin at eave (0.009 m^2/m) + ridge slot (0.018 m^2/m); b) eave tile corrugation (0.009 m^2/m) + 20 mm slot

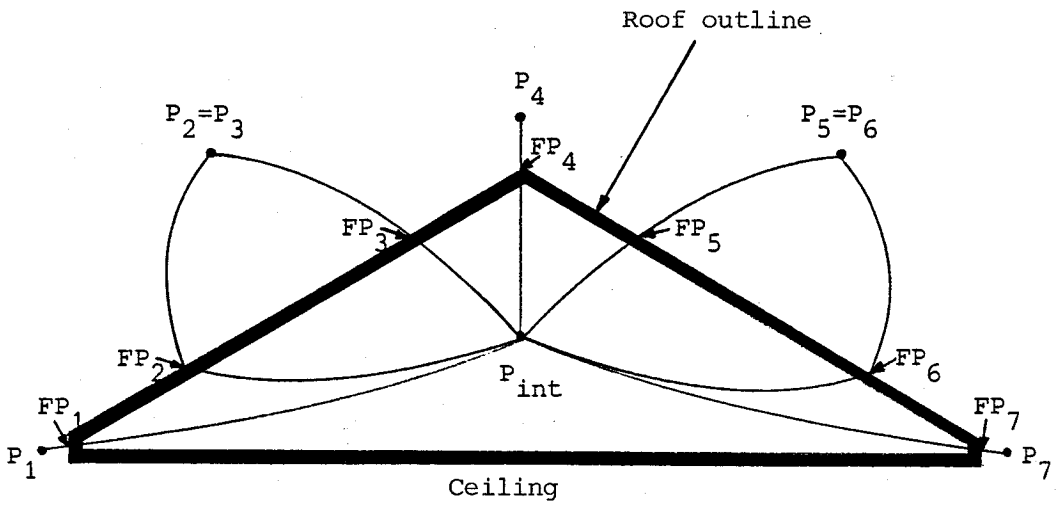

P_1 to P_9 - airflow pressures

P_{int} - internal attic pressure

FP_1 to FP_9 - airflow paths

(P_8, P_9, FP_8 and FP_9 are the airflow pressures and airflow paths through the gables. Not represented in diagram.)

Figure 3.1 Network representation of the attic ventilation model showing the nine flow paths.

along the eaves (0.02 m^2/m); c) eave tile corrugation (0.009 m^2/m) + 50 mm slot along the eaves (0.05 m^2/m).

(2) Clay tiled: a) no intentionally provided openings, only a crack of 2 mm between tiles and purlin at eave; b) 29 mm slot along the eaves (0.029 m^2/m); c) 59 mm slot along the eaves (0.059 m^2/m).

Note that the eave slots on the clay tiled roof are bigger than that on the asbestos cement roof, in order to provide the same eave opening area (tile corrugation + slot).

- Wind exposures: (1) exposed in open country and (2) sheltered in a town with the building surrounded on all sides by similar buildings.
- Length to width ratio: 1:1 (best approximation for 6 m by 7 m)
- Wind directions: (1) normal and (2) 45° to the eaves.
- Inside/outside air temperature differences: (1) 5 K and (2) 20 K.

3.3 RESULTS

The results obtained from the simulations with the model are presented in figures 3.2 to 3.5 for the asbestos cement roof and figures 3.6 to 3.9 for the clay tiled roof. Ventilation is expressed by volume flow rate (m^3/s). To convert this to air changes per hour, multiply by 79 (3600 divided by the volume of the attic) for the asbestos cement roof (slope 20°) and by 50 for the clay tiled roof (slope 30°). The difference in ventilation by changing the inside/outside air temperature difference from 5 to 20 K was very small due to the small difference in height between ridge and eaves. The results discussed below are those calculated for a 5 K difference in temperature.

Figure 3.2 shows the ventilation flow rate of an asbestos cement roof located in open country with wind normal to the eaves. For wind speeds above 0.5 m/s, higher ventilation flow rates were obtained using eave slots (20mm and 50mm) rather than eaves + ridge openings. Without wind, eaves + ridge opening provided a small ventilation flow rate by stack effect. For a wind speed of 2 m/s (average wind speed during typical summer day in Porto Alegre, table 1.1) the ventilation flow rate was 0.055 m^3/s for eaves + ridge openings, 0.136 m^3/s for the 20mm eave slots and 0.271 m^3/s for the 50mm eave slots.

Figure 3.3 shows the ventilation flow rate of an asbestos cement roof located in open country with a wind with direction 45° to

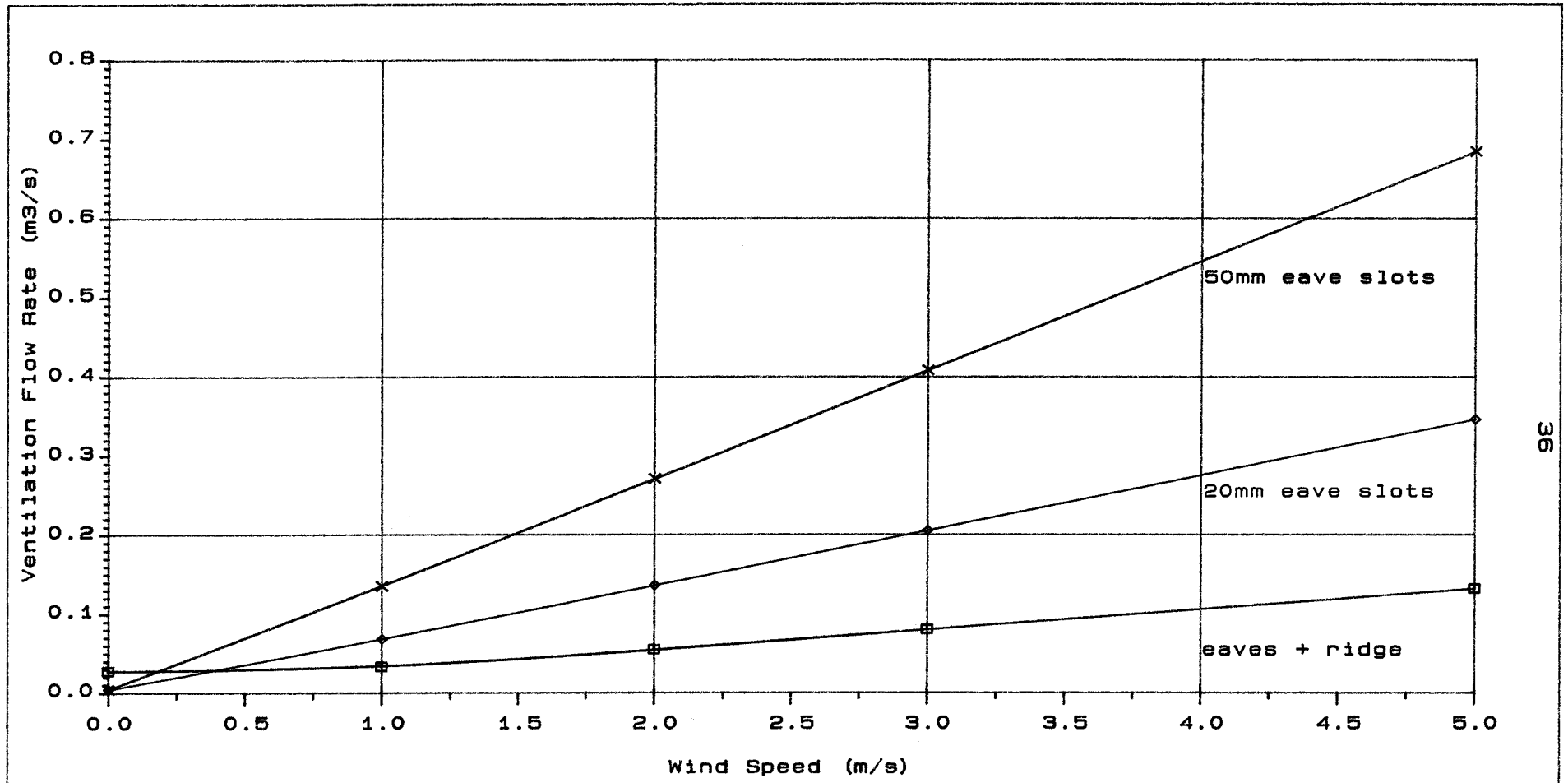

Figure 3.2 Ventilation flow rates through the asbestos cement roof with different opening configurations (-Location: open country -Wind direction: normal to the eaves).

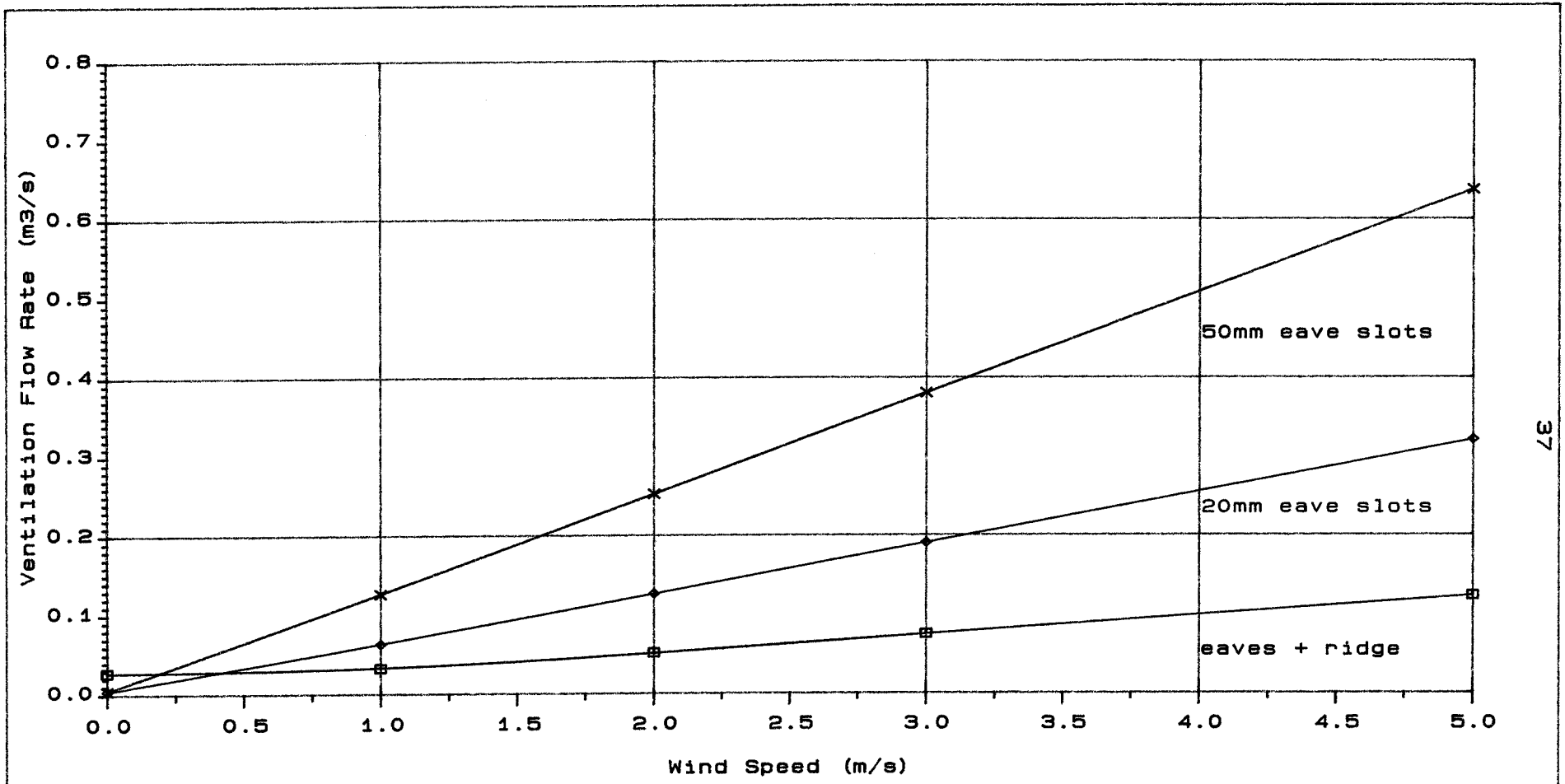

Figure 3.3 Ventilation flow rates through the asbestos cement roof with different opening configurations (-Location: open country -Wind direction: 45° to the eaves).

the eaves. The pattern observed was very similar to the one shown in figure 3.2. The values of the ventilation flow rate were slightly lower. For a wind speed of 2 m/s the ventilation was 0.052 m^3/s for eaves + ridge openings, 0.127 m^3/s for the 20mm eave slots and 0.253 m^3/s for the 50mm eave slots. These values are about 7% lower than the previous ones.

Figure 3.4 shows the ventilation flow rate of an asbestos cement roof located in a town with wind normal to the eaves. Again a similar pattern was observed, but the ventilation flow rates were much lower and the wind speed at which eave slots became more efficient than eaves + ridge was slightly higher (1 m/s). For a wind speed of 2 m/s the ventilation was 0.039 m^3/s for eaves + ridge openings, 0.055 m^3/s for the 20 mm eave slots and 0.109 m^3/s and for the 50 mm eave slots.

Figure 3.5 shows the ventilation flow rate of an asbestos cement roof located in a town with a wind 45° to the eaves. The same pattern as shown in figure 3.4 was observed, but the ventilation flow rates were slightly lower. For a wind speed of 2 m/s the ventilation was 0.035 m^3/s for eaves + ridge openings, 0.047 m^3/s for the 20 mm eave slots and 0.092 m^3/s and for the 50 mm eave slots. These values are 10% lower than those for figure 3.4 for eaves + ridge openings and 16% for the eave slots.

The change in location of an asbestos cement roof from open country (figure 3.2 and 3.3) to town (figure 3.4 and 3.5) causes reductions in the ventilation flow rate. For a wind speed of 2 m/s the reduction was about 30% for eaves + ridge and about 60% for the eave slots.

Figure 3.6 shows the ventilation flow rate of a clay tiled roof located in open country and wind normal to the eaves. The roof without openings had a ventilation flow rate of about 0.030 m^3/s for wind speeds up to 2 m/s, this increased to 0.098 m^3/s at 5 m/s. For a wind speed of 2 m/s the ventilation flow rate was 0.161 m^3/s for the 29mm eave slots and 0.310 m^3/s for the 59mm eave slots.

Figure 3.7 shows the ventilation flow rate of a clay tiled roof located in open country with a wind 45° to the eaves. The pattern was very similar to the one shown in figure 3.6. The values were slightly lower. The roof without openings had the same ventilation as for wind normal to the eaves for wind speeds up to 3 m/s. For a wind speed of 2 m/s the ventilation was 0.149 m^3/s for

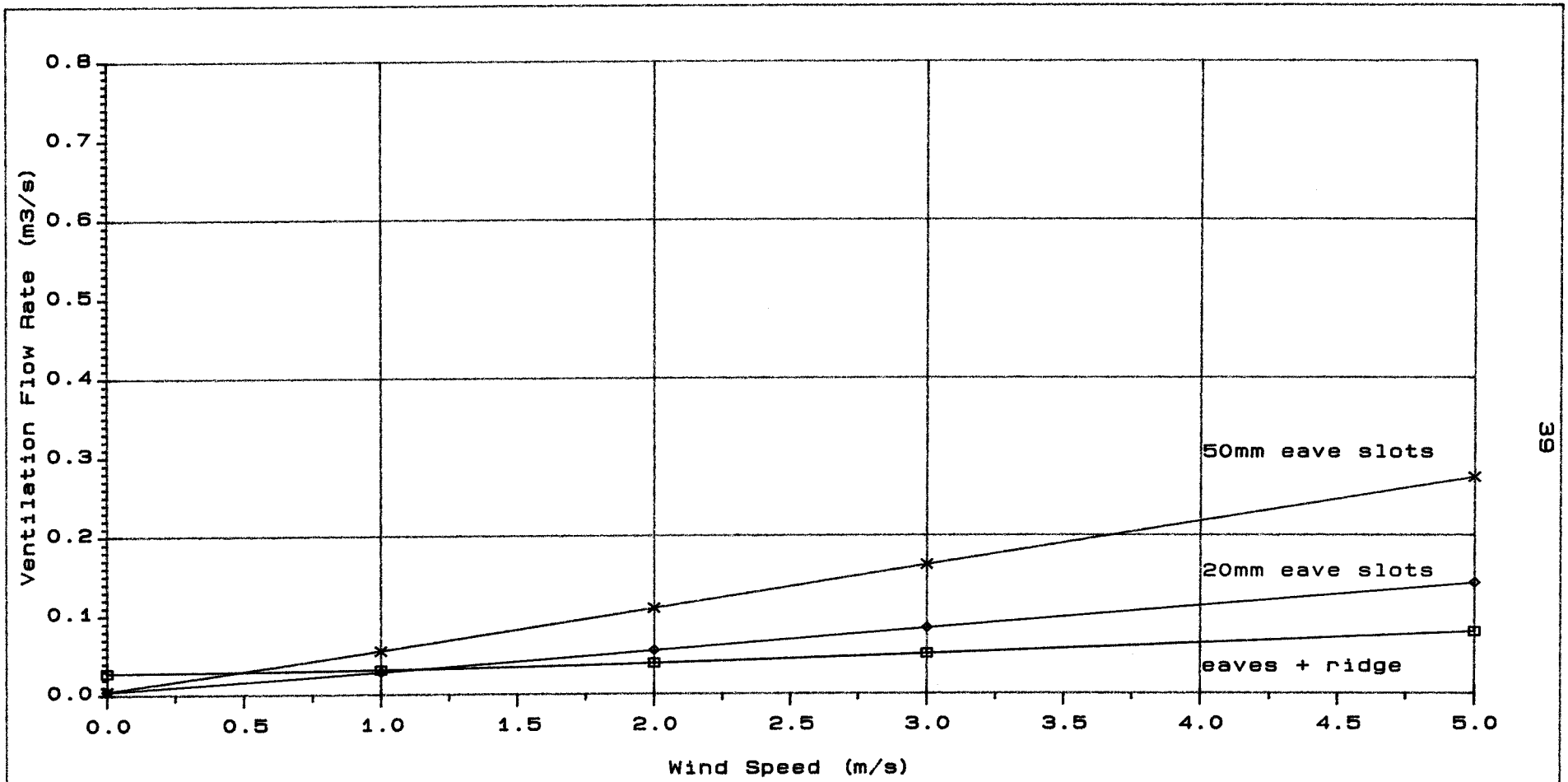

Figure 3.4 Ventilation flow rates through the asbestos cement roof with different opening configurations (-Location: town -Wind direction: normal to the eaves).

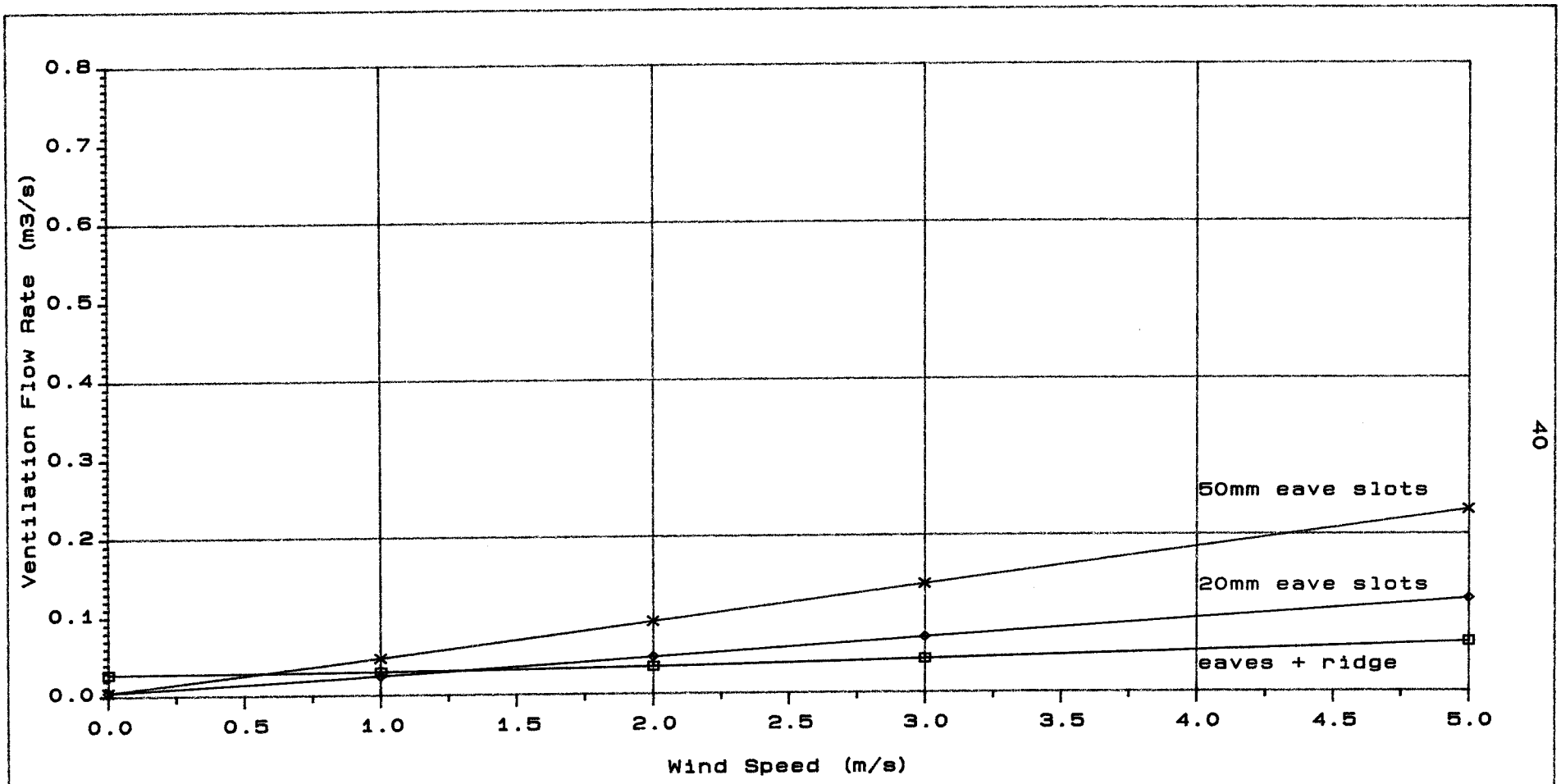

Figure 3.5 Ventilation flow rates through the asbestos cement roof with different opening configurations (-Location: town -Wind direction: 45° to the eaves).

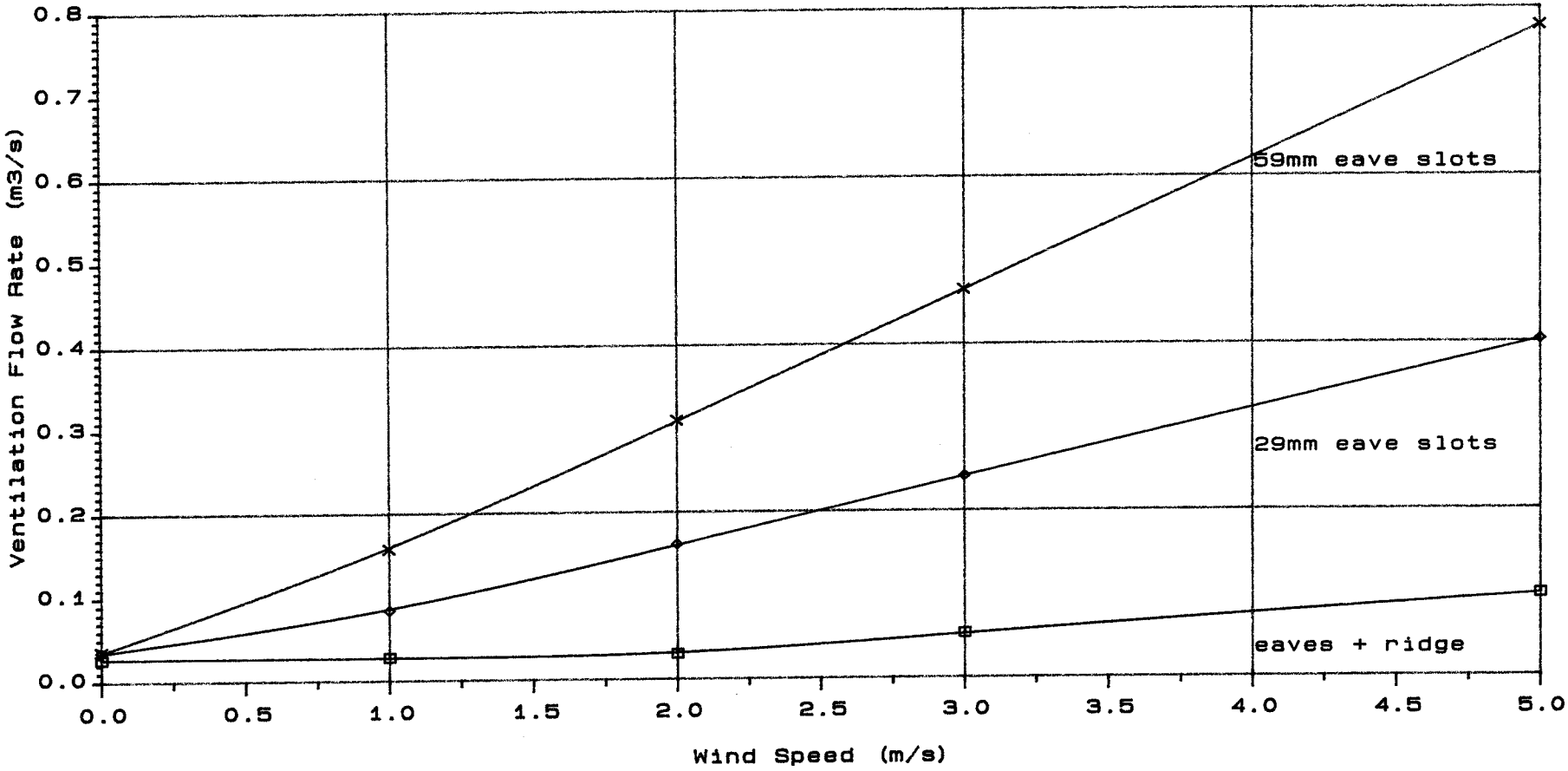

Figure 3.6 Ventilation flow rates through the clay tiled roof with different opening configurations (-Location: open country -Wind direction: normal to the eaves).

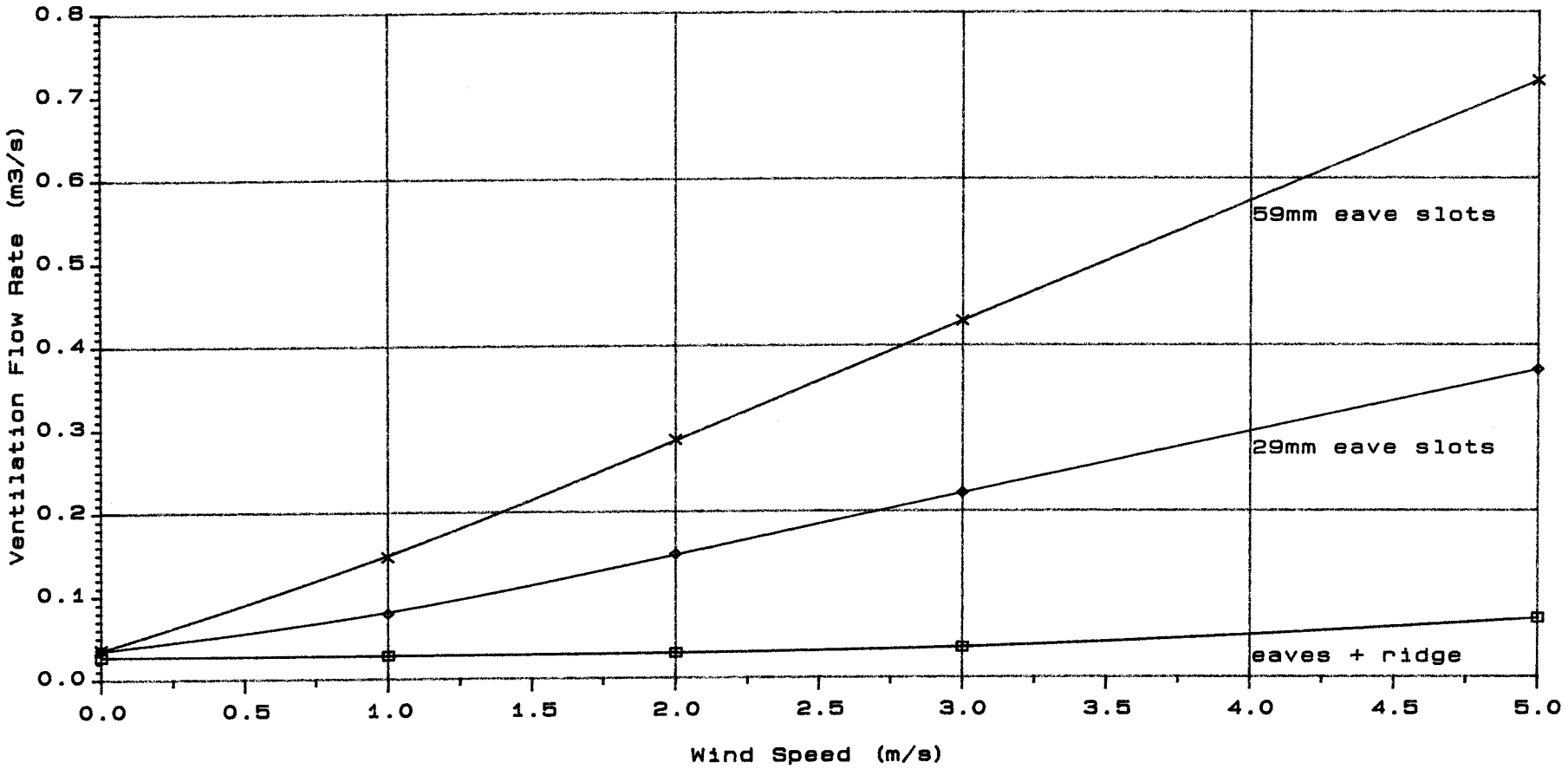

Figure 3.7 Ventilation flow rates through the clay tiled roof with different opening configurations (-Location: open country -Wind direction: 45° to the eaves).

the 29mm eave slots and 0.287 m^3/s for the 59mm eave slots. These values are 7% lower than for normal wind (figure 3.6).

Figure 3.8 shows the ventilation flow rate of a clay tiled roof located in a town with wind normal to the eaves. Ventilation flow rates were much lower than in open country. The roof without openings had the same ventilation flow rate for wind speeds up to 4 m/s. For a wind speed of 2 m/s the ventilation was 0.071 m^3/s for the 29mm eave slots and 0.134 m^3/s for the 59mm eave slots.

Figure 3.9 shows the ventilation flow rate of a clay tiled roof located in a town with a wind 45° to the eaves. Again a similar pattern to the case with normal wind was observed. The roof without openings had the same ventilation for wind speeds up to 5 m/s. For a wind speed of 2 m/s the ventilation was 0.061 m^3/s for the 29mm eave slots and 0.114 m^3/s for the 59mm eave slots. These values are about 15% smaller than those for frontal wind (figure 3.8).

The change in location of a clay tiled roof from open country (figure 3.6 and 3.7) to town (figure 3.8 and 3.9) causes reductions in the ventilation flow rate. For a wind speed of 2 m/s the reduction was about 60% for the eave slots. No reduction was found for the roof without openings.

When there was no wind, the ventilation provided by eaves + ridge openings in the asbestos cement roof was similar to the ventilation found in the clay tiled roof without openings and equal to about two attic air changes per hour.

Table 3.1 shows the ventilation flow rate through the nine flow paths for both types of roofs in a urban environment, sheltered by surrounding buildings, a wind of 2 m/s normal to the eaves and an air temperature difference between interior/exterior of 5 K. Comparing the asbestos cement roof with the clay tiled roof, the asbestos cement roof with eave + ridge openings gave more ventilation than the clay tiled roof without specially provided openings. Considering the results with the slot ventilation openings, the clay tiled roof produced higher ventilation rates than the asbestos cement roof, due to higher air permeability. It is interesting to note that in the asbestos cement roof with slots, most of the flow (more than 80%) is from one slot to the other and, in the clay tile roof, the flow is more homogeneously distributed by the various paths and only 44% is from slot to slot.

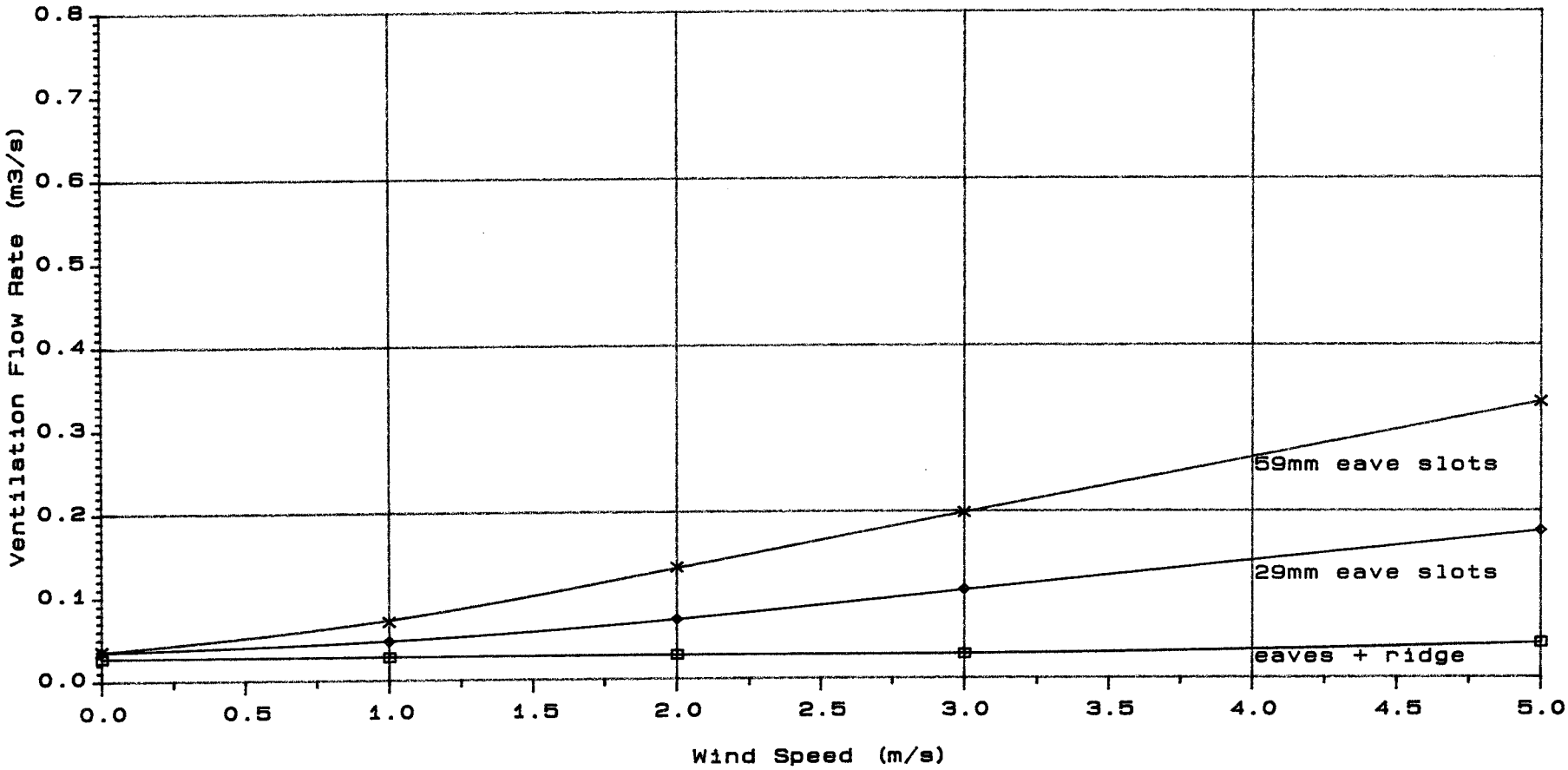

Figure 3.8 Ventilation flow rates through the clay tiled roof with different opening configurations (-Location: town -Wind direction: normal to the eaves).

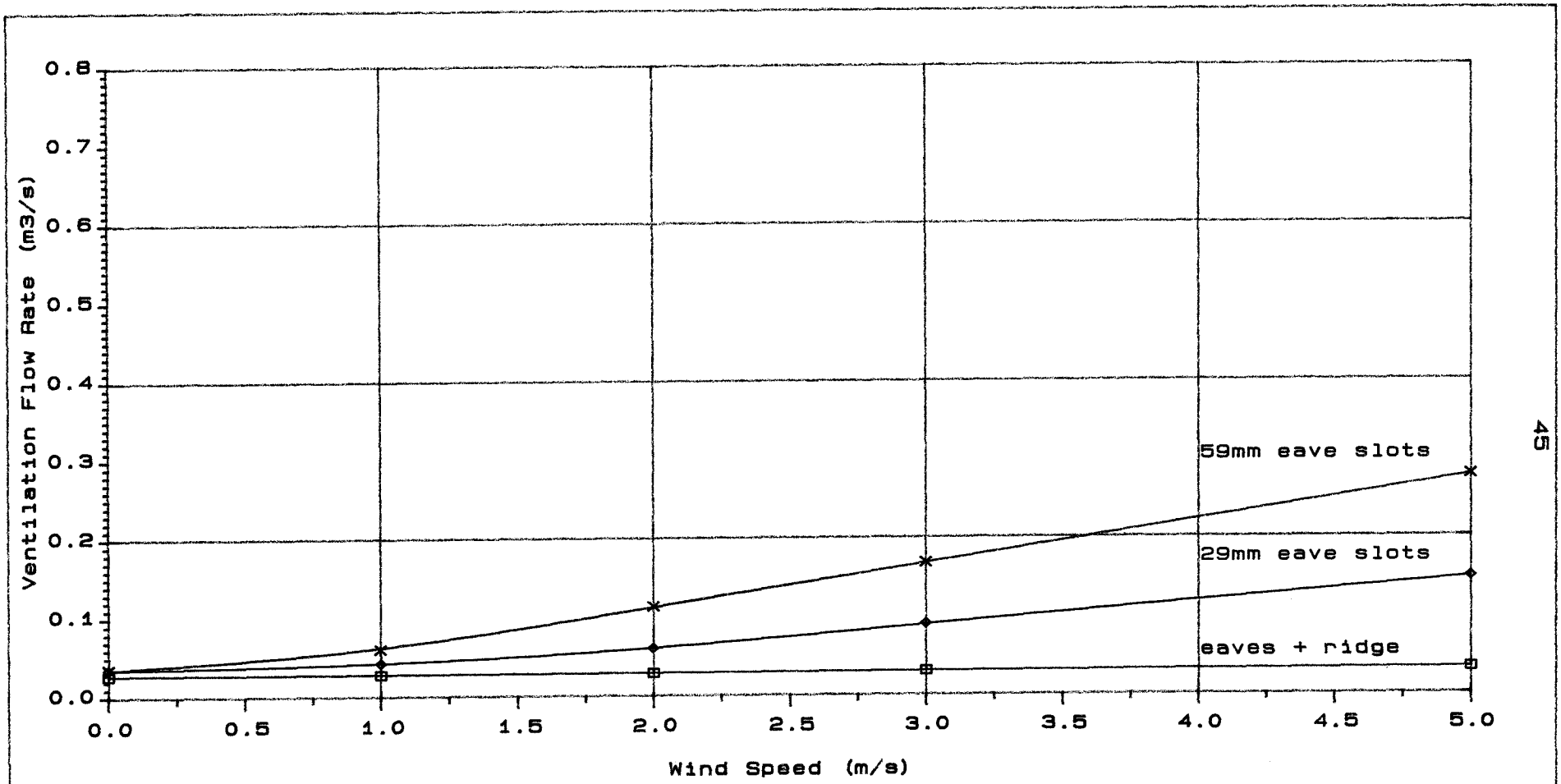

Figure 3.9 Ventilation flow rates through the clay tiled roof with different opening configurations (-Location: town -Wind direction: 45° to the eaves).

Table 3.1 Ventilation flow rate through the nine flowpaths of an asbestos cement roof and a clay tiled roof.

	Asbestos Cement			Clay Tiled		
Flow-paths	Eave+ Ridge	Slot 20mm	Slot 50mm	No Opening	Slot 29mm	Slot 59mm
	(m^3/s)			(m^3/s)		
1	0.025	0.055	0.109	0.007	0.071	0.134
2	-0.001	-0.002	-0.002	0.007	-0.013	-0.015
3	-0.002	-0.003	-0.004	-0.016	-0.024	-0.025
4	-0.037	---	---	---	---	---
5	0.001	-0.003	-0.003	-0.013	-0.021	-0.023
6	0.001	-0.002	-0.002	0.011	-0.009	-0.012
7	0.013	-0.045	-0.098	0.004	-0.004	-0.059
8	0.000	0.000	0.000	0.000	0.000	0.000
9	0.000	0.000	0.000	0.000	0.000	0.000
total	0.040	0.055	0.109	0.029	0.071	0.134

3.4 DISCUSSION AND CONCLUSION

The model was very useful in identifying and quantifying the relative importance of the several variables concerned.

Attic ventilation is more sensitive to the shelter provided by neighbouring buildings (town) than to changes in wind direction in both kinds of roofs. The reduction in attic ventilation by changing the exposure from country to town for attics with slots was 60 %. For changes in wind direction from normal to 45° to the eaves it was 7% in open country and about 15% in a town.

The use of ridge ventilators for increasing attic ventilation in asbestos cement roofs gets more important as the house becames sheltered from the wind and the wind speed is reduced.

The clay tiled roof produced a more diffuse air flow through the attic than the asbestos cement and is, therefore, potentially more efficient at moisture and heat removal.

High ventilation flow rates are possible with the provision of large openings in any kind of roof. Design should carefully consider the local micro climate, summer and winter ventilation needs. The average summer day wind speed in Porto Alegre is 2 m/s (table 1.1). Considering that the house studied here (6m x 7m in

plan) is built in a new development (town) near Porto Alegre, the mean attic ventilation with frontal wind for an asbestos cement roof would be 3 ach with eaves + ridge openings, 4 ach with the 20mm eave slots and 9 ach with the 50mm eave slots. For a clay tiled roof, the mean ventilation would be 2 ach without openings, 4 ach with the 29mm eave slots and 7 ach with the 59mm eave slots. The reduction to ceiling heat flux caused by such ventilation flow rates was studied theoretically and is reported in chapter 7.

CHAPTER 4 STEADY STATE HEAT TRANSFER MODELS

4.1 INTRODUCTION

The steady state models described in this chapter were developed to mathematically simulate the heat transfer process in the test roof (chapter 5) so that modelled and measured ceiling heat flux could be compared. Modelling the heat transfer through a roof and ceiling to the room in a double pitched roof can be made with several degrees of complexity. The aim was to establish by steady state methods, the important heat flow paths and the best way of modelling them mathematically. With the knowledge gained, an unsteady state model was developed to simulate real roofs (chapter 7).

The steady state models developed had four main differences:

- number of surfaces,
- treatment of the ventilation air,
- natural convection coefficients at roof surface,
- ventilation air speed.

The models follow the theory described in section 2.4. Throughout their development a compromise was sought between accuracy and simplicity.

4.1.1 Number of surfaces

The number of surfaces considered in each model influences the accuracy with which radiation heat transfer is modelled and determines the number of heat flow paths analyzed. In reality, seven surfaces can be found in a double pitched roof: the two roof surfaces, two gables, two eave walls and the ceiling. To consider all these, a seven surface model is required. The radiation heat transfer analysis is carried out by solving the heat balance at each surface, by considering its radiosity and emissive power as described in section 2.3.1. Simplifications can be made that reduce the number of surfaces involved. Assuming the heat transfer through the eave walls to be small a model with five surfaces is derived. The radiation heat transfer analysis is done in the same way as for the seven surfaces model. Furthermore, assuming the two roof surfaces to be at the same

temperature and the heat transfer through the gables to be small, a model with only two surfaces can be developed.

Considering two surface models, comprising of roof and ceiling, the radiation heat transfer can be represented using a radiation heat transfer coefficient given by

$$h_r = \sigma \frac{(T_r^2 + T_{co}^2)(T_r + T_{co})}{\frac{1}{\epsilon_r} + \frac{1}{\epsilon_{co}} - 1} \quad W/m^2K \qquad (4.1)$$

where

co - refers to the ceiling upper surface
r - refers to the roof under surface

4.1.2 Treatment of the ventilation air

Three ways of simulating the heat removed by ventilation have been considered. In the first, the ventilation air is assumed to mix well with the attic air and the temperature of the air leaving the attic is the mean temperature of the air in the attic. As described in section 2.3.4, the ventilation conductance is

$$C_v = \rho\ c\ V \quad W/K \qquad (4.2)$$

In the second way, the air was assumed to increase in temperature as it travels through the attic and the attic air temperature was assumed to be the mean between input and output air temperatures. The ventilation conductance then is

$$C_v = 2\ \rho\ c\ V \quad W/K \qquad (4.3)$$

The third way of modelling the heat removed by ventilation was that suggested by Peavy (1979), expanded to include the gables. He assumed the attic air temperature to increase as it travels through the attic, and the following heat balance equation applies to the attic air temperature, T ,as a function of a dimension y for the air flow path.

$$V \rho c l \frac{dT_y}{dy} = \sum_{i=1}^{i=ns} S_i h_{ci} (T_i - T_y) \qquad (4.4)$$

where

l - air flow path length, m
S_i - area of surface i, m^2
h_{ci} - convection heat transfer coefficient of surface i, W/m^2K
T_i - temperature of surface i, K
T_y - attic air temperature at position y, K
ns - number of surfaces

The differential equation is solved and the average attic air temperature (T_a) found by integrating with respect to y over the air flow path from y=0 to y=l, l being the distance from air entry point to its exit. The integration gives

$$T_a = C_1 B_2 + C_2 T_{in} \qquad (4.5)$$

where

$$C_1 = \frac{1}{B_1} - \frac{C_2}{B_1} \qquad B_1 = \frac{\sum_{i=1}^{i=ns} S_i h_{ci}}{V \rho c l}$$

$$C_2 = \left(\frac{1 - e^{-B_1 l}}{B_1 l} \right) \qquad B_2 = \frac{\sum_{i=1}^{i=ns} S_i h_{ci} T_i}{V \rho c l}$$

T_{in} - temperature of air entering the attic, K

4.1.3 Natural convection coefficients at roof surface

Two kinds of natural convection heat transfer coefficients have been used for the under-side of the roof surface: fixed coefficients from the CIBSE Guide (1986) and coefficients varying with temperature difference and surface dimensions from Alamdari and Hammond (1983) (see 2.3.2). These relationships are for horizontal and for vertical surfaces. For a sloping surface, two assumptions were made. The first assumption was from Peavy (1979) who suggested an interpolation between the horizontal and the vertical coefficient

according to the slope angle. This is appropriate for free standing plates and so applicable to a roof with ridge ventilation. In a roof ventilated only by the eaves, this is not expected to apply. Later, observations (Chapter 5) showed a very high degree of stratification in the attic air, therefore a second assumption was incorporated. This was that horizontal heat transfer coefficients would represent the convection under the sloping roof surfaces.

4.1.4 Ventilation air speed

The first assumption about the ventilation air speed was that it could be represented by the ventilation flow rate divided by the cross sectional area. This gave very low values for the average air speed (0.04 m/s for 0.04 m^3/s). With approximate measurements made at the test roof (see section 5.4), this was seen to be unrepresentative. To bring the value of the air speed to the order of magnitude found in the test roof (chapter 5), an empirical relationship was adopted

$$v = 10\ V_t \quad m/s \tag{4.6}$$

where

V_t - total attic volume air flow rate, m^3/s

4.2 THE MODELS

Several models have been developed combining the variations described. The nomenclature used for these is that the first number represents the number of surfaces considered (eg model 5.1 considers five surfaces) and the second number represents the different assumptions for heat removal by ventilation, natural convection coefficient at the roof surface and ventilation air speeds. For each model a computer program has been developed.

4.2.1 Models considering two surfaces

The simplest mathematical models assume that the roof and the ceiling are represented by infinite parallel planes and that the gables and eaves have an insignificant heat flux.

The general representation of the two surfaces model is given in figure 4.1 using an electrical analogy.

The heat balance gives

$$(h_{cr} + h_{cc} + C_v)\ T_a - h_{cc}\ T_{co} = C_v\ T_o + h_{cr}\ T_r \qquad (4.7)$$

where

h_{cr} - convection heat transfer coefficient at the roof surface, $W/m^2\ K$
h_{cc} - convection heat transfer coefficient at the ceiling surface, $W/m^2\ K$
T_a - attic air temperature, K
T_o - outside air temperature, K

and

$$-h_{cc}\ T_a + (h_r + h_{cc} + \lambda/l)\ T_{co} = h_r\ T_r + T_{ci}\ \lambda/l \qquad (4.8)$$

where

λ - ceiling thermal conductivity, W/m K
l - ceiling thickness, m

The different assumptions in models 2.1, 2.2 and 2.3 are listed in table 4.1.

Table 4.1 Different assumptions considered for the two surface models.

Assumptions			Model		
			2.1	2.2	2.3
Attic ventilation	Air well mixed		x	x	
	Air not well mixed	Eq 4.3			x
		Eq 4.5			
Natural convection coefficient under the sloping roof	Fixed values CIBSE		x		
	Alamdary and Hammond	Horizontal		x	x
		Peavy's interpolation			
Ventilation air speed	Air flow rate / area		x	x	x
	Eq 4.6				

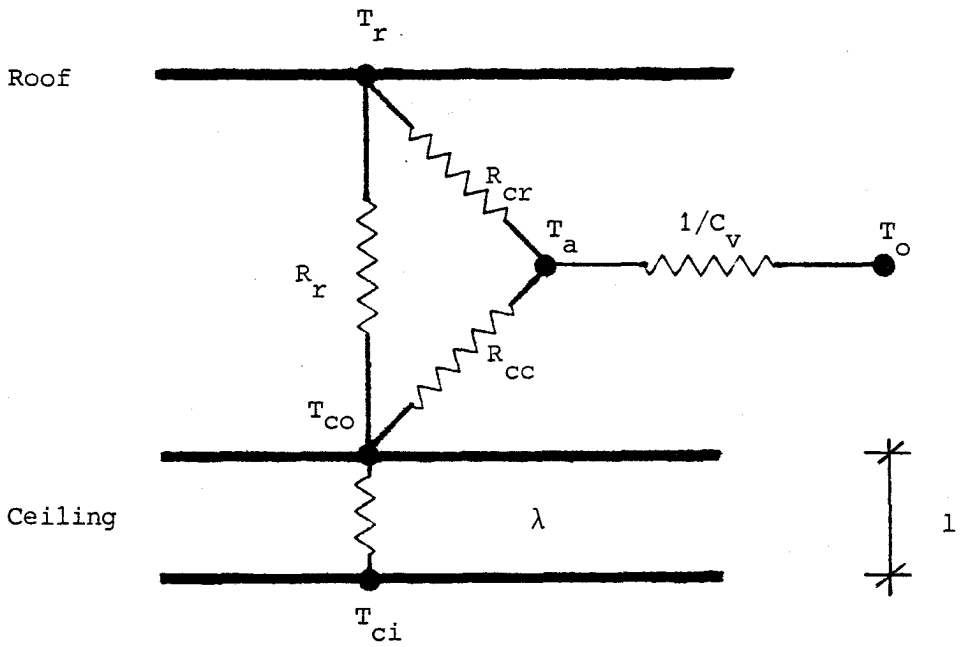

$R = 1/h$

Figure 4.1 Electrical analogy of the two surface models.

4.2.2 Models considering five surfaces

The five surfaces are the two sloping roofs, two gables and the ceiling. The general representation of the five surfaces models is given in figure 4.2.

The heat balance gives 11 non-linear equations

$$- \left(\sum_{i=1}^{i=5} h_{ci} S_i + C_v \right) T_a + \sum_{i=1}^{i=5} h_{ci} S_i T_i = -C_v T_o \qquad (4.9)$$

and

$$h_{ci} T_a - (h_{ci} + \lambda_i/l_i) T_i - (\sigma\epsilon_i/(1-\epsilon_i)) T_i^4 + (\epsilon_i/(1-\epsilon_i)) J_i = -(\lambda_i/l_i) T_{si}$$

for i=1 to i=5 (4.10)

and

$$- (\epsilon_i \sigma / (1-\epsilon_i)) T_i^4 + (1/(1-\epsilon_i)) J_i - \sum_{j=1}^{j=5} F_{ij} J_j = 0$$

for i=1 to i=5 (4.11)

This system of non-linear equations is solved by a computer subroutine (C05NBF) that uses a modification of the Powell hybrid method (NAG 1984).

The different assumptions in models 5.1 to 5.8 are listed in table 4.2.

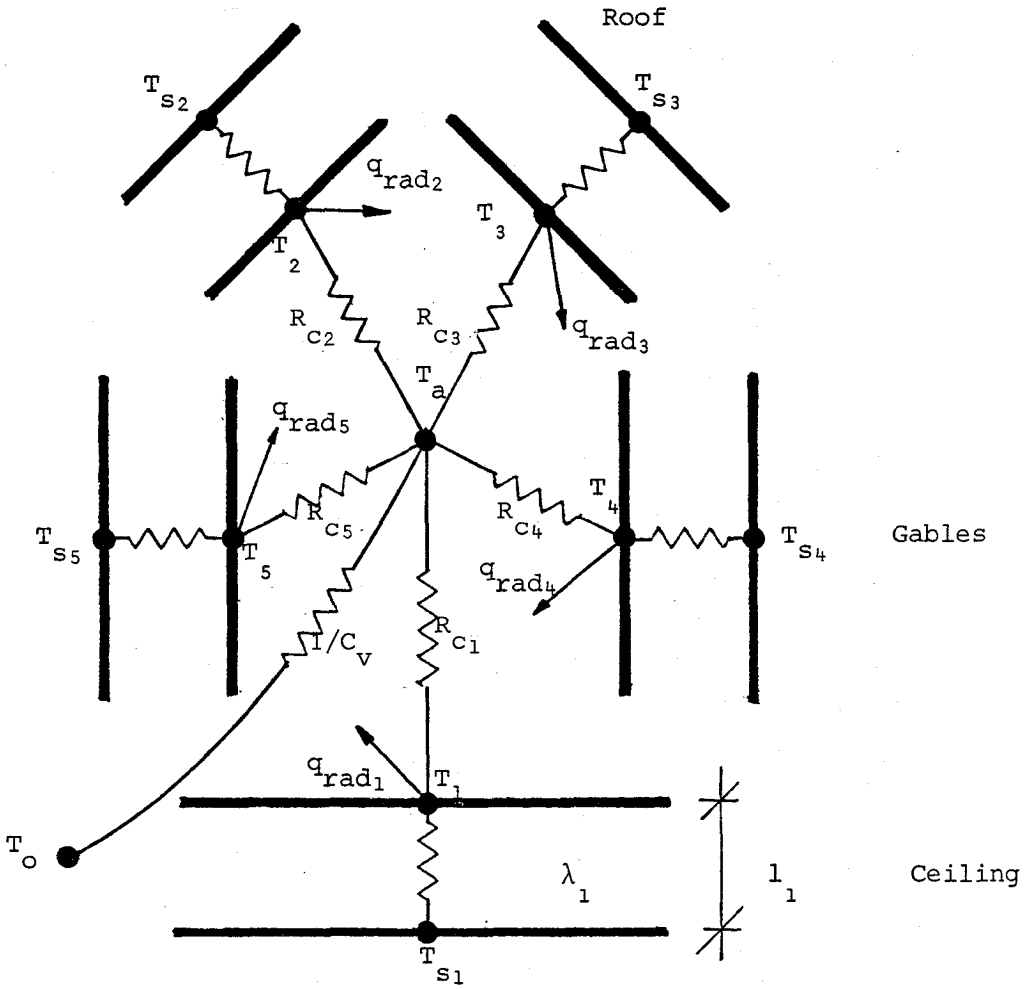

$R_{ci} = 1/h_{ci}$

q_{radi} - heat flux leaving the surface by radiation

Figure 4.2 Electrical analogy of the five surface models.

Table 4.2 Different assumptions considered for the five surface models.

Assumptions			Model			
			5.1	5.2	5.3	5.4
Attic ventilation	Air well mixed		x	x	x	
	Air not well mixed	Eq 4.3				x
		Eq 4.5				
Natural convection coefficient under the sloping roof	Fixed values CIBSE					
	Alamdary and Hammond	Horizontal		x	x	
		Peavy's interpolation	x			x
Ventilation air speed	Air flow rate / area		x	x		x
	Eq 4.6				x	

Table 4.2 (cont.) Different assumptions considered for the five surface models.

Assumptions			Model			
			5.5	5.6	5.7	5.8
Attic ventilation	Air well mixed					
	Air not well mixed	Eq 4.3	x	x		
		Eq 4.5			x	x
Natural convection coefficient under the sloping roof	Fixed values CIBSE					
	Alamdary and Hammond	Horizontal	x	x	x	x
		Peavy's interpolation				
Ventilation air speed	Air flow rate / area		x		x	
	Eq 4.6			x		x

4.2.3 Models considering seven surfaces

The seven surfaces are two sloping roofs, two gables, two eaves and the ceiling. The general representation of the seven surfaces models is given in figure 4.3.

The heat balance gives 13 non-linear equations

$$- \left(\sum_{i=1}^{i=7} h_{ci} S_i + C_v \right) T_a + \sum_{i=1}^{i=7} h_{ci} S_i T_i = - C_v T_o \qquad (4.12)$$

and

$$h_{ci} T_a - (h_{ci} + \lambda_i/l_i) T_i - (\sigma\epsilon_i/(1-\epsilon_i))T_i^4 + (\epsilon_i/(1-\epsilon_i)) J_i = -(\lambda_i/l_i) T_{si}$$

for i=1 to i=7 (4.13)

and

$$- (\epsilon_i \sigma / (1-\epsilon_i)) T_i^4 + (1/(1-\epsilon_i)) J_i - \sum_{j=1}^{j=7} F_{ij} J_j = 0$$

for i=1 to i=7 (4.14)

The computer program uses the same NAG subroutine to solve the non-linear equations as used for models considering five surfaces.

The different assumptions in models 7.1 and 7.2 are listed in table 4.3.

The 13 models described in this chapter were used to obtain empirical data. The data were then compared with measurements obtained experimentally from the test roof. The experimental procedure is described in the following chapter.

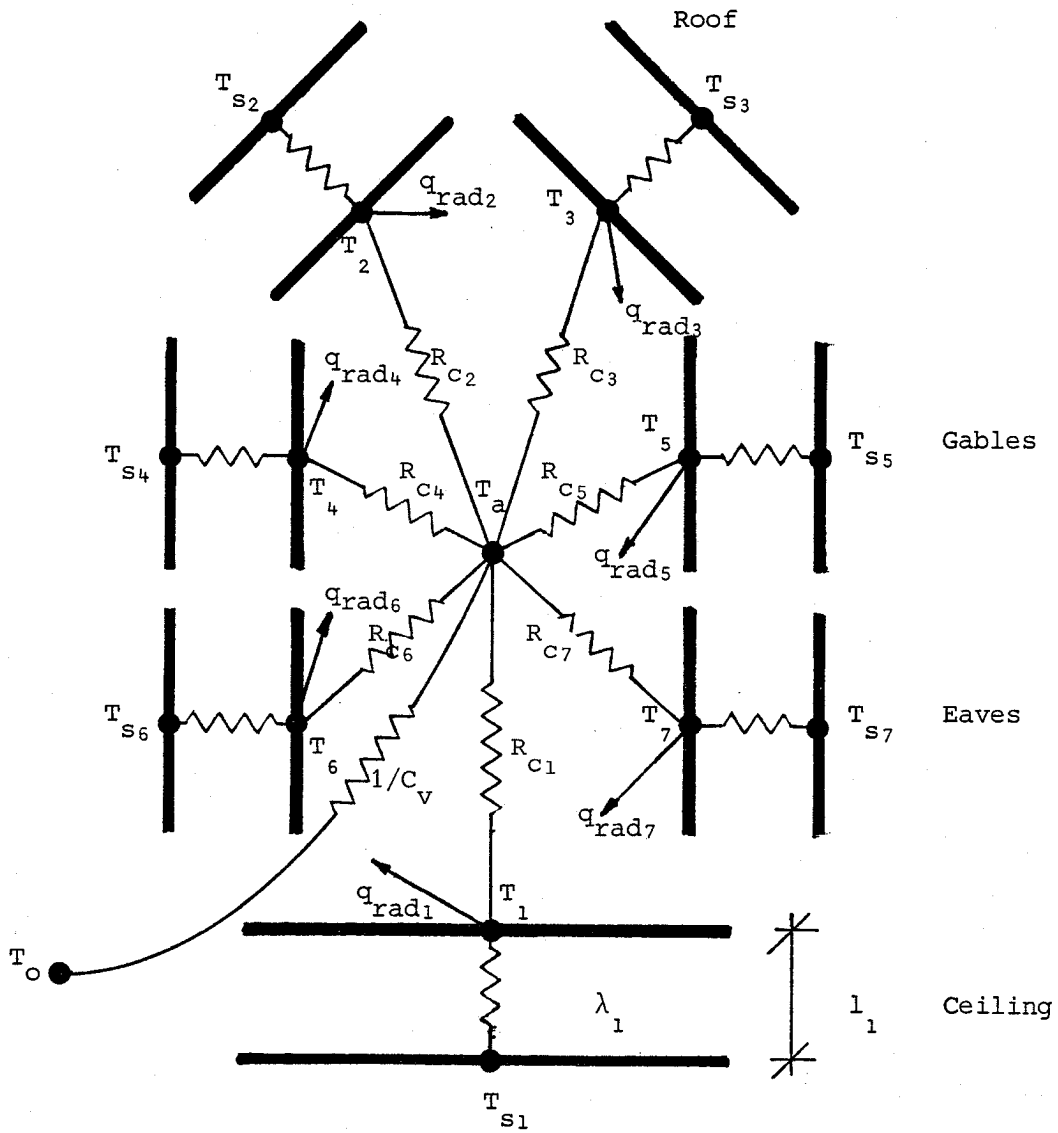

$R_{ci} = 1/h_{ci}$

q_{radi} - heat flux leaving the surface by radiation.

Figure 4.3 Eletrical analogy of the seven surface models.

Table 4.3 Different assumptions considered for the seven surface models.

Assumptions			Model	
			7.1	7.2
Attic ventilation	Air well mixed		x	x
	Air not well mixed	Eq 4.3		
		Eq 4.5		
Natural convection coefficient under the sloping roof	Fixed values CIBSE			
	Alamdary and Hammond	Horizontal	x	x
		Peavy's interpolation		
Ventilation air speed	Air flow rate / area		x	
	Eq 4.6			x

CHAPTER 5 MEASUREMENTS ON THE TEST ROOF

5.1 INTRODUCTION

The roof was designed to test the validity of the models and to gain experience into summer heat transfer mechanisms in ventilated attics.

The use of a scale model was considered but rejected since some physical observations are affected by changes in scale as shown by Pitts and Ward (1983). A full scale roof was chosen. In the early stages of design, a roof slice having a span of 5.5 m (same as house described in chapter 1) was considered. Unfortunately, shortage of space in the department restrained the plan dimensions. A room measuring 4.8 m by 3.6 m was allocated. This led to the design of a roof 2 m by 4 m in plan with a double pitch of 30° over a chamber 0.6 m high.

The design followed the basic guide lines of a guarded hot box as described in Rucker and Mumaw (1981). The outside environment would be represented by a roof surface temperature generated by electric heaters in a heating chamber over the roof. The problem of guarding these heaters from back and edge losses was analyzed and a difficulty emerged. As the attic air would be subjected to high thermal stratification depending on the ventilation, the heating chamber would also be stratified. This stratification would be variable from test to test and consequently guard heaters would be very difficult to control. The same problem was found when the design of the guard heaters for the gables was considered.

It was then decided to measure the heat transfer through the roof by installing heat flux meters in the ceiling.

The gables and the heating chamber were well insulated to minimize losses through them.

The experiment was designed to allow changes to attic surface emissivities, roof surface temperatures, area of ventilation entrance, ventilation flow rate and visualization of the air flow.

5.2 PHYSICAL DESCRIPTION

The observations were carried out on a test roof located in a room in the basement of the Civil Engineering Building at the University of Leeds. The roof (figure 5.1) was a slice (1.7m) of a double pitch full scale roof having a span of 4 m between the side walls. It was built over a chamber 0.6 m high where the downward heat flow was collected and removed. The roof cover was corrugated galvanized iron over two rafters in each side of the roof. It was painted black on the upper surface to absorb radiant heat from the electric rod heaters. The gables were a double wall of 'Purldek' (10 mm exterior grade plywood, 50 mm rigid polyurethane foam insulation and aluminium foil laminate, total resistance 2.32 m^2 K/W) with a 50 mm air gap between them. One aluminium foil faced the air gap and the other faced the attic. This composite wall had a thermal resistance of 5.0 m^2 K/W (from surface to surface). The attic was separated from the bottom chamber by a plywood ceiling 18 mm thick. A door was made in one gable to gain access to the attic for instrumentation and inspections. The door used during the tests was made of the same material as the gables, this was removed and replaced by 'perspex' during flow visualization tests. The walls of the bottom chamber were made of a single layer of 'Purldek' as heat losses in this part were not important. There was also an access door into this chamber.

The attic was ventilated by air brought in from a basement corridor where the temperature was stable. It came in through a pipe, incorporating an air flow meter, to an expansion box and then into the attic through the eaves. The output was through a second expansion box to a duct and back to the corridor. This configuration created minimal pressure on the output side and so simulated an attic air flow similar to that expected in reality. Ventilation through the bottom chamber was transverse to the attic ventilation direction and distributed by a duct with a lateral slot. In this way the air travelled a short distance in the chamber giving an uniform air temperature. Both ventilation systems, attic and bottom chamber, were tested and gave an uniform discharge along the slots.

Each side of the roof had, 15 rod heaters (Metrel MSR7, 1750 W) evenly distributed. These were connected in blocks of three in series and these blocks were than connected in parallel. This

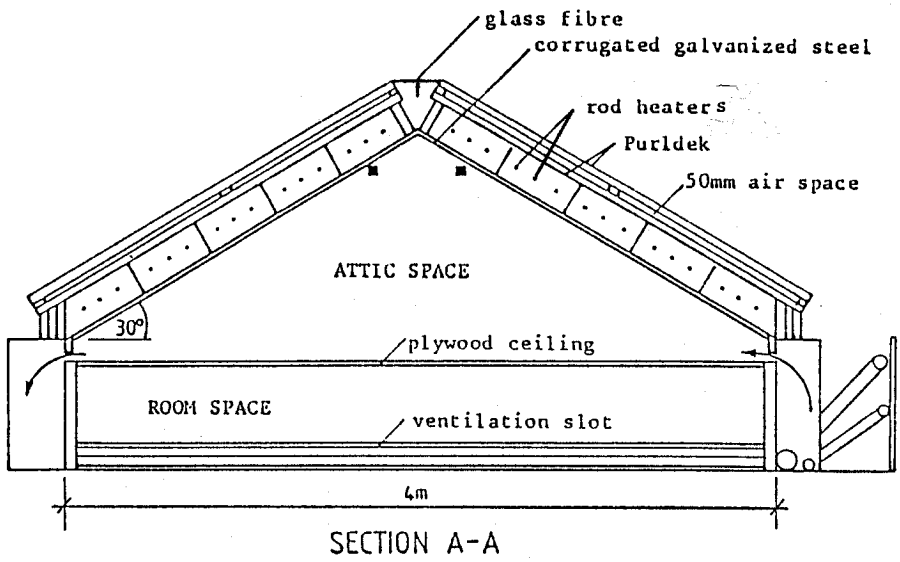

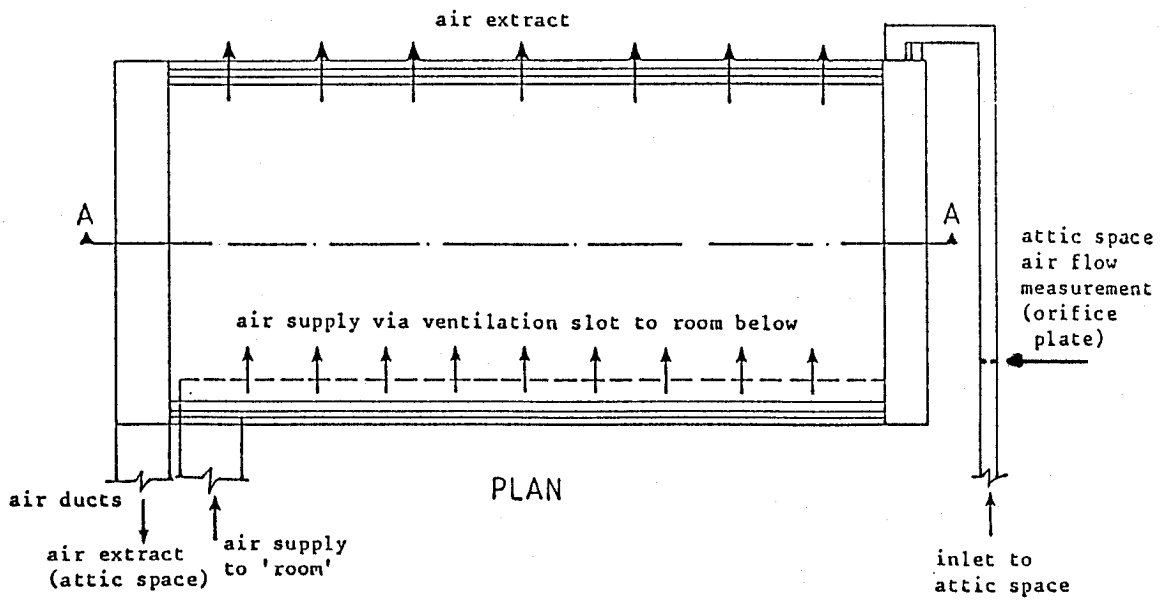

Figure 5.1 Diagram of the test roof.

arrangement gave a power output of 3 kW that was well distributed over the surface. The heaters were placed mid-height in a chamber (200 mm high) formed by an extension of the gable walls over the roof cover and a lid of double 'Purldek' (same as gable walls).

All gaps and cracks were filled with mastic.

5.3 INSTRUMENTATION AND CONTROL

Temperature, heat flux, air volume flow rate and air speed were measured. Facilities to enable visualization of the attic air flow, temperature control of the heaters and speed control of the fans were incorporated.

5.3.1 Temperatures

Temperatures were measured by copper-constantan thermocouples connected to a 'Comark 5000' digital thermometer via a 50 channels switch. The switch was wired in copper-constantan wire and insulated with 50 mm polystyrene foam to avoid temperature difference between the inputs. All thermocouples were made from the same reel of wire.

Calibration of the thermocouples was performed in a large bath of well stirred water. The water temperature was varied from ambient to 100 °C and measured by a 0.1 K resolution mercury in glass precision thermometer and readings were taken at 20, 30, 40, 50, 60 and 100 °C. The maximum difference found among the thermocouples was 0.2 K. The accuracy of any temperature measurement made with the thermocouples is estimated to be ± 0.2 K.

Air temperature sensors were protected from radiation by a 30 mm diameter 150 mm long cylinder of 0.3 mm polished aluminium sheet.

Surface temperature sensors were glued to a 50 mm square plate of 0.3 mm aluminium sheet (except for the ones on the roof cover, that were glued directly to the sheet). Their emissivity was matched to that of the surface upon which they were used. The wires were kept in contact with the surface for at least 100 mm to avoid false readings due to conduction along the wires.

The location of the temperature sensors can be seen in figure 5.2.

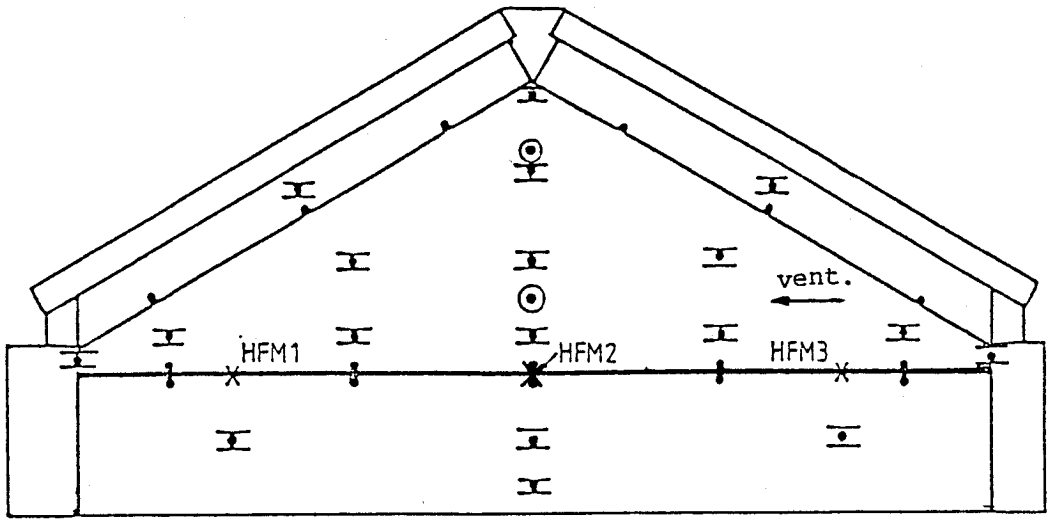

- Surface temperature thermocouple
- Air temperature thermocouple (screened from radiation)
- Surface temperature thermocouple on gable walls
- Heat flux meter (HFM)

Figure 5.2 Location of thermocouples and heat flux meters.

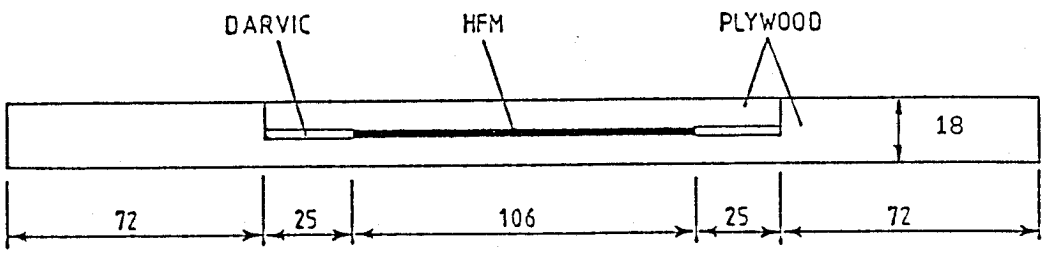

Figure 5.3 Section showing a heat flux meter (HFM) embedded in plywood (all values in milimetres).

5.3.2 Heat Flux

The ventilation heat flux (Q_v) is given by

$$Q_v = \rho \; c \; V \; \Delta t \qquad (5.1)$$

where

Δt - temperature difference between input and output air, K

The gable heat flux (Q_g) is given by

$$Q_g = S \; \Delta t / R_g \qquad (5.2)$$

where

S - gable area, m^2
Rg - gable thermal resistance, m^2K/W
Δt - temperature difference across it, K

The uncertainty in both calculations is estimated to be $\pm$ 7%.

The ceiling heat flux was measured by three WS31 heat flux meters (106 mm diameter) from 'TPD-TNO' (Delft, Netherlands), connected to a 'Thurlby 1905' intelligent multimeter.

Measurements of heat flux using heat flux meters are very difficult to make to any degree of accuracy. If care is not taken, large errors can arise. As discussed by Flanders (1985) and Ferraro et al. (1983), the sensor is a disturbance in the environment where it should measure heat flux. The main factors that can lead to errors in this measurement are the following;

a) sensor disturbing the convective heat transfer from the surface,
b) sensor having a different emissivity to that of the surface,
c) poor thermal contact between sensor and ceiling material,
d) sensor and ceiling material having different thermal conductivity.

To avoid factors a) and b) the sensors were embedded in the ceiling (figure 5.3). Good thermal contact (factor c) was assured by applying heat sink compound between the meter and the plywood. Factor d) remained a source of error and calibration was necessary. For this reason, the ceiling heat flux sensors were not embedded directly in the ceiling, but in the middle of 300 by 300 mm pieces of the same

plywood as used for the ceiling (figure 5.3). It was then possible to calibrate the sensors in a hot plate apparatus embedded in their actual surrounding material (see Appendix 1). For the heat flux measurements, the calibrated meters in their plywood surrounding were fitted in correctly sized holes in the ceiling. The position of the sensors during tests can be seen in figure 5.2. The calibration of the heat flux meters generated new constants that were multiplied by the output emf to give the actual ceiling heat flux (W/m^2). Overall measurement error (Δq), including random and systematic errors is estimated to be ± 5%.

5.3.3 Air Flow

The air was blown through the attic by a fan having a speed controller. The air volume flow rate was measured before it entered the attic by orifice plates designed to British Standard 1042 (1982). Two independent pipes (diameters 107 mm and 53 mm) were used to allow a wide range of air flows to be measured. A gate valve was used to close the pipe not in use. On the 107 mm pipe, an orifice plate with orifice diameter of 75 mm was used. This gave a range of air flow measurement from 0.013 m^3/s to 0.04 m^3/s . On the 53 mm pipe, orifice plates with orifice diameters of 23 mm and 41 mm were used, giving a measuring air flow range from 0.003 m^3/s to 0.013 m^3/s.

The pressure difference across the orifice plate was measured by a 'Furness' micromanometer (MDC-FC001) capable of reading a maximum of 100 Pa, using 5 scales calibrated to show at full scale 100%, 30%, 10%, 3%, 1% of the maximum.

The uncertainty of the orifice plates was ± 2% because it was impossible to provide the upstream length required in the British Standard for 'zero additional uncertainty'. Some uncertainty can also be attributed to the micromanometer, making a total error of about ± 5% more realistic.

The air flow rates can be converted to attic air changes per hour by multiplying them by 784 (3600 divided by attic volume).

5.3.4 Air Speed

The determination of the air speed in the attic was very difficult because of the jet behaviour of the air as it enters the thermally stratified attic.

The instrumentation available to measure air speed was a thermistor anemometer 'Testovent 4100'. When this instrument is exposed to high thermal radiation, its accuracy is poor due to radiation being absorbed by the sensor. As screening from radiation would disturb the flow, measurements have only been made during flow visualization tests in order to find the order of magnitude of the air speed at the bottom of the attic. Velocity measurements were made in the middle of the attic and 50 mm above the ceiling. They were confirmed approximately by timing some smoke movement during the flow visualization tests.

5.3.5 Flow Visualization

Smoke pellets (Smoke Products Ltd) were used in the input air stream for flow visualization. The attic door was replaced by 'perspex' to allow the smoke to be seen when passing through the attic.

Attempts were made to photograph the smoke traces, but results were not satisfactory because of the small size of the door and the reflexions caused by the gable covered with aluminium foil. Drawings of the observations were made.

5.3.6 Temperature Control

Two time proportioning temperature controllers (Anglicon DH series), were used to control the temperature generated on each side of the roof by the heaters placed over the roof cover. The sensing elements of the controllers were placed at mid-height in the middle of the heating chamber.

5.3.7 Fan Speed Control

The fan (Fischbach) providing the attic ventilation was connected to a speed controller to allow fine changes to be made to the attic ventilation flow rate.

5.4 THE TESTS

The ceiling heat flux and ventilation heat removal were analysed using different roof temperatures, surface emissivities, attic ventilation flow rates and ventilation entrances. The roof temperatures used were 70, 60, 50, 40 and 30 °C, with 70 °C and 50 °C

being used most frequently. A temperature of 70 °C was considered to be the maximum that a black roof will reach under intense sunshine. The emissivity of the materials used in the underside of the roof cover were 0.13 for new corrugated galvanized sheet and 0.9 for a black paint. The emissivity of the ceiling to the attic was taken as 0.9 for normal plywood and 0.05 for aluminium foil laid over it. Attic ventilation flow rates up to 0.04 m^3/s were used. Ventilation entrances were either the normal aperture due to corrugation of the sheets or this plus a 50 mm slot in the eaves.

A total of 40 tests were performed under steady state conditions. To assure steady state conditions had been achieved, each test was run for 24 hours before the readings were taken. Three one hourly readings were taken and averaged. The maximum ceiling heat flux variation accepted between the hourly readings was ± 3%.

The tests were divided into seven groups (A-G), Group A consisted of tests without ventilation, roof emissivity of 0.13, ceiling emissivity of 0.9 and roof temperatures of 30, 40, 50, 60 or 70 °C. Groups B to G had ventilation flow rates from 0 to 0.04 m^3/s; the other variables are given in table 5.1.

Table 5.1 Differences between the groups of tests.

Group	Emissivities		Roof Temperature (°C)	Ventilation Opening
	Roof	Ceiling		
B	0.13	0.90	70	small
C	0.13	0.05	70	small
D	0.90	0.90	70	small
E	0.90	0.90	70	large
F	0.90	0.90	50	small
G	0.13	0.90	50	small

small= corrugation only
large= corrugation plus 50mm slot

In each test, the roof temperature was maintained constant but the air temperature in the bottom chamber was not controlled. The temperature of the ventilation air used in the bottom chamber was fairly constant (basement temperature), the maximum variation during each group of experiments being about 2 K.

Tests for flow visualization and air speed measurements were also performed.

5.5 RESULTS

5.5.1 Gable Heat Flux

The significance of the gable heat loss in each test was assessed by dividing it by the corresponding ceiling heat flux. The results fell into three categories. The first category was formed by tests from group C. They had ceiling and roof with low emissivities. The gable heat flux varied from 22 to 54% of the ceiling heat flux. The second category consists of tests from groups A, B and G (low emissivity roof, high emissivity ceiling) with gable heat flux varying from 9 to 13% of the ceiling heat flux. The third category is composed of groups D, E and F (roof and ceiling with high emissivity) where the gable heat flux was only 6 to 10% of the ceiling heat flux.

5.5.2 Ceiling Heat Flux

The ceiling heat flux was measured at three positions along the attic ventilation flow path:

a) near the inlet,

b) in the middle,

c) near the outlet.

Analyses of the data showed that in all the test groups except C, the trend was that the ceiling heat flux in the middle was greater than near the inlet or outlet.

In tests without ventilation, the ceiling heat flux at the inlet side was similar to that of the outlet side, but less than that in the middle : 10% less when the roof emissivity was low and 5% less when this emissivity was high.

In tests with ventilation, the ceiling heat flux at the inlet side was different to that at the outlet side. As the ventilation increased, the ceiling heat flux at the inlet side reduced below that measured at the outlet side and kept decreasing until a minimum was reached (0.025 m^3/s) in tests of groups B, D, F. After this, in tests of group B it remained constant, and in tests of groups D and F it started to increase. This indicates that increasing ventilation may be disadvantageous. In tests of group E, the inlet side ceiling heat flux kept decreasing throughout the ventilation range studied. The difference in behaviour between tests in group E (large ventilation opening) and group D (small ventilation opening)

indicates that large ventilation openings are more effective in reducing the ceiling heat flux.

Tests in group C were a special case. The roof and ceiling had low emissivities. All tests using ventilation showed the ceiling heat flux at the inlet side to be greater than that at the outlet side. Tests with the same ventilation flow rate showed considerable differences in the ceiling heat flux at the input side. This indicates that the ceiling heat flux is very sensitive to the temperature of the ventilation air. The ceiling heat flux at the outlet side and in the centre were similar in all the tests in group C.

An average ceiling heat flux was calculated from the three measured values in each test. Ceiling heat fluxes obtained from tests in group A are plotted against the temperature difference between roof and underside of the ceiling in figure 5.4. A quadratic regression analysis of the data yielded a regression coefficient of 0.9997 ($P<0.0001$). The regression line is plotted through the data in figure 5.4 with 95% confidence limits shown by dotted lines on either side of the data.

Figure 5.5 shows how the ceiling heat flux varied with ventilation flow rate for tests in groups B to G. Attic ventilation was generally beneficial in reducing the ceiling heat flux. This reduction, for an increase in the ventilation flow rate from 0 to 0.04 m^3/s, was about 40% for groups B and G and about 30% for groups D, E and F. More than 70% of the total reduction occurred in the range 0 to 0.012 m^3/s. Group C behaved differently, the ceiling heat flux increased for ventilation flow rates exceeding 0.012 m^3/s. This was probably due to the disturbance in the stratification of the attic air.

Changing roof emissivity (in the attic) from 0.9 to 0.13 (group D to B) reduced the ceiling heat flux by about 40%. This change, together with the change in ceiling emissivity from 0.90 to 0.05 (group D to C) caused a total ceiling heat flux reduction of about 80%.

5.5.3 Removal of Heat by Ventilation

In all groups, increasing the attic ventilation flow rates increased the heat removed from the attic space as one would expect.

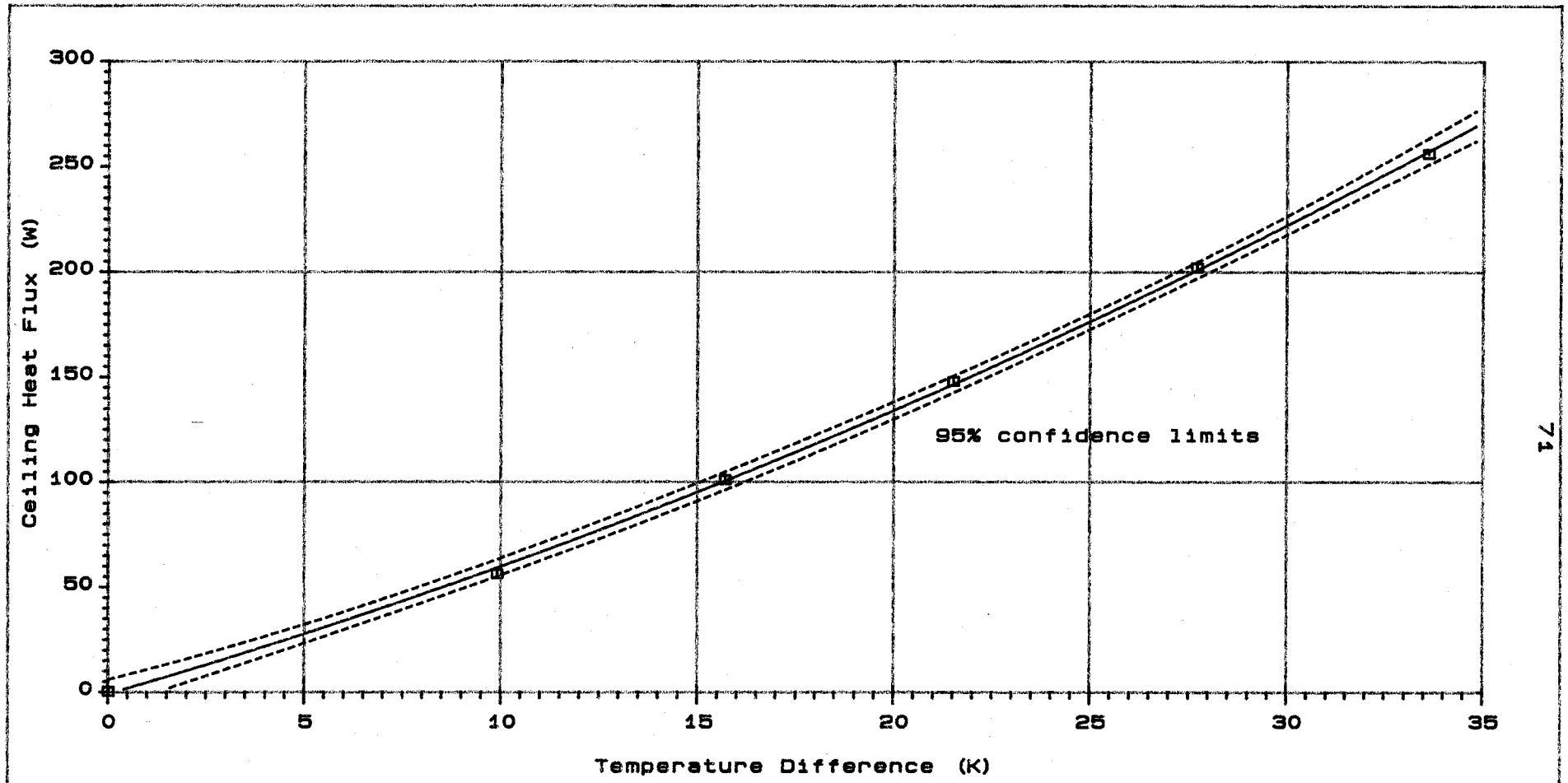

Figure 5.4 Ceiling heat flux plotted against temperature difference between roof and under-side of ceiling for tests in group A.

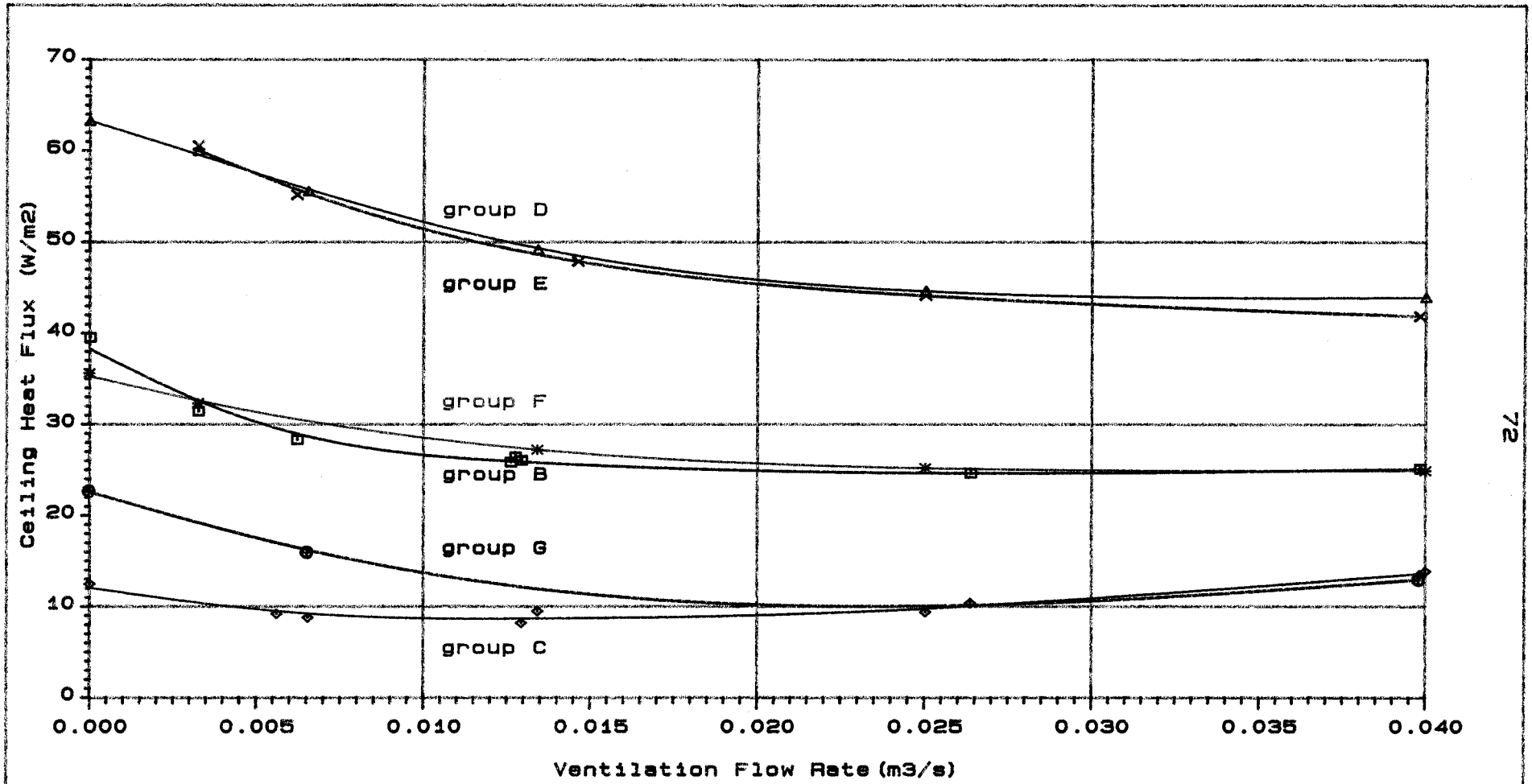

Figure 5.5 Ceiling heat flux plotted against ventilation flow rate for tests in groups B to G.

Tests in groups D and E (which differed only by the ventilation opening) had very similar ceiling heat fluxes (figure 5.5). However, the heat removed by ventilation in the two groups was similar only up to ventilation flow rates of 0.012 m^3/s. From 0.012 to 0.04 m^3/s the amount of heat removed by ventilation in group D tests started to increase faster than in tests of group E and at 0.04 m^3/s was 74% larger. In tests of group E, the air moved parallel to the ceiling while in tests of group D it moved towards the ridge. This movement towards the ridge disturbed the stratification of the attic air and therefore more heat was removed by ventilation.

5.5.4 Flow Visualization

When the air entered the attic, there was a sudden enlargement of the cross-sectional flow area. The ratio between the larger and the smaller cross section is 14:1 for the corrugation opening (group D) and 2:1 for the corrugation plus slot opening (group E). Furthermore, there is a density difference between the air in the attic and that entering. Thus the formation of different jets for the two kinds of opening is to be expected.

With the corrugation opening, due to the slope of the input, the air initially tends to flow in the direction of the ridge in contact with the tiles. Eventually density forces exceed the vertical component force of the velocity, and then the air starts flowing horizontally. The height at which this happened varied with the input velocity and is shown in figure 5.6. High degrees of turbulence were observed at high ventilation flow rates (0.024, 0.040 m^3/s). When the emissivity of the roof was changed, the behaviour of the air movement remained the same.

With the slot plus corrugation opening, as the change in area was smaller (2:1), the flow was only slightly turbulent and the flow path followed the line of the ceiling rather than that of the tiles. The depth of flow was less than in the former case, as can be seen in figure 5.7.

5.5.5 Air Speed

Attic air speeds that were calculated by dividing the ventilation flow rate by the mean cross sectional area and those measured by thermistor anemometer (R.M.S. value and fluctuations) for different attic ventilation flow rates are shown in table 5.2. The

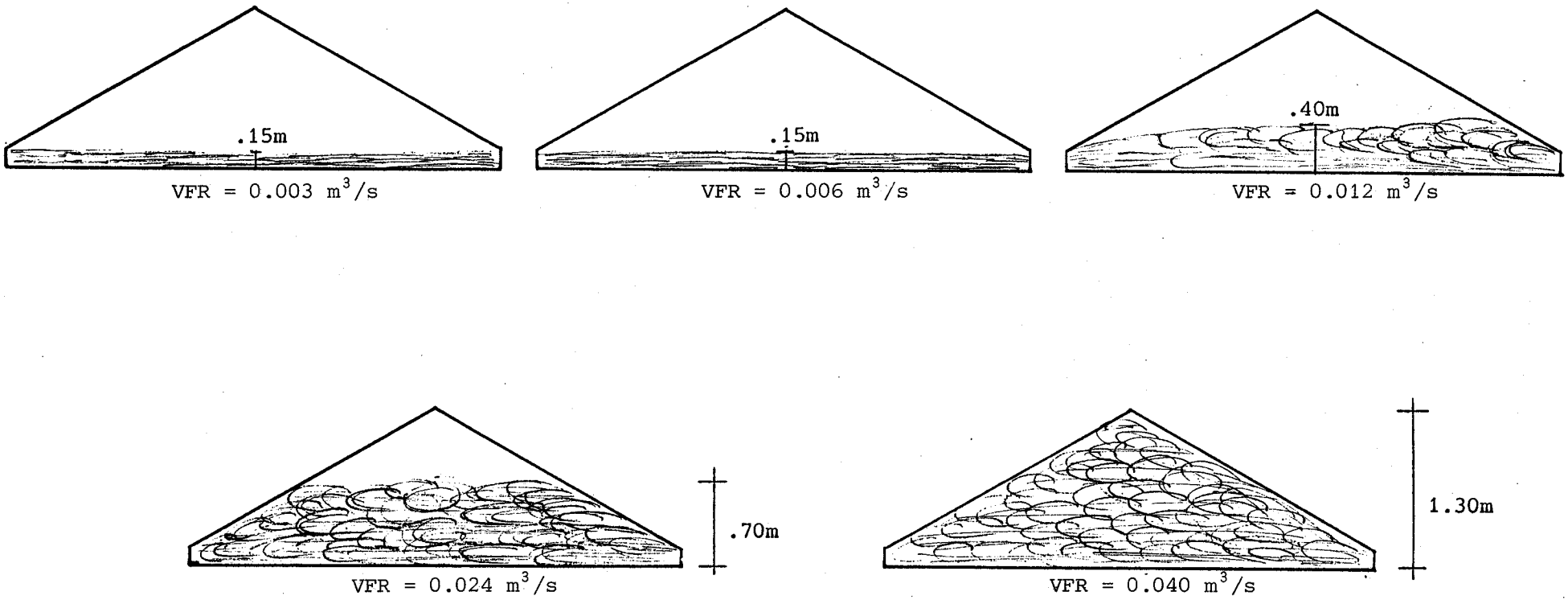

VFR - ventilation flow rate

Figure 5.6 Observed air flow patterns (small ventilation opening).

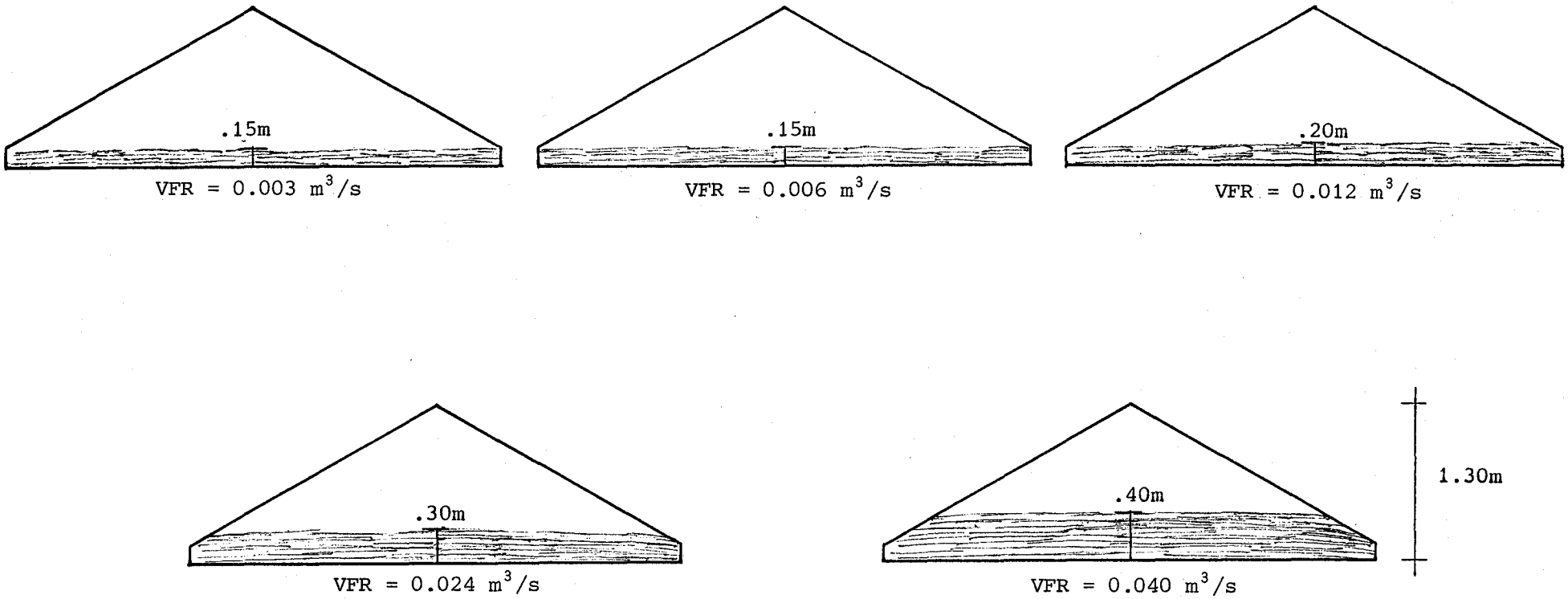

VFR - ventilation flow rate

Figure 5.7 Observed air flow pattern (large ventilation opening).

measured air speeds are one order of magnitude higher than the ventilation flow rate and very different from the ones calculated.

Table 5.2 Calculated and measured air speeds in the attic.

Ventilation Flow Rate (m^3/s)	Calculated (flow/area) (m/s)	Measured (R.M.S.) (m/s)	Fluctuation on Measurement (m/s)
0.003	0.003	0.05	0 to 0.1
0.012	0.01	0.15	0.1 to 0.2
0.025	0.02	0.3	0.2 to 0.4
0.040	0.04	0.4	0.3 to 0.5

5.5.6 Effective Attic Thermal Resistance

The effective thermal resistance (ER) of the attic in each test was calculated by dividing the temperature difference between the roof and the top of the ceiling by the ceiling heat flux. Surface temperatures used were an average of the values measured over the surface. Values obtained are presented in table 5.3.

ER's for tests in group A increased as the temperature difference across the attic decreased. E.g.: reducing the roof temperature from 70 °C to 30 °C increased the ER by 40%.

In tests of group B, ER increased with ventilation flow rate up to a maximum of 0.026 m^3/s; an increase of 57%. Further increase in ventilation caused the ER to reduce.

In tests of group C, ER's were very high and only increased with ventilation rates up to 0.006 m^3/s. Total increase in ER of 41%. Further increases in ventilation caused ER's to reduce. Values of ER at a ventilation flow rate of 0.040 m^3/s were lower than those without ventilation. Tests with the same ventilation rate, in group C, showed different ER's. This is attributed to the high thermal resistance of the attic space under these particular tests conditions (different corridor temperature for different tests, changing the temperature of the ventilation air).

ER's for tests in group D increased with ventilation rates up to 0.025 m^3/s; total increase of 61%. Increasing the ventilation rate above 0.025 m^3/s up to 0.04 m^3/s caused a slight reduction in ER.

Table 5.3 Effective attic thermal resistance calculated for each test.

Ventilation (m^3/s)	Ventilation (ach)	Roof Temp. (°C)	Effective Attic Thermal Resistance (m^2 K/W)
Group A			
0.0	0	70	0.70
0.0	0	60	0.74
0.0	0	50	0.80
0.0	0	40	0.86
0.0	0	30	0.99
Group B			
0.0	0	70	0.70
0.003	2	70	0.84
0.006	5	70	0.94
0.013	10	70	1.03
0.013	10	70	1.03
0.013	10	70	1.02
0.026	20	70	1.10
0.040	31	70	1.06
Group C			
0.0	0	70	2.99
0.006	5	70	4.09
0.006	5	70	4.22
0.013	10	70	4.17
0.013	10	70	3.56
0.025	20	70	3.56
0.025	20	70	3.35
0.040	31	70	2.55
0.040	31	70	2.32
Group D			
0.0	0	70	0.18
0.003	2	70	0.20
0.006	5	70	0.23
0.013	10	70	0.26
0.025	20	70	0.29
0.040	31	70	0.27
Group E			
0.003	2	70	0.22
0.006	5	70	0.25
0.013	10	70	0.33
0.024	20	70	0.37
0.039	31	70	0.41
Group F			
0.0	0	50	0.21
0.003	2	50	0.23
0.013	10	50	0.29
0.025	20	50	0.30
0.040	31	50	0.30
Group G			
0.0	0	50	0.80
0.007	5	50	1.06
0.040	31	50	1.19

Tests in Group E showed ER's to increase over the entire ventilation range studied; total increase of 86%. ER values were higher than those for tests in group D. The ER of a test having ventilation flow rate of 0.04 m^3/s was 52% higher in group E than in group D. This shows the value of the additional insulation obtained from the undisturbed stratification of the attic air.

Tests in group F had ER's slightly higher than those of tests in group D (11% to 17%). These showed the same trend as for tests in group A, i.e. increasing resistance with decreasing temperature difference across the attic. The same was observed when ER's for tests in groups G and B were compared.

5.6 DISCUSSION AND CONCLUSION

In all groups of tests other than C the gable heat flux was small when compared with the ceiling heat flux. The results are therefore considered to be representative of the phenomena occurring in reality.

Tests in group A have shown that for an attic having a low emissivity roof, the heat transfer through it is well described by a quadratic regression between temperature difference and ceiling heat flux. This non-linearity demonstrates the importance of providing effective attic thermal resistance values for the various temperature differences to be found in the field.

The reductions in ceiling heat flux obtained by ventilation were significant but it should be remembered that they are related to the temperature of the ventilation air. In all tests this temperature was lower than the bottom chamber temperature and therefore represented an extreme situation.

Reducing the emissivity of the roof and ceiling reduced the ceiling heat flux by about 80%. This shows the paramount importance of the radiation component in the heat transfer through attics.

Tests in group E are likely to be difficult to model mathematically because of the additional insulation offered by the thermally stratified air undisturbed by the ventilation. Although E and D had similar average ceiling heat fluxes, the temperature difference between roof and ceiling was greater for E. Thus the insulating properties of E were better, in spite of D having a higher ventilation heat removal rate.

Heat flux was greater in the middle of the ceiling than near the inlet or outlet for all groups of test except C. This contradicts what would be expected from surfaces behaving as diffuse emitters for radiation. There is possibly some departure from diffuse behaviour.

In tests of group C, the attic had such a high thermal resistance due to the double low emissivity, that even with highly insulated gables the heat losses where high. The stratification of the attic air was so remarkable, that only small ventilation flow rates helped in reducing the ceiling heat flux. The cause was that at low ventilation flow rates, the air was moving only at the bottom of the attic and did not disturb the stratification. Large ventilation flow rates had the opposite effect and increased the ceiling heat flux. Consequently, group C is anticipated to be very difficult to model mathematically. These tests illustrated that multiple low emissivity is very effective in reducing the heat transfer through attics and that ventilation has generally little effect and can even be disadvantageous.

The effective thermal resistances (ER) calculated gave a clear picture of the insulation value of the attic in each test. These ER's will be compared with the values available from the literature and with those calculated using the unsteady state model in chapter 7.

The tests provided a good insight into the mechanisms of heat transfer through ventilated attics and a sound base for analysing the accuracy of the mathematical models developed in chapter 4. The experimental data reported in this chapter is compared with the empirical data in the next chapter.

CHAPTER 6 COMPARISON BETWEEN EXPERIMENTAL AND MATHEMATICALLY MODELLED DATA

6.1 INTRODUCTION

The steady state heat transfer models described in chapter 4 were used to predict the heat transfer through various roof configurations. These configurations were tested on the experimental roof (chapter 5). Results from each technique were then compared.

Parameters input into the models were the length, width and height of the attic, the thermal properties of its components (see table 6.1) and the outside surface temperatures of the bounding components. The outside surface temperature that was considered for each component was determined from an area weighted average of the measured values over the surface.

Table 6.1 Materials, dimensions and thermal properties of the roof components.

Component	Material	Thickness (mm)	Conductivity (W/m K)	Area (m^2)	Emissivity Facing the Attic
Roof	galvanized steel	2	40	2x3.81	0.13 or 0.85
Gable	'Purldek'/ air gap/ 'Purldek'	180	0.036*	2X2.30	0.05
Eave	timber	50	0.15	2X0.17	0.90
Ceiling	plywood	18	0.13	6.51	0.05 or 0.90

* - equivalent conductivity allowing for the air gap, equal to thickness divided by the total resistance (without surface resistances).

For each test, the models predicted the attic air temperature, the heat flux through each surface bounding the attic and the heat removed by ventilation. These were then compared with those measured. The values for gable and eave heat fluxes were not

compared as their influence on the overall heat transfer process was very small.

To give a sound basis to the comparison, an uncertainty analysis of the measured and simulated values was undertaken. The uncertainty on the measured ceiling heat flux was determined to be ± 5% (chapter 5). The uncertainty of the simulated ceiling heat flux is associated with the uncertainties in the input data. It is rather complex to attempt a theoretical analysis of the uncertainties propagated in the mathematical models as the ceiling heat flux is calculated from a system of several non-linear equations. To simplify the situation, an error analysis was carried out on the most critical input variables using model 5.3. These variables are listed in table 6.2 with their associated uncertainties.

Table 6.2 Input data to which models are considered to be more sensitive.

Parameters	Uncertainty (μ)
Ventilation flow rate (V)	± 5.0%
Ceiling conductivity (λ)	± 3.0%
Ceiling thickness (l)	± 1 mm
Temperature (t) - roof and ceiling	± 0.2 K
Emissivities (ϵ) low	± 0.02
high	± 0.05

Assuming that the uncertainties in the simulated ceiling heat flux caused by each input variable are random and independent, according to Taylor (1982) they can be combined by adding them in quadrature. An analysis of the most unfavourable combination of input uncertainties was also performed. The results for each group of tests are given in table 6.3.

Table 6.3 Uncertainty in the ceiling heat flux simulated by model 5.3 for each input variable.

Group	Variable (± %)					$\sqrt{\sum \mu^2}$	Maximum Uncertainty
	V	λ	l	t	ε		
A	-	1	1	4	10	11	16
B	1	1	1	3	13	14	18
C	1	1	1	3	20	20	24
D	1	1	3	3	7	8	15
E	1	1	3	2	6	7	12
F	1	1	3	5	7	9	16
G	1	1	1	5	13	14	20

Analysis showed that the uncertainties in the simulated ceiling heat flux due to uncertainties in ventilation flow rate or conductivity are about ± 1%. Those due to uncertainty in ceiling thickness are also about ± 1% for tests of groups A, B, C and G (low ceiling heat flux) increasing to ± 3% for tests of groups D, E and F. The uncertainty in the temperature measurements caused an uncertainty of ± 2% to ± 5% in the simulated ceiling heat flux. The uncertainty in the emissivity caused the highest uncertainty in the predicted ceiling heat flux, particularly for tests with low emissivity. An uncertainty of 10 to 15% was found for tests with one low emissivity surface and 20% for tests with two low emissivity surfaces (group C). The analysis done by unfavourable combination of input data is the most extreme case possible. The addition in quadrature of the uncertainties due to each input data seems more realistic due to the rare possibility of the unfavourable combination.

In general, the uncertainty associated with predicting the ceiling heat flux under simulated conditions where the roof and ceiling had high emissivities (groups D, E and F) is about ± 10%. This may increase up to ± 15%, when one of the two surfaces has low emissivity (groups A, B and G) and further increases up to ± 20%, when the two surfaces have low emissivity (group C).

6.2 RESULTS

The percentage difference between simulated (S) and measured (M) ceiling heat flux values (100((S/M) - 1)) are presented in tables 6.4, 6.5 and 6.6, for the various models.

As predicted in chapter 5, tests in group C were very difficult to simulate because of the high thermal stratification of the attic air.

Table 6.4 shows the percentage difference between the ceiling heat flux simulated by the two surface models (model 2.1, 2.2, 2.3) and the observed for each test.

Model 2.1 predicted negative ceiling heat fluxes at ventilation rates of 0.04 m^3/s in groups B and G and at ventilations rates above 0.025 m^3/s in group C. The highest overestimation was 186% for the test without ventilation in group C. The agreement obtained over tests in group E is regarded as fortuitous.

Values predicted by model 2.2 were similar to those predicted by model 2.3. Although they did not predict negative ceiling heat fluxes, they overestimated the same by 201% for the tests without ventilation in group C and underestimated by about 45% in tests with ventilation rates of 0.04 m^3/s in the same group.

These results indicate that two surface models are too simple to realistically represent the heat transfer through the test roof.

Table 6.5 shows the percentage difference between the ceiling heat fluxes simulated by the five surface models (models 5.1 to 5.8) and those observed for each test.

Model 5.1 showed a maximum overestimation of 140% for tests with ventilation rates of 0.006 m^3/s in group C. The worst underestimation was 25%. This was in tests having ventilation rates of 0.04 m^3/s in the same group.

Model 5.2 showed a maximum overestimation of 83% for the test without ventilation in group C. The worst underestimation was 71% for tests with ventilation rates of 0.04 m^3/s in the same group.

The reduction in the maximum overestimation from model 5.1 (140%) to model 5.2 (83%) shows the importance of assuming the convection coefficient under the sloping roof to be taken as if the surface was horizontal.

Table 6.4 Comparison between simulated (S) and measured (M) ceiling heat flux. Two surface models.

Ventilation (m^3/s)	Roof Temp. (°C)	Percentage Difference = 100((S/M)-1) Model 2.1	2.2	2.3
Group A				
0.0	70	20	26	26
0.0	60	23	31	31
0.0	50	27	38	38
0.0	40	31	48	48
0.0	30	46	72	72
Group B				
0.0	70	20	26	26
0.003	70	-6	-3	-18
0.006	70	-25	-10	-13
0.013	70	-70	-8	-10
0.013	70	-68	-7	-9
0.013	70	-69	-9	-11
0.026	70	-90	-3	-4
0.040	70	*	-6	-7
Group C				
0.0	70	186	201	201
0.006	70	74	84	5
0.006	70	73	84	9
0.013	70	29	31	6
0.013	70	-17	-13	-14
0.025	70	-88	-14	-17
0.025	70	*	-21	-24
0.040	70	*	-44	-46
0.040	70	*	-46	-48
Group D				
0.0	70	18	21	21
0.003	70	2	17	16
0.006	70	-7	24	23
0.013	70	-22	32	32
0.025	70	-33	39	39
0.040	70	-44	31	31
Group E				
0.003	70	6	22	21
0.006	70	1	32	31
0.015	70	-4	54	53
0.024	70	-4	66	65
0.039	70	0	76	76
Group F				
0.0	50	19	23	23
0.003	50	1	17	16
0.013	50	-29	28	27
0.025	50	-42	32	32
0.040	50	-46	30	29
Group G				
0.0	50	27	38	38
0.007	50	-37	-11	-15
0.040	50	*	-10	-11

* the ceiling heat flux calculated was negative.

Table 6.5 Comparison between simulated (S) and measured (M) ceiling heat flux. Five surface models.

Ventilation (m^3/s)	Roof Temp. (°C)	Percentage Difference = 100((S/M)-1) Model 5.1	5.2	5.3	5.4
Group A					
0.0	70	13	2	2	13
0.0	60	14	3	3	14
0.0	50	15	4	4	15
0.0	40	16	5	5	16
0.0	30	24	13	13	24
Group B					
0.0	70	13	2	2	13
0.003	70	21	5	5	13
0.006	70	25	8	8	14
0.013	70	21	-1	5	10
0.013	70	23	1	7	11
0.013	70	20	-1	5	9
0.026	70	18	-20	10	-10
0.040	70	1	-40	1	-34
Group C					
0.0	70	119	83	83	119
0.006	70	139	78	78	106
0.006	70	140	78	78	105
0.013	70	104	47	82	66
0.013	70	69	19	50	35
0.025	70	38	-2	66	8
0.025	70	27	-11	51	-1
0.040	70	-22	-71	8	-52
0.040	70	-25	-57	12	-40
Group D					
0.0	70	10	8	8	10
0.003	70	14	10	10	13
0.006	70	21	11	11	12
0.013	70	18	5	8	2
0.025	70	10	-5	6	-10
0.040	70	-9	-22	-6	-27
Group E					
0.003	70	20	16	16	18
0.006	70	28	19	19	19
0.015	70	38	23	28	21
0.024	70	38	23	33	18
0.039	70	38	22	40	18
Group F					
0.0	50	9	8	8	9
0.003	50	15	11	11	12
0.013	50	14	2	6	-1
0.025	50	4	-10	2	-15
0.040	50	-9	-20	-2	-25
Group G					
0.0	50	15	4	4	15
0.007	50	23	6	7	12
0.040	50	-9	-46	-3	-42

Table 6.5(cont.) Comparison between simulated (S) and measured (M) ceiling heat flux. Five surface models.

Ventilation	Roof Temp.	Percentage Difference = 100((S/M)-1)			
		Model			
(m^3/s)	(°C)	5.5	5.6	5.7	5.8
Group A					
0.0	70	2	2	2	2
0.0	60	3	3	3	3
0.0	50	4	4	4	4
0.0	40	5	5	5	5
0.0	30	13	13	13	13
Group B					
0.0	70	2	2	2	2
0.003	70	-2	-2	3	3
0.006	70	-4	-4	3	3
0.013	70	-30	-25	-18	-13
0.013	70	-28	-23	-17	-11
0.013	70	-30	-24	-19	-12
0.026	70	-53	-25	-43	-15
0.040	70	-69	-34	-65	-26
Group C					
0.0	70	83	83	83	83
0.006	70	46	46	62	62
0.006	70	46	47	60	60
0.013	70	21	41	27	54
0.013	70	-37	8	-28	21
0.025	70	-50	-10	-40	8
0.025	70	*	-58	*	-47
0.040	70	-90	-41	-85	-30
0.040	70	-3	13	2	24
Group D					
0.0	70	8	8	8	8
0.003	70	4	4	9	9
0.006	70	0	0	7	8
0.013	70	-12	-9	-4	-1
0.025	70	-24	-15	-18	-8
0.040	70	-39	-26	-35	-21
Group E					
0.003	70	9	9	14	14
0.006	70	7	7	15	15
0.015	70	5	9	13	17
0.024	70	4	13	9	19
0.039	70	5	19	9	24
Group F					
0.0	50	8	8	8	8
0.003	50	4	4	9	9
0.013	50	-14	-10	-7	-3
0.025	50	-28	-19	-24	-11
0.040	50	-34	-22	-32	-18
Group G					
0.0	50	4	4	4	4
0.007	50	-12	-12	-2	-2
0.040	50	-70	-36	-67	-29

* the ceiling heat flux calculated was negative.

Model 5.3 showed the same maximum overestimation of 83% as model 5.2 for the test without ventilation in group C. Nevertheless, the maximum underestimation was only 6% for the test with a ventilation flow rate of 0.04 m^3/s in group D. This shows the importance of using attic air velocities closer to the ones measured in the test roof.

A maximum overestimation of 119% was obtained with model 5.4 for the test without ventilation in group C. The worst underestimation was 52% at a ventilation rate of 0.04 m^3/s in the same group.

Model 5.5 showed the same maximum overestimation of 83% as did models 5.2 and 5.3 for the tests without ventilation in group C. But the underestimations were worse and negative ceiling heat fluxes were estimated for tests with ventilation rates of 0.025 m^3/s in group C.

Model 5.6 produced the same overestimations as model 5.5. The worst underestimation was 58% for the same test that model 5.5 predicted negative ceiling heat flux (0.025 m^3/s in group C).

The results from models 5.4, 5.5 and 5.6 did not compare well with measured. This indicates that the assumption that the attic air temperature was the mean between input and output temperatures (eq. 4.3) is not as good as the well mixed assumption.

Model 5.7 showed very similar results to model 5.5 with the same maximum over and underestimation.

Model 5.8 showed the same maximum overestimation as models 5.2, 5.3, 5.5, and 5.7 in group C. The worst underestimation was 47% for the test with ventilation rate of 0.025 m^3/s in the same group.

Ceiling heat fluxes simulated by model 5.8 compare better with measured ones than those simulated by model 5.6.. This supports the assumption that the attic air temperature increases as it travels through the attic (eq. 4.5) rather than the assumption that the attic air temperature is the mean between input and output temperatures. Nevertheless these results are not as good as those from model 5.3 that assumes a good mixture in the attic air.

The agreement between observed and predicted ceiling heat fluxes by the five surface model is much better than for the two surface models. Model 5.3 was the best for all groups of tests except E. For group E, model 5.5 was the best.

Table 6.6 shows the percentage difference between the ceiling heat flux simulated by the seven surface models and the observed for each test.

Model 7.1 produced a maximum overestimation of 75% for the test without ventilation in group C. The worst underestimation was 53% at ventilation rates of 0.04 m^3/s in the same group.

The same maximum overestimation of 75% was obtained with model 7.2 but for a different test (0.013 m^3/s) in the same group C. The worst underestimation was only 11% for a ventilation rate of 0.04 m^3/s in group D. This shows again the importance of using attic velocities closer to the ones measured in the test roof.

The agreement between observed and simulated ceiling heat flux by the seven surface models is slightly better than for the five surfaces models. Model 7.2 was the best for all groups except E.

The ceiling heat fluxes simulated by the best models for each group of tests are compared with observations in figure 6.1 to 6.7.

Figure 6.1 shows the observed ceiling heat fluxes for tests in group A and the ones simulated by models 5.3 and 7.2. The agreement is very good for all tests. The maximum difference was 13% for model 5.3 with a temperature difference of 10 K.

Figure 6.2 shows the observed ceiling heat fluxes for tests in group B and the ones simulated by models 5.3 and 7.2. The agreement for both models in all tests is good but model 7.2 predicted ceiling heat fluxes slightly closer to the observed ones. The maximum difference was 10% for model 5.3 with a ventilation rate of 0.026 m^3/s.

Figure 6.3 shows the observed ceiling heat fluxes for tests in group C and the ones simulated by models 5.3 and 7.2. Model 7.2 predicted ceiling heat fluxes slightly closer to the observed ones than did model 5.3. The difference between simulated and observed ceiling heat fluxes was the largest without ventilation, decreasing as ventilation flow rates increased. Good agreement is found for a ventilation rate of 0.04 m^3/s. The maximum difference was 83% for model 5.3 without ventilation.

Figure 6.4 shows the observed ceiling heat fluxes for tests in group D and the ones simulated by models 5.3 and 7.2. Model 7.2 predicted ceiling heat fluxes slightly lower than model 5.3. Both models overestimated the ceiling heat flux up to a ventilation rate

Table 6.6 Comparison between simulated (S) and measured (M) ceiling heat flux. Seven surface models.

Ventilation (m^3/s)	Roof Temp. (°C)	Percentage Difference = 100((S/M)-1) Model 7.1	7.2
Group A			
0.0	70	2	1
0.0	60	3	2
0.0	50	4	3
0.0	40	5	4
0.0	30	14	12
Group B			
0.0	70	2	1
0.003	70	0	2
0.006	70	-1	4
0.013	70	-17	1
0.013	70	-15	2
0.013	70	-17	1
0.026	70	-19	6
0.040	70	-30	-3
Group C			
0.0	70	75	74
0.006	70	53	70
0.006	70	51	70
0.013	70	44	75
0.013	70	15	44
0.025	70	13	60
0.025	70	-1	44
0.040	70	-53	3
0.040	70	-35	8
Group D			
0.0	70	4	4
0.003	70	5	6
0.006	70	3	7
0.013	70	-6	4
0.025	70	-14	1
0.040	70	-26	-11
Group E			
0.003	70	10	11
0.006	70	10	14
0.013	70	12	22
0.024	70	13	28
0.039	70	18	34
Group F			
0.0	50	4	4
0.003	50	5	6
0.013	50	-8	1
0.025	50	-17	-3
0.040	50	-23	-7
Group G			
0.0	50	4	3
0.007	50	-6	3
0.040	50	-34	-7

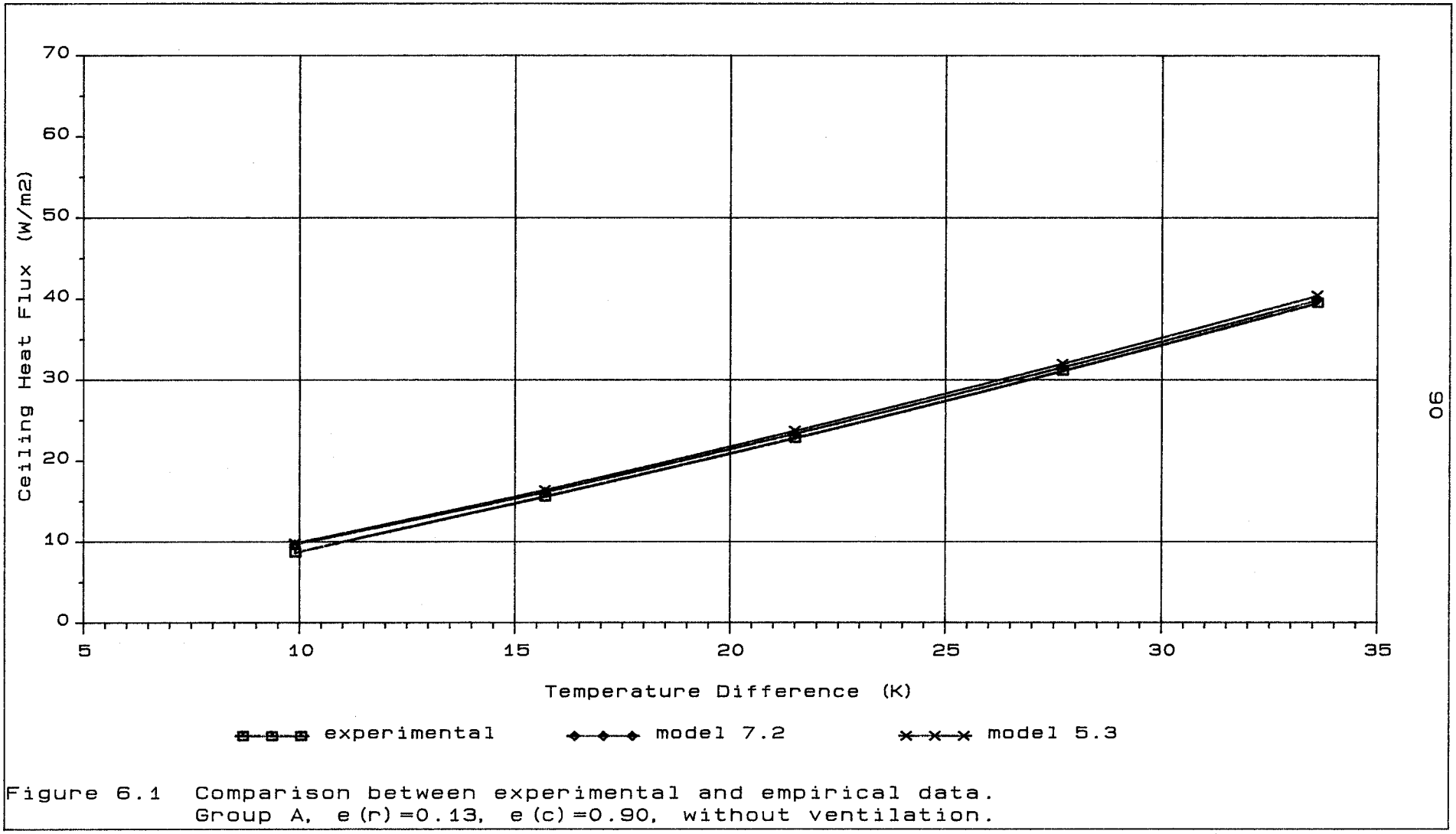

Figure 6.1 Comparison between experimental and empirical data.
Group A, e(r)=0.13, e(c)=0.90, without ventilation.

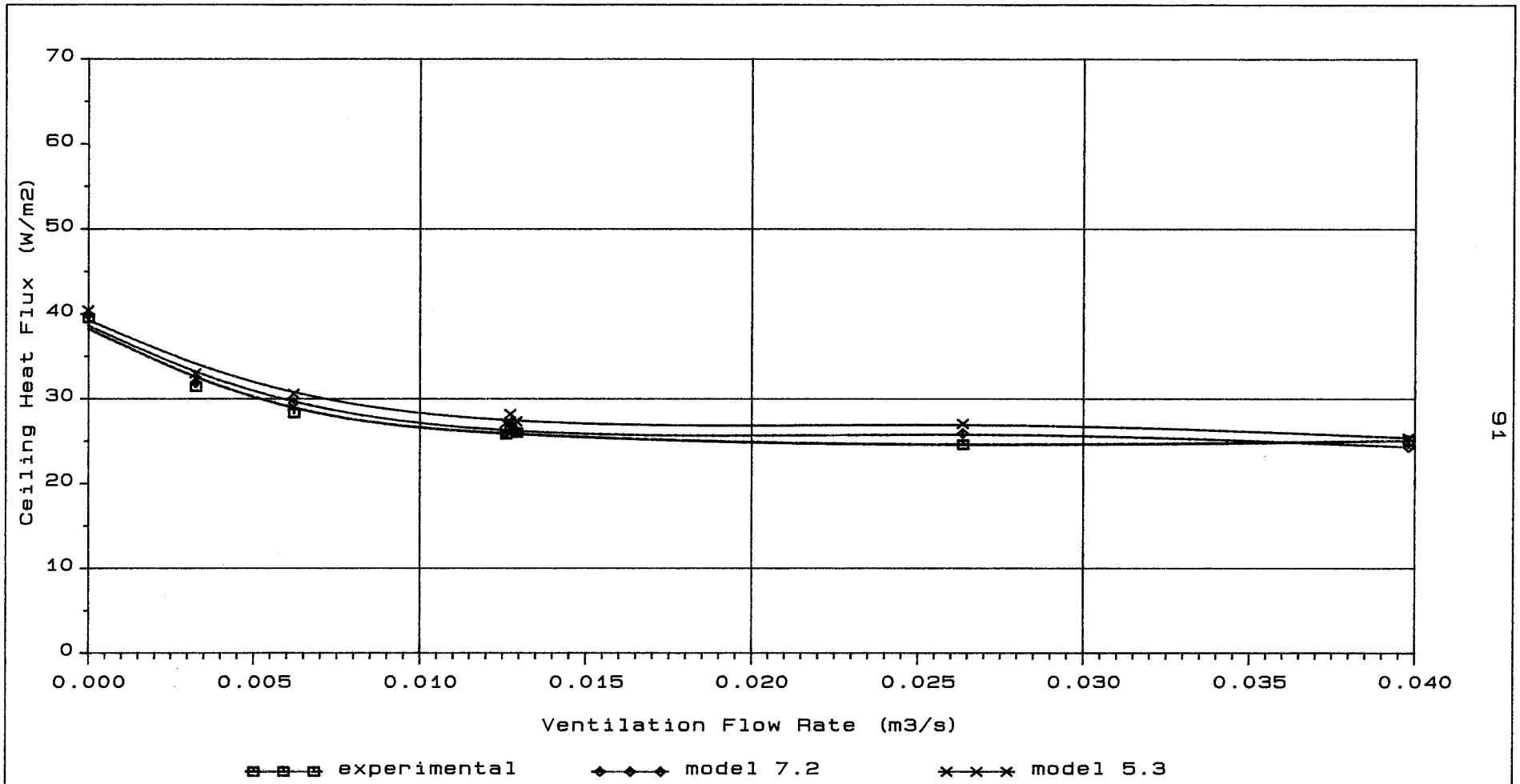

Figure 6.2 Comparison between experimental and empirical data.
Group B, e(r)=0.13, e(c)=0.90, roof temperature 70 C, ventilation entrance- small.

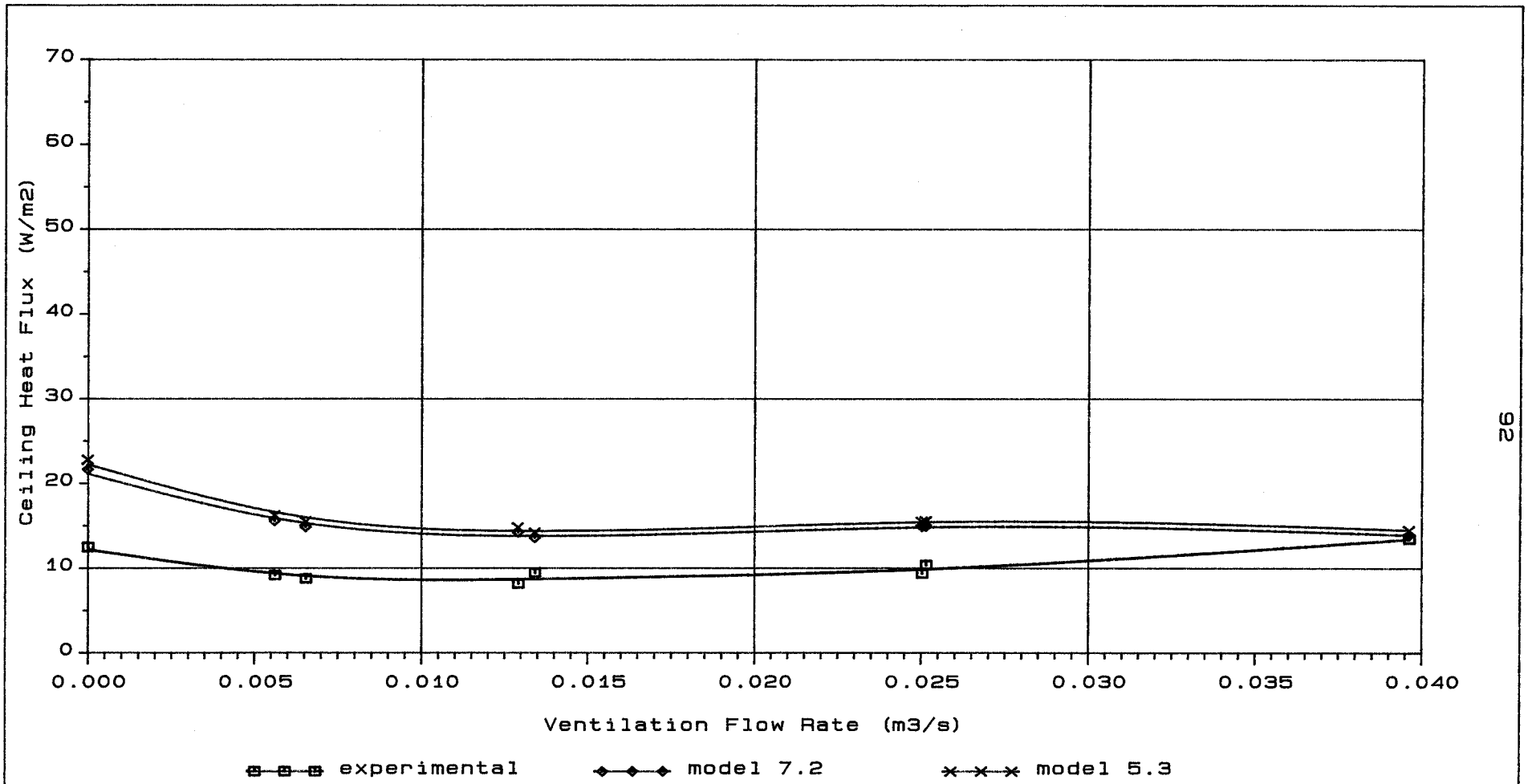

Figure 6.3 Comparison between experimental and empirical data.
Group C, e(r)=0.13, e(c)=0.05, roof temperature 70 C, ventilation entrance- small.

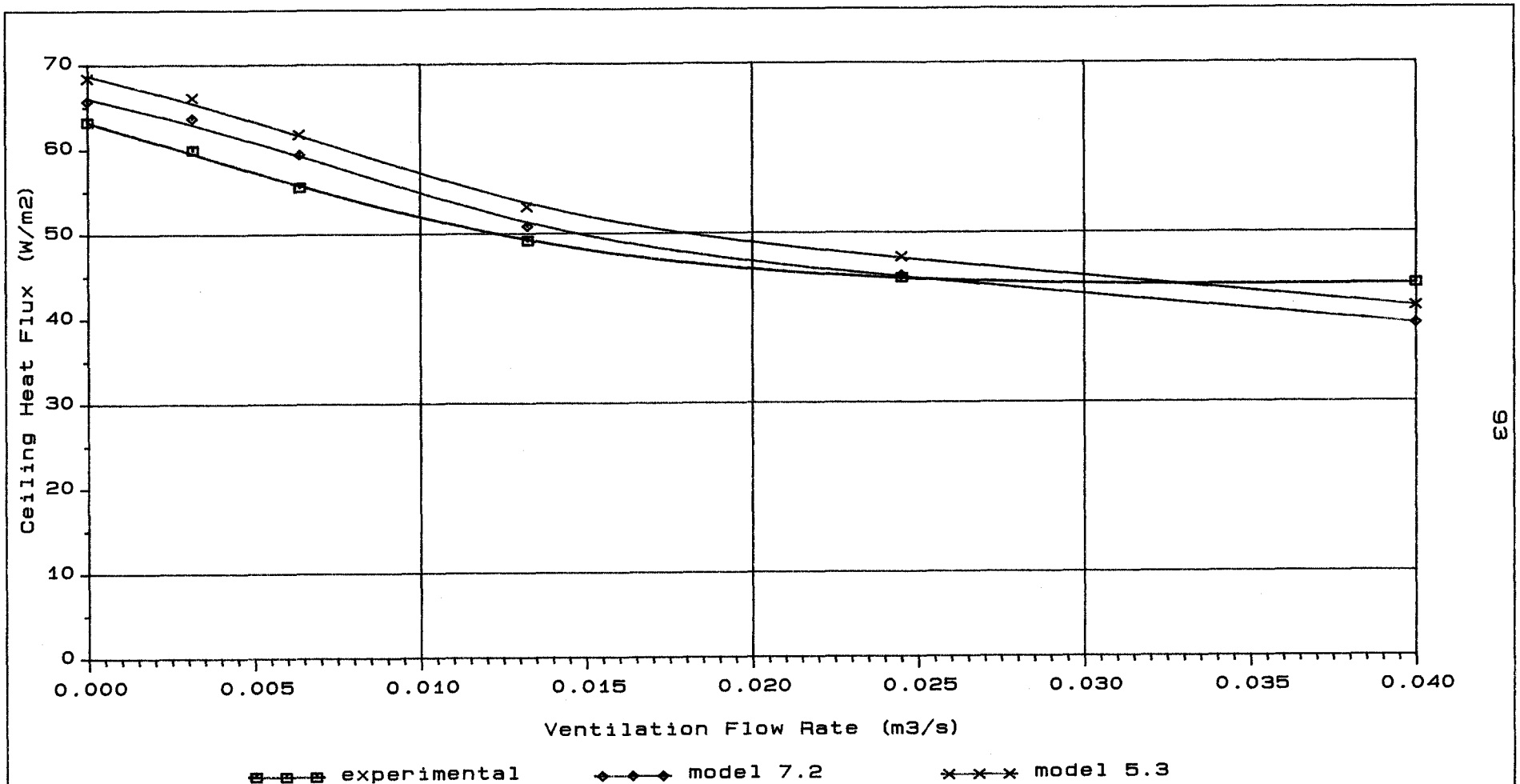

Figure 6.4 Comparison between experimental and empirical data.
Group D, e(r)=0.90, e(c)=0.90, roof temperature 70 C, ventilation entrance- small.

of 0.025 m^3/s, above this they underestimated it. The maximum overestimation was 11% for model 5.3 with a ventilation rate of 0.006 m^3/s. The worst underestimation was also 11% for model 7.2 with a ventilation rate of 0.04 m^3/s.

Figure 6.5 shows the observed ceiling heat fluxes for tests in group E and the ones simulated by models 5.3, 5.5, 5.7 and 7.2. Models 5.5 and 5.7 predicted ceiling heat fluxes closer to the observations than models 5.3 and 7.2. Model 5.5 was the most accurate. Its maximum overestimation was 9% at low ventilation flow rate.

Figure 6.6 shows the observed ceiling heat fluxes for tests in group F and the ones simulated by model 5.3 and 7.2. Model 7.2 predicted slightly lower ceiling heat fluxes than model 5.3. The agreement is good for both models. The maximum overestimation was 11% for model 5.3 at a ventilation rate of 0.003 m^3/s. The maximum underestimation was 7% for model 7.2 at a ventilation rate of 0.04 m^3/s.

Figure 6.7 shows the observed ceiling heat fluxes for tests in group G and the ones simulated by model 5.3 and 7.2. The agreement is good. The maximum overestimation was 7% for models 5.3 with a ventilation rate of 0.007 m^3/s. The worst underestimation was also 7% for and model 7.2 with a ventilation rate of 0.04 m^3/s.

Table 6.7 lists the measurements of the heat removed by ventilation and predictions obtained from models 5.3 and 7.2 - the models that best simulated all groups of tests except E - and models 5.5 and 5.7 - that best simulated tests of group E.

In tests of groups B, C, D, F and G the heat removed by ventilation was overestimated at low ventilation flow rates by models 5.3 and 7.2. The reverse happened at high ventilation flow rates. At medium ventilation flow rates (0.013 m^3/s) the agreement between predicted and measured values was good.

For tests in group E, models 5.3, 5.5, 5.7 and 7.2 overestimated the heat removed by ventilation at all ventilation flow rates. Models 5.5 and 5.7, gave the most accurate predictions of ceiling heat flux. These models highly overestimated the heat removed by ventilation at low ventilation flow rates.

Table 6.8 presents the difference between simulated attic air temperatures and mean of measured ones. Table 6.9, lists the difference between simulated attic air temperatures and measured

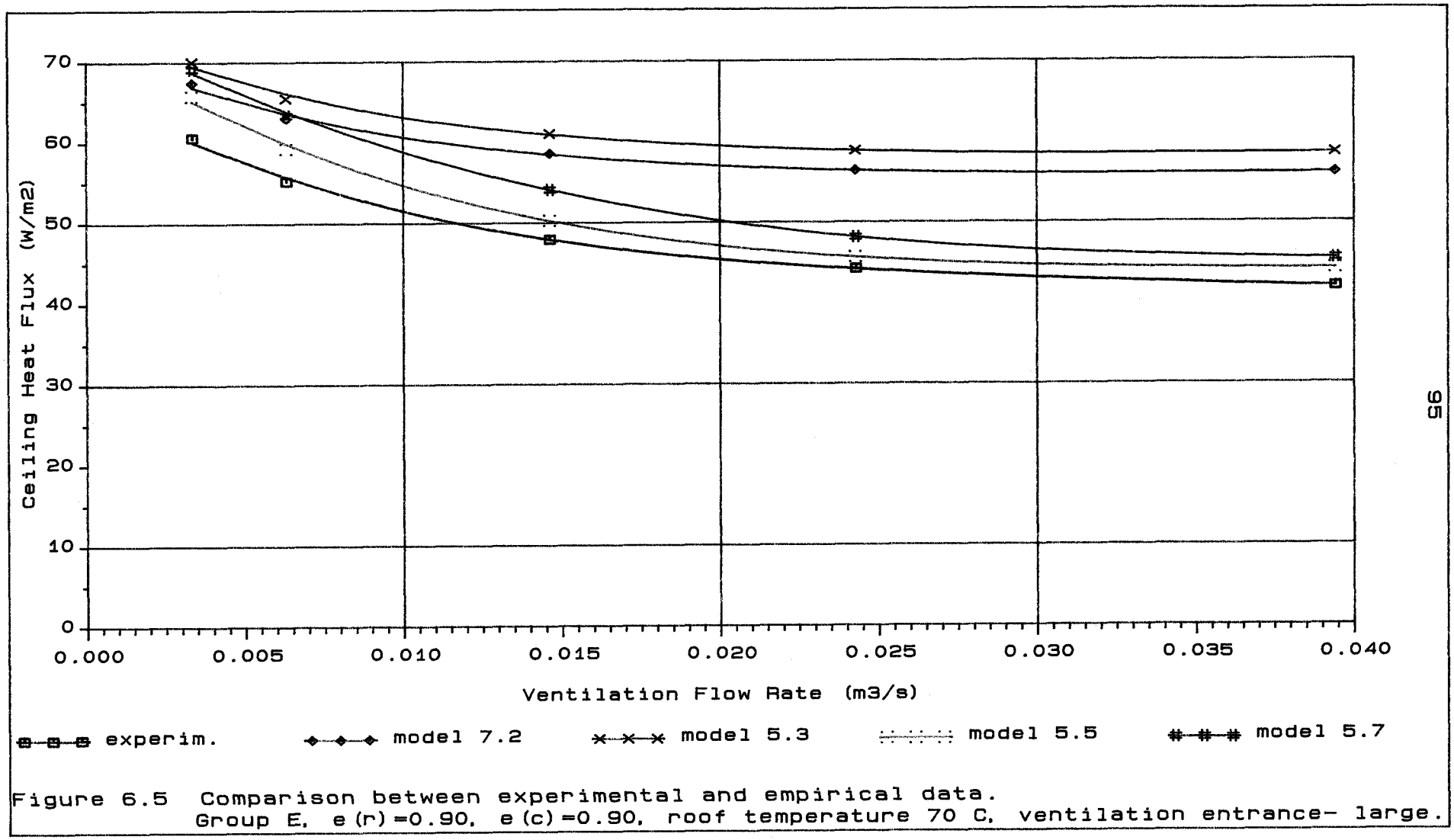

Figure 6.5 Comparison between experimental and empirical data.
Group E, e(r)=0.90, e(c)=0.90, roof temperature 70 C, ventilation entrance- large.

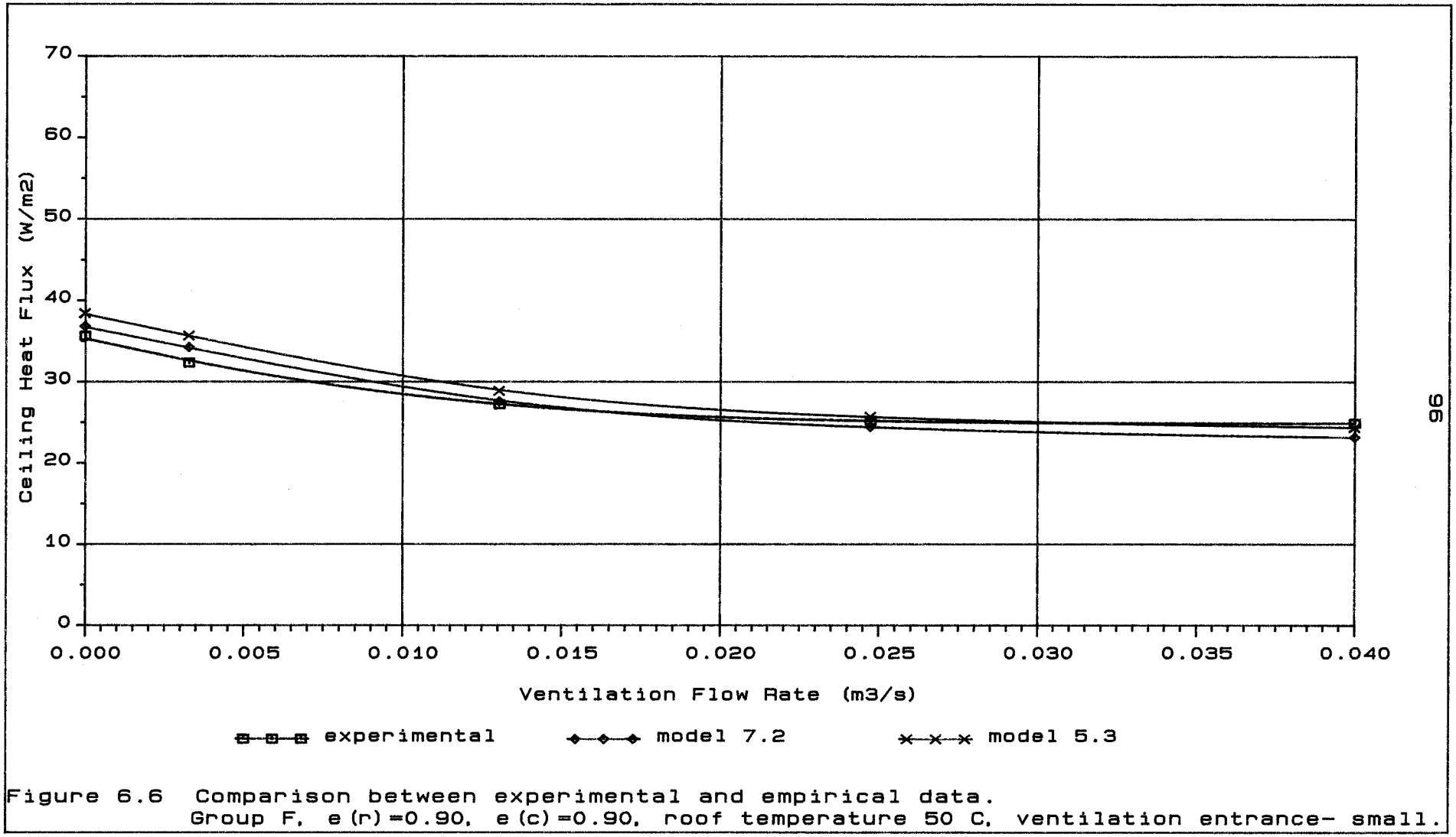

Figure 6.6 Comparison between experimental and empirical data.
Group F, e(r)=0.90, e(c)=0.90, roof temperature 50 C, ventilation entrance- small.

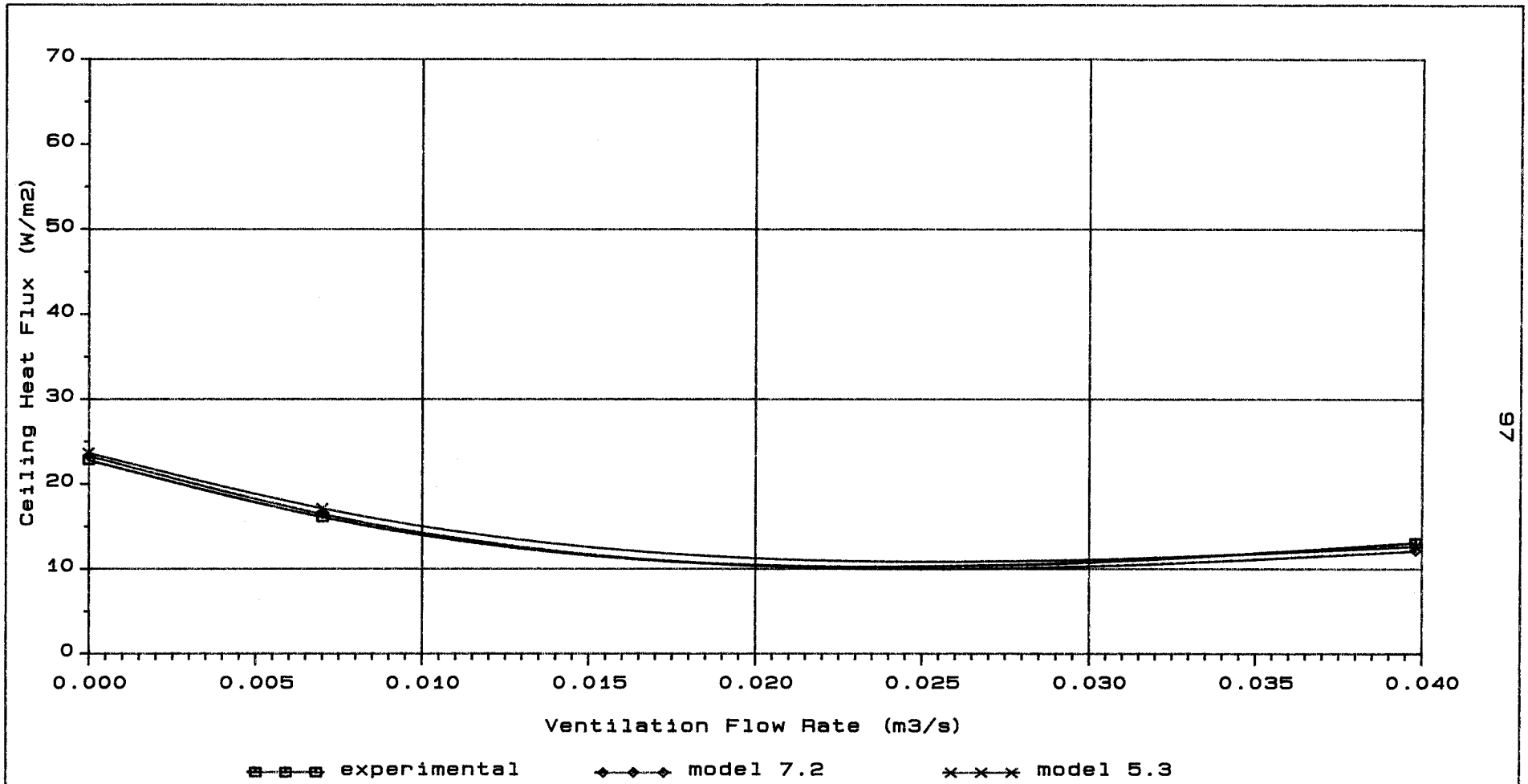

Figure 6.7 Comparison between experimental and empirical data.
Group G, e(r)=0.13, e(c)=0.90, roof temperature 50 C, ventilation entrance- small.

Table 6.7 Simulated and measured heat removed by ventilation.

Ventilation (m^3/s)	Observations (W)	Model 5.3 (W)	Model 7.2 (W)	Model 5.5 (W)	Model 5.7 (W)
Group B					
0.0	0	0	0		
0.003	38	77	75		
0.006	104	123	121		
0.013	220	208	207		
0.013	215	214	212		
0.013	217	210	209		
0.026	409	386	384		
0.040	685	553	551		
Group C					
0.0	0	0	0		
0.006	118	123	123		
0.006	121	128	129		
0.013	172	179	181		
0.013	163	193	196		
0.025	375	341	345		
0.025	357	362	366		
0.040	814	588	593		
0.040	619	524	527		
Group D					
0.0	0	0	0		
0.003	63	87	86		
0.006	125	154	153		
0.013	257	275	274		
0.025	499	435	434		
0.040	781	582	582		
Group E					
0.003	62	95	94	168	109
0.006	129	157	156	260	191
0.013	291	306	305	425	365
0.024	389	431	430	494	456
0.039	449	586	584	527	507
Group F					
0.0	0	0	0		
0.003	33	50	50		
0.013	150	152	151		
0.025	291	245	244		
0.040	465	326	327		
Group G					
0.0	0	0	0		
0.007	74	81	80		
0.040	452	327	326		

Table 6.8 Difference between simulated attic air temperature (T_{as}) and mean of measured ones(T_{am}).

Ventilation (m^3/s)	Roof Temp. (°C)	$\Delta t = T_{as} - T_{am}$ (K) Model 5.3	7.2	5.5	5.7
Group A					
0.0	70	1.6	0.4		
0.0	60	1.3	0.2		
0.0	50	0.5	-0.3		
0.0	40	0.7	0.1		
0.0	30	0.6	0.2		
Group B					
0.0	70	1.6	0.4		
0.003	70	-2.8	-3.4		
0.006	70	-5.8	-6.1		
0.013	70	-8.5	-8.6		
0.013	70	-8.8	-8.9		
0.013	70	-8.4	-8.5		
0.026	70	-6.0	-6.1		
0.040	70	-5.6	-5.6		
Group C					
0.0	70	-4.9	-5.5		
0.006	70	-11.7	-11.5		
0.006	70	-11.5	-11.4		
0.013	70	-11.6	-11.4		
0.013	70	-11.9	-11.7		
0.025	70	-8.8	-8.6		
0.025	70	-9.2	-9.1		
0.040	70	-8.9	-8.8		
0.040	70	-7.3	-7.2		
Group D					
0.0	70	-1.2	-2.3		
0.003	70	-6.9	-7.2		
0.006	70	-8.9	-9.1		
0.013	70	-9.9	-10.0		
0.025	70	-8.0	-7.9		
0.040	70	-7.4	-7.4		
Group E					
0.003	70	-7.9	-8.2	-10.9	-8.5
0.006	70	-9.9	-10.1	-13.7	-11.2
0.015	70	-12.4	-12.5	-18.0	-16.1
0.024	70	-11.5	-11.6	-18.2	-17.0
0.039	70	-10.1	-10.1	-17.3	-16.7
Group F					
0.0	50	-0.7	-1.3		
0.003	50	-4.3	-4.5		
0.013	50	-5.6	-5.7		
0.025	50	-4.9	-4.9		
0.040	50	-4.0	-4.0		
Group G					
0.0	50	0.5	-0.3		
0.007	50	-4.5	-4.7		
0.040	50	-3.4	-3.4		

Table 6.9 Difference between simulated attic air temperature (T_{as}) and measured temperature of output air from attic (T_{aom}).

Ventilation	$\Delta t = T_{as} - T_{aom}$			
	Model			
	5.3	7.2	5.5	5.7
(m^3/s)	(K)			
Group B				
0.003	11.1	10.5		
0.006	3.1	2.8		
0.013	-0.1	-0.2		
0.013	0.5	0.4		
0.013	0.0	-0.1		
0.026	-0.3	-0.4		
0.040	-2.5	-2.5		
Group C				
0.006	1.2	1.4		
0.006	1.4	1.5		
0.013	0.8	1.0		
0.013	2.4	2.6		
0.025	-0.8	-0.6		
0.025	0.7	0.8		
0.040	-4.3	-4.2		
0.040	-1.7	-1.6		
Group D				
0.003	7.4	7.1		
0.006	4.5	4.3		
0.013	1.6	1.5		
0.025	-2.0	-1.9		
0.040	-3.9	-3.9		
Group E				
0.003	8.8	8.5	5.8	8.2
0.006	4.2	4.0	0.4	2.9
0.015	1.4	1.3	-4.2	-2.3
0.024	2.0	1.9	-4.7	-3.5
0.039	3.4	3.4	-3.8	-3.2
Group F				
0.003	5.1	4.9		
0.013	0.6	0.5		
0.025	-1.3	-1.3		
0.040	-2.6	-2.6		
Group G				
0.007	1.3	1.1		
0.040	-2.8	-2.8		

temperatures of output air from attic. The mean of the measured attic air temperatures was calculated as a volume weighted average of the temperatures recorded at ten different positions. By referring to table 6.8 it can be seen that the agreement between simulated and mean of measurements is only good for tests without ventilation. When there is ventilation, the simulated attic air temperature agrees better with the temperature of the output air from the attic, as can be seen in table 6.9.

6.3 DISCUSSION AND CONCLUSION

Two surface models are unable to represent the phenomena studied because they assume too many simplifications.

The importance of assuming the convection coefficient under the sloping roof surface to be that of an horizontal surface was made clear in the five surface models for small ventilation flow rates. See table 6.5 where the results of model 5.1 are compared with those of model 5.2 (or models 5.4 x 5.5).

Considering the velocity of the attic air to be closer to the measured value, instead of just dividing the velocity flow rate by the cross sectional area was shown to be important in the five surface models. Using this assumption caused the predicted values to be close to the ones observed at high ventilation flow rates for all groups except E. See the results of model 5.3 as compared with those of model 5.2 in table 6.5 (or models 7.2 x 7.1, table 6.6).

Assuming the attic air to be well mixed and at the same temperature gave better results than assuming it to increase as it travels through the attic. This assumption applied to all groups of tests except E. In other words, it applied for all tests with small ventilation opening. In group E, models 5.5 and 5.7 (air not well mixed) showed better agreement (see figure 6.5). Model 5.5 (attic air temperature = mean between input and output) is a simplification of model 5.7, and the fact that it agreed better is considered to be fortuitous.

Good predictions of ceiling heat flux in tests having small ventilation openings were obtained with models 5.3 and 7.2. These models predicted well the ceiling heat flux of tests in group C at very high ventilation flow rates, when the stratification of the attic air is minimized. At low ventilation flow rates, the models

grossly overestimate the ceiling heat flux. In this case, a more elaborate model, dividing the attic air in elements, would have to be developed. As an attic with two low emissivity surfaces is quite unusual, the development of a further model was considered to be beyond the scope of this work.

For groups A, B, D, F and G the best models were 5.3 and 7.2. For these models the maximum disagreement between simulated and observed ceiling heat fluxes was ± 13% (model 5.3 - table 6.5) and ± 12% (model 7.2 - table 6.6). Bearing in mind the uncertainties associated with the input data, particularly emissivity (10 to 15%), these results are very good. The improvement in accuracy between the five and the seven surfaces models was very small. The use of five surfaces is therefore considered to be a good balance between accuracy and simplicity.

The comparisons made between simulated and measured heat removal by ventilation and attic air temperatures demonstrated how complex and difficult it is to model the phenomenon of heat removal by ventilation. The convective heat transfer process assumed in the models is a simplification. Nevertheless, the simulations yielded ceiling heat fluxes that agreed reasonably well with the observations and this is what actually matters in practice.

Large openings are necessary to achieve high attic ventilation rates (chapter 3). Group E tests had large openings and were better simulated by models 5.5 and 5.7 (air not well mixed). In the tests , air entered the attic by one eave and left by the other. In chapter 3, an old asbestos cement roof exposed to the weather was shown to have about 80% of its ventilation from eave to eave and the rest spread among other flow paths. A clay tiled roof distributed the flow well and only about 40% was from eave to eave (see table 3.1). Thus, assuming the attic air to be well mixed seems appropriate for general application. Also, considering the natural convection coefficient at the under-side of the roof surface, an interpolation between the horizontal and vertical value seems more realistic because the air permeability of the roof disturbs the stratification. Ventilation air speeds as high as those used in the test roof are not expected in the field, because large openings are necessary to achieve high ventilation flow rates. The values obtained by dividing the flow rate by the mean cross sectional area are nevertheless, expected to be too small due to some concentration on the flow from

eave to eave. Field observations are necessary before a general assumption about this point can be made.

Model 5.1 considers the attic air to be well mixed, the natural convection coefficient under the sloping roof to be an interpolation between vertical and horizontal values and the ventilation air speed as the air flow rate divided by mean cross sectional area. It was therefore selected as the basis for the unsteady state model which is developed in the next chapter.

CHAPTER 7 UNSTEADY STATE HEAT TRANSFER MODEL

7.1 INTRODUCTION

The steady state model 5.1 was used as a basis for developing a dynamic model using a finite difference technique for solving the heat transfer equations. The initial dynamic model only simulated the heat transfer through a roof. This was expanded to predict the effect that changes in the roof have upon the thermal behaviour of the living quarters.

Simulations were performed using typical summer and winter weather data of Porto Alegre (table 1.1 and 1.2) for the low cost house described in chapter 1. This had the following specification:

-roof: 6mm old corrugated asbestos cement sheet (solar absorptivity 0.8) with a slope of 20°, ventilated at the eaves;

-ceiling: 10mm plaster board;

-walls: 25mm plaster + 100mm brickwork + 25mm external render painted white (solar absorptivity 0.3);

-windows: single glazing with outside solar protection (louvered shutters);

-floor: concrete in contact with the earth;

-orientation: east-west.

Appropriate thermal properties for these materials were taken from the CIBSE Guide (1986) and are given in table 7.1.

Table 7.1 Thermal properties of the materials considered in the simulations.

Material	Thermal Conductivity (W/m K)	Specific Heat Capacity (J/kg K)	Density (kg/m^3)
Asbestos cement	0.36	1050	700
Brickwork	0.84	800	1700
Glass fibre quilt	0.04	840	12
Plaster	0.50	1000	1300
Plasterboard	0.16	840	950
Rendering	0.50	1000	1300
Cast concrete	1.13	1000	2000
Glass	1.05	750	2500

The effective resistances of the ventilated attic (chapter 2, section 2.5) were computed according to equation 2.26. ER's provide simple indices for comparing different solutions and allow heat gains and losses calculations to be performed by simpler models like the Admittance Procedure (CIBSE 1986).

7.2 THE MODEL

The model divides the house into two cells, attic and living quarters. The attic cell is formed by two roof surfaces, two gables and the ceiling. The living quarter cell is formed by the ceiling, the floor and four walls. The heat flow paths are shown in figure 7.1. One-dimensional heat flow is assumed through each component. As suggested by Clarke (1985) the mass associated with each component was divided into three nodes, one on each surface and one in the middle of the mass. The temperature of the ground 0.2 m below the floor was assumed to be constant, equal to the monthly average outside air temperature. Ventilation heat removal was considered as a conductance between the inside and outside air. The ventilation air was considered to be well mixed and coming from outside. Solar gain through windows into the living quarters was calculated using the solar gain factor given in CIBSE (1986). All the solar gain was input to the ground surface node.

Heat balances were evaluated at future time giving the fully implicit finite difference formulation. The implicit formulation was chosen because of the unconditional stability for space and time discretizations (Clarke 1985).

The heat balance for surface nodes exposed to the outside environment gives

$$\alpha_{wo}\, I_t^{t+1} + \epsilon_{wo}\, I_{lt}^{t+1} + h_{wind}\left(T_o^{t+1} - T_{wo}^{t+1}\right) - \epsilon_{wo}\sigma\left(T_{wo}^{t+1}\right)^4 + \frac{\left(T_{wm}^{t+1} - T_{wo}^{t+1}\right)}{R_{wo}} = \frac{\rho_{wo}\, c_{wo}\, l_{wo}}{\Delta t}\left(T_{wo}^{t+1} - T_{wo}^{t}\right) \qquad (7.1)$$

where

t - time, s
wo- refers to outside surface node

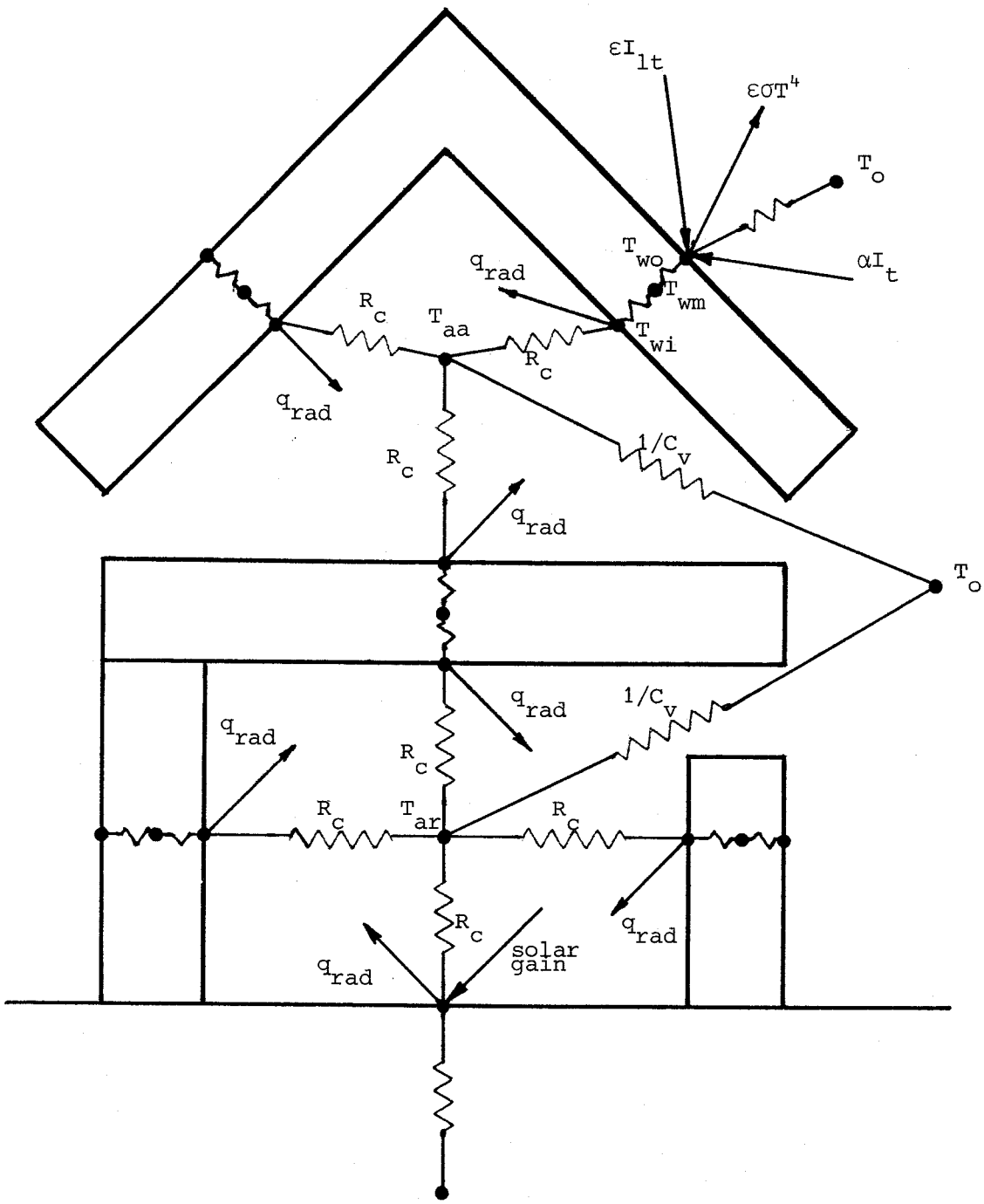

$R_c = 1/h_c$ T_g

q_{rad} - heat flux leaving the surface by radiation.

Figure 7.1 Diagramatic representation of the unsteady state heat transfer model.

wm- refers to node inside the component
α - solar absorptivity
R - thermal resistance, m^2K/W

For the node inside the component it gives

$$\frac{\left(T_{wo}^{t+1} - T_{wm}^{t+1}\right)}{R_{wo}} + \frac{\left(T_{wi}^{t+1} - T_{wm}^{t+1}\right)}{R_{wi}} = \frac{\rho_{wm}\, c_{wm}\, l_{wm}}{\Delta t}\left(T_{wm}^{t+1} - T_{wm}^{t}\right) \quad (7.2)$$

where

wi- refers to inside surface node

For nodes exposed to the inside environment it gives

$$\frac{\left(T_{wm}^{t+1} - T_{wi}^{t+1}\right)}{R_{wi}} + \left(T_a^{t+1} - T_{wi}^{t+1}\right) h_{ci}^{t+1} - \frac{\epsilon_{wi}\sigma}{(1 - \epsilon_{wi})}\left(T_{wi}^{t+1}\right)^4$$

$$+ \frac{\epsilon_{wi}}{(1-\epsilon_{wi})} J_{wi}^{t+1} = \frac{\rho_{wi}\, C_{wi}\, l_{wi}}{\Delta t}\left(T_{wi}^{t+1} - T_{wi}^{t}\right) \quad (7.3)$$

where

T_a - inside air temperature (room or attic), K

plus one equation to determine the radiosity

$$- \frac{\epsilon_{wi}\sigma}{(1-\epsilon_{wi})}\left(T_{wi}^{t+1}\right)^4 + \frac{J_{wi}^{t+1}}{(1-\epsilon_{wi})} - \sum_{j=1}^{j=n} F_{ij}\, J_{wj} = 0 \quad (7.4)$$

where

i - surface number, 1 to 5 in attic and 1 to 6 in room
n - number of surfaces

For air nodes it gives

$$\sum_{i=1}^{i=n}\left(\left(T_{wi}^{t+1} - T_a^{t+1}\right) S_i\, h_{ci}^{t+1}\right) + \left(T_o^{t+1} - T_a^{t+1}\right) C_v = 0 \quad (7.5)$$

These expressions give a system of 41 non-linear equations with temperatures and radiosities at time t+1 as unknowns.

A computer program was written to calculate solar and longwave radiation incident on all the external surfaces together with the wind convection coefficient, according to the theory described in chapter 2. The system of non-linear equations was solved in the same way as the steady state models described in chapter 4.

The program starts with a steady state solution and then repeats the unsteady state calculations for three days to allow the masses to reach a stable temperature. The time interval can be varied. The calculations were repeated for attic ventilations up to 130 air changes per hour (ach). Ventilation air speed was assumed to be the volume flow rate divided by mean cross sectional area of the attic.

7.3 VARIABLES STUDIED

Preliminary simulations showed that considering the roof to attic convection coefficient as if the surface was horizontal (as done in chapter 6) made little difference when compared with interpolating it between the values for horizontal and vertical surfaces. Variations in ceiling heat flux and temperatures predicted by the model were very small over time intervals of 15 or 60 minutes. Therefore, to reduce computer time an interval of one hour was chosen.

The simulations performed during the summer day used the following input parameters.

-SR1: standard house as described in section 7.1 with window solar protection (louvered shutters) closed, house ventilation 10 ach.

-SR2: same as SR1 but roof solar absorptivity 0.3.

-SR3: same as SR1 but roof to attic emissivity 0.05.

-SR4: same as SR1 plus 25mm glass fibre quilt attached below the roof.

-SR5: same as SR1 plus 25mm glass fibre quilt over the ceiling.

-SR6: same as SR1 but outside roof convection coefficient (eq. 3.13, chapter 3) doubled.

-SR7: same as SR1 but roof slope 10°.

-SR8: same as SR1 but roof slope 30°.

-SR9: same as SR1 but roof solar absorptivity of 0.3 and roof to attic emissivity 0.05.

-SR10: same as SR9 with 25mm glass fibre over the ceiling.

The simulations performed during the winter day used input parameters, WR1 to WR10, as summer (SR1 to SR10), but without solar protection to the window and house ventilation 5 ach.

7.4 RESULTS FOR TYPICAL SUMMER DAY

Figure 7.2 presents the temperatures reached in various points of the standard house (SR1) without attic ventilation. The room air temperature is equal to the outside air temperature. The under-side of ceiling surface temperature is much higher, reaching a peak of 43 °C at 13h, almost 11K higher than the temperature of the room air. The floor temperature stayed cool throughout the day. The difference between the ceiling and room air temperatures for all the summer data at the peak time (13h) is given in table 7.2.

Table 7.2 Temperature difference between under-side ceiling temperature (T_{ci}) and room air (T_a) during summer at peak conditions (13h).

	$\Delta t = T_{ci} - T_a$ (K)	
Data Sets	Attic Ventilation (ach) 0	130
SR1	10.8	7.5
SR2	1.9	1.4
SR3	-1.0	-1.7
SR4	1.3	0.6
SR5	1.5	-0.3
SR6	6.1	4.4
SR7	10.6	7.8
SR8	10.1	7.1
SR9	-2.6	-2.5
SR10	-3.0	-3.0

Figure 7.3 shows the temperatures at the same locations as figure 7.2 for the standard house (SR1), but with 130 attic ach. The room air temperature is 0.4K lower than the outside air temperature during the day. The attic air temperature dropped below the upper-side of ceiling temperature, but the under-side of ceiling

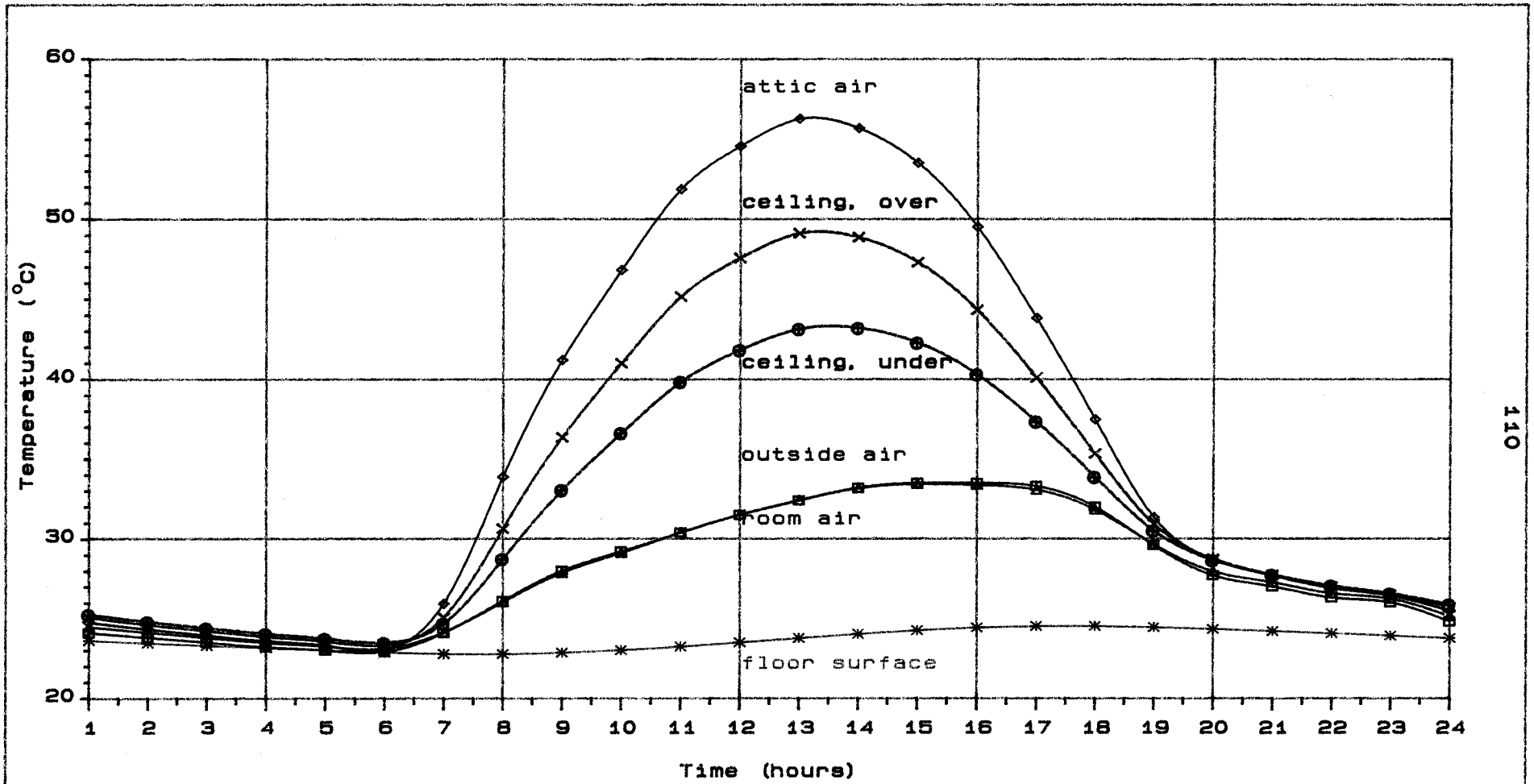

Figure 7.2 Temperatures associated with the standard house (summer, SR1), without attic ventilation

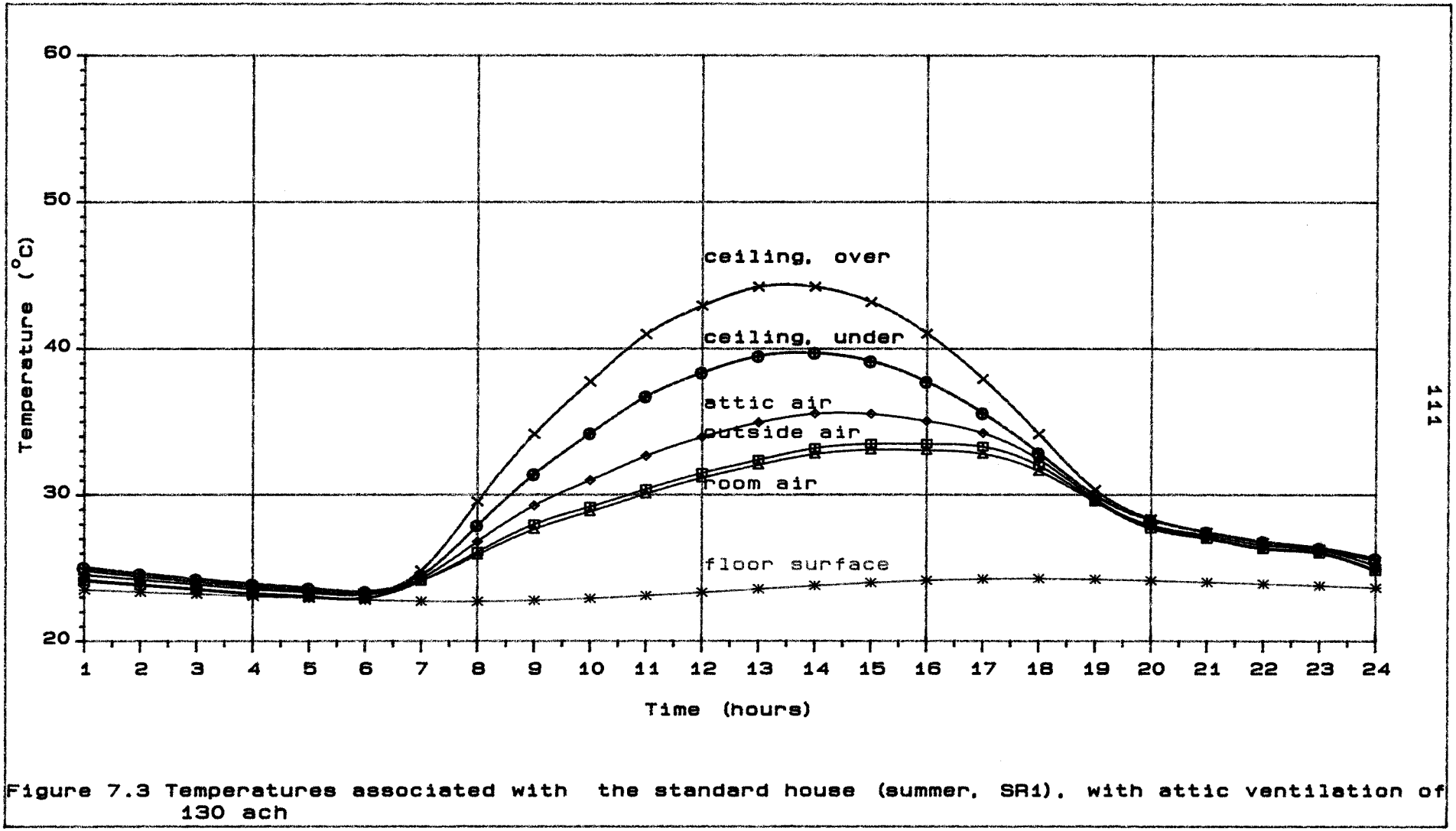

Figure 7.3 Temperatures associated with the standard house (summer, SR1), with attic ventilation of 130 ach

temperature was still high, peaking to 40 °C at 13h, almost 8K higher than the room air temperature.

Figure 7.4 shows the ceiling heat flux for different rates of attic ventilation in the standard house (SR1). A ventilation of 33 ach reduced the peak ceiling heat flux by 14%. The maximum attic ventilation considered (130 ach) reduced the peak ceiling heat flux by 21%, from 94 W/m^2 to 74 W/m^2. Night time ceiling heat fluxes were very similar unrespective of the attic ventilation rate.

Figure 7.5 presents the ceiling heat flux at peak time (13h) for all the summer data (SR1 to SR10)*. Changing the slope of the roof from 20° (SR1) to 10° (SR7) reduced the ceiling heat flux by 1%, changing the slope from 20° to 30° (SR8) reduced it by 4%. Doubling the wind convection coefficient (SR6) effectively altered the outside roof surface energy balance, this reduced the ceiling heat flux by 28%. Lowering the solar absorptivity (SR2) reduced the ceiling heat flux by 54%. Adding the glass fibre quilt under the roof cover (SR4) gave an average reduction of 59% while adding it over the ceiling (SR5), gave an average reduction of 62%. At low rates of attic ventilation the results for both solutions (SR4 and SR5) are similar. As the ventilation increases, putting the insulation over the ceiling is more beneficial. Lowering the roof to attic emissivity (SR3) reduced the ceiling heat flux by 79%. When ceiling to attic emissivity was additionally lowered (SR9), the ceiling heat flux was reduced by 90%; and adding ceiling insulation to these (SR10) increased the reduction to 95%. Increasing the attic ventilation from 0 to 130 ach caused reductions in ceiling heat flux ranging from 10% (SR2) to 35% (SR3).

Reductions in ceiling heat flux produced by changing the standard roof configuration caused the temperature at the under-side of the ceiling to reduce at peak times. The lowest value attained (SR10 with high attic ventilation) was almost 5K below the outside air temperature. The temperature of the room air at this time also reduced to almost 2K below the outside air temperature.

The effective thermal resistances of the ventilated attics were computed throughout the day. Values of ceiling heat flux at peak time (13h) were chosen as representative for design purposes. The values obtained for each set of input data are given in table 7.3.

* The attic ventilation is given in air changes per hour for a roof slope of 20°.

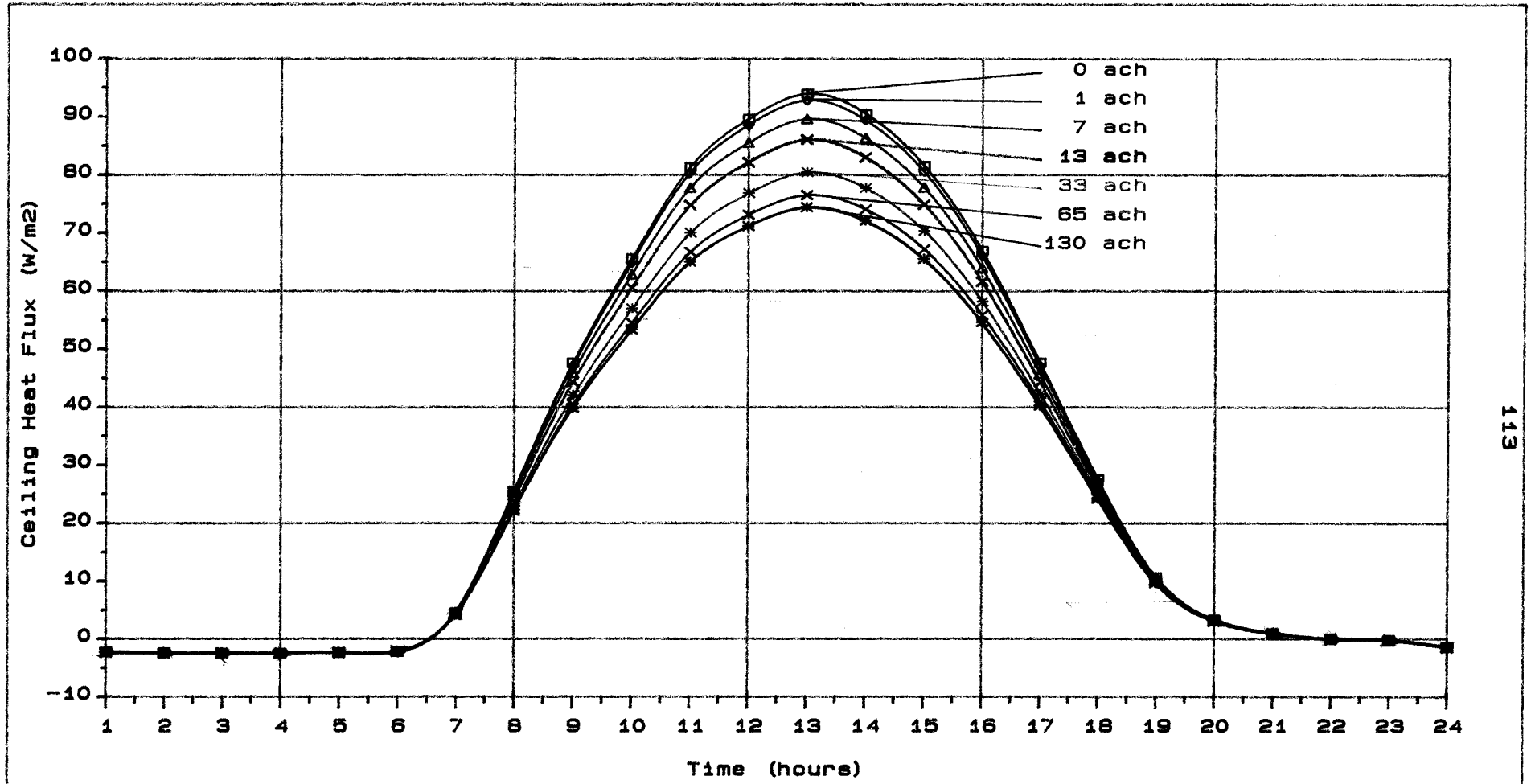

Figure 7.4 Ceiling heat flux under different rates of attic ventilation (summer, SR1).

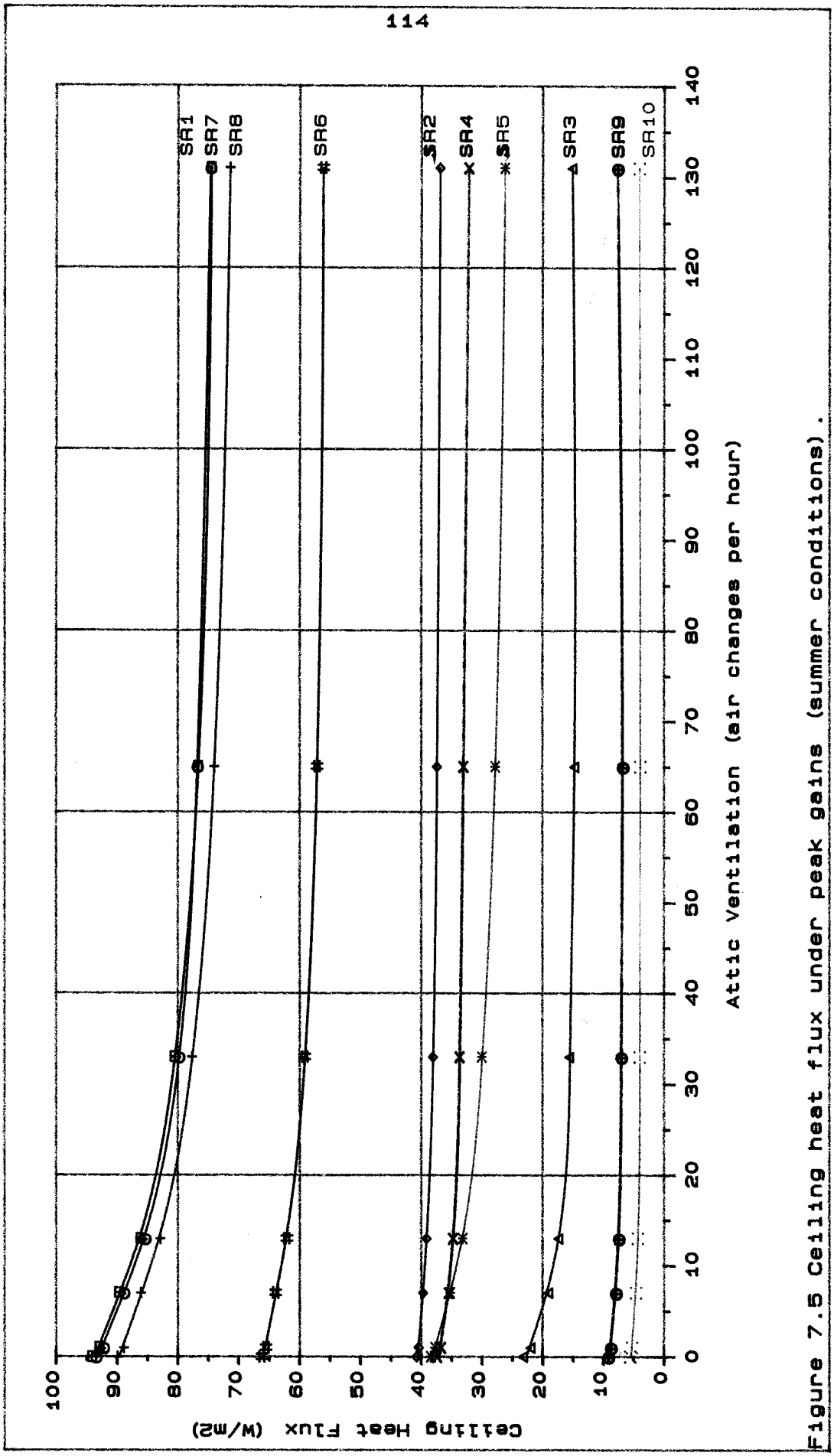

Figure 7.5 Ceiling heat flux under peak gains (summer conditions).

Table 7.3 Effective thermal resistance of ventilated attics during the summer day.

	Attic Ventilation (ach)						
	0	1	7	13	33	65	130
	(m^2 K/W)						
SR1	0.16	0.16	0.17	0.18	0.20	0.22	0.23
SR2	0.18	0.19	0.19	0.20	0.20	0.21	0.21
SR3	1.61	1.71	1.99	2.19	2.45	2.60	2.52
SR4	0.19	0.19	0.19	0.20	0.20	0.21	0.21
SR5	0.20	0.21	0.27	0.32	0.41	0.48	0.54
SR6	0.17	0.17	0.18	0.19	0.21	0.22	0.23
SR7	0.15	0.15	0.16	0.17	0.20	0.21	0.22
SR8	0.16	0.17	0.17	0.19	0.21	0.23	0.24
SR9	1.89	1.98	2.19	2.33	2.49	2.57	2.25
SR10	2.69	2.89	3.38	3.68	4.04	4.14	3.90

7.5 RESULTS FOR TYPICAL WINTER DAY

Figure 7.6 presents some temperatures for the standard house (WR1) without attic ventilation. At the time of the lowest outside air temperature, 7h , the inside ambient air temperature was about 3K higher. At this time the temperature of the under-side of ceiling was similar to that of the room air. The floor temperature was warmer than the room air temperature throughout the day.

Figure 7.7 shows temperatures at the same locations as figure 7.6 for the standard house (WR1), but with 130 attic ach. The room air temperature and under-side of ceiling temperature are very similar to those without attic ventilation (figure 7.5) although the attic air temperature has dropped to lower values.

Figure 7.8 shows the ceiling heat flux for different rates of attic ventilation in the standard house (WR1). Attic ventilation reduced the heat gained during the day by 30% (13h) and increased night losses by 10% (7h).

Figure 7.9 presents the ceiling heat flux at the time of peak losses (7h) for all the variables studied (WR1 to WR10). Changing the roof slope now shows a significant difference. The shallower the roof slope, the more heat it looses to the sky by longwave radiation. Changing the roof slope from 20° to 10° (WR7) increased the losses by about 35%. (Note that this was the only case were the ventilation was beneficial). Changing from 20° to 30° (WR8), decreased the loss by about 8%. Doubling the wind convection

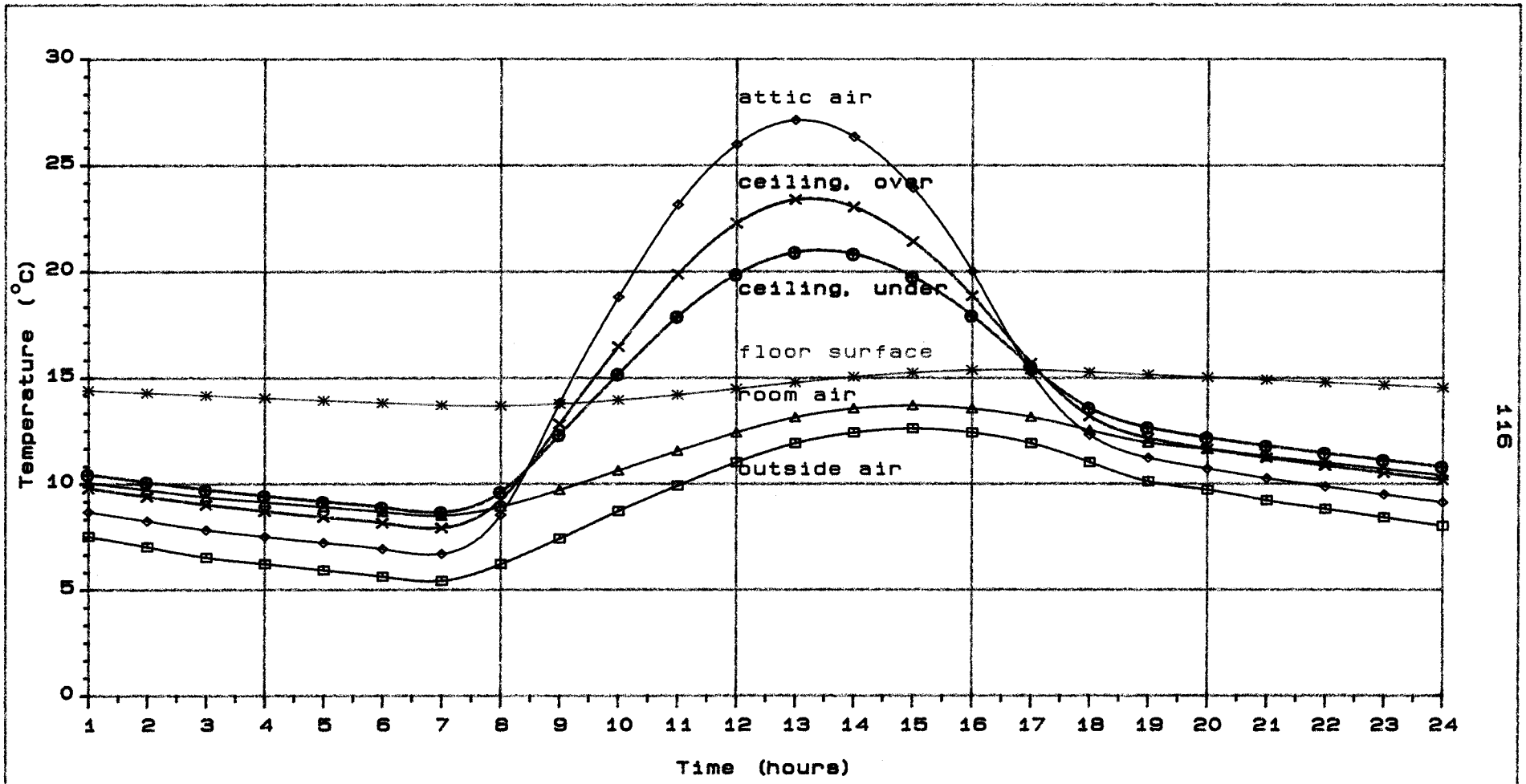

Figure 7.6 Temperatures associated with the standard house (winter, WR1), without attic ventilation

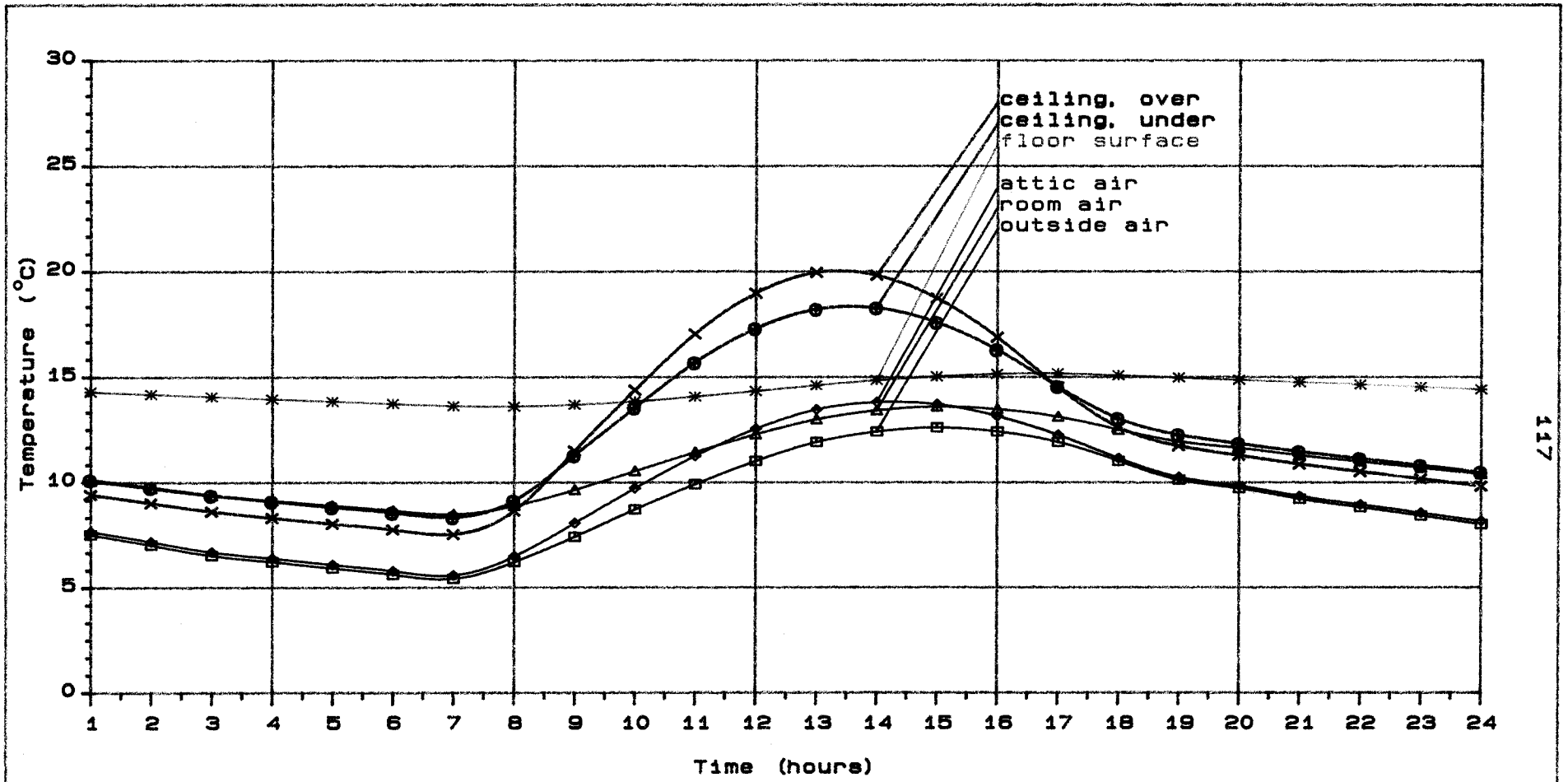

Figure 7.7 Temperatures associated with the standard house (winter, WR1), with attic ventilation of 130 ach

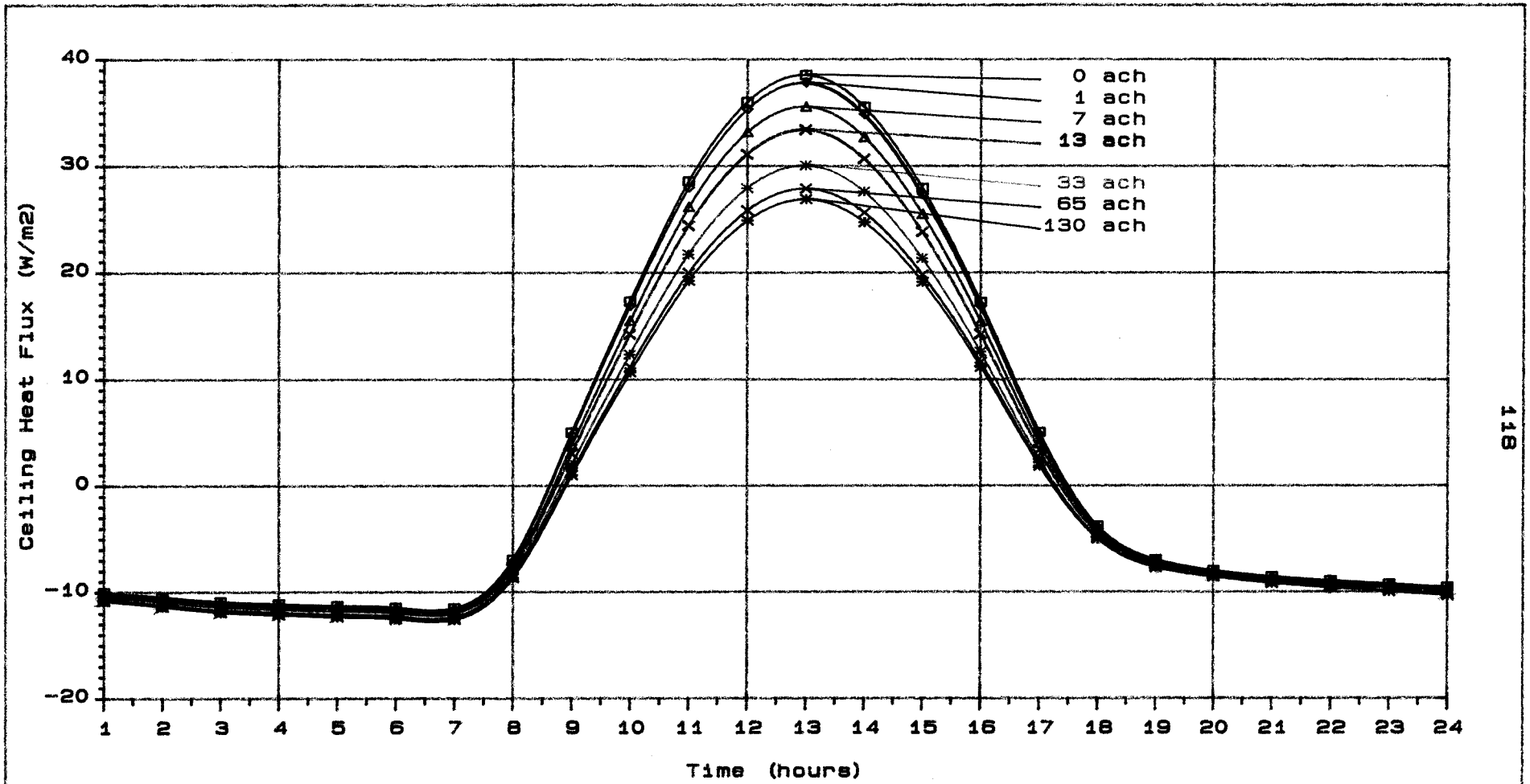

Figure 7.8 Ceiling heat flux under different rates of attic ventilation (winter, WR1).

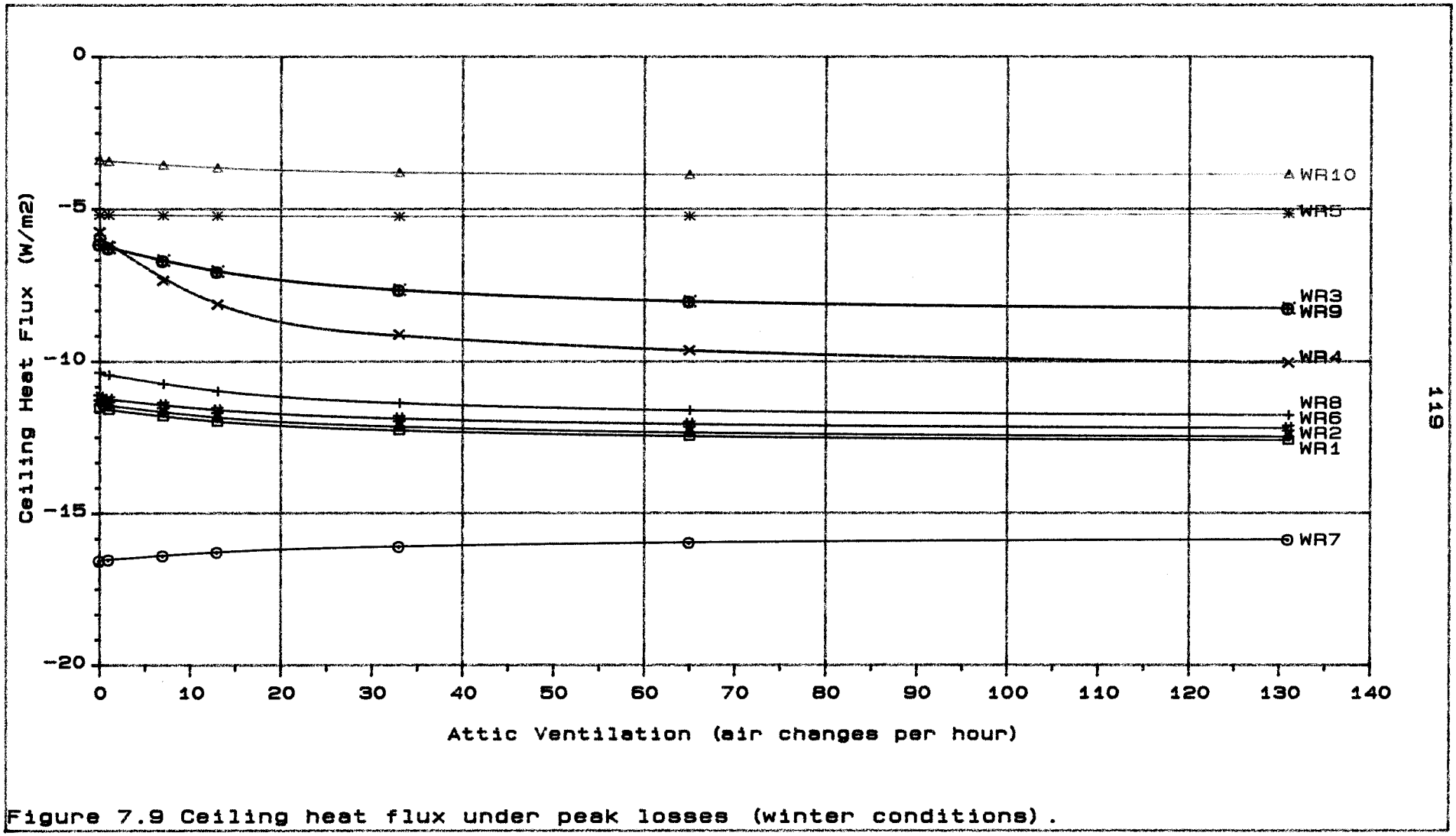

Figure 7.9 Ceiling heat flux under peak losses (winter conditions).

coefficient (WR6) reduced the losses by 3%. Lowering the solar absorptivity (WR2) decreased the losses by 1%. A glass fibre quilt under the roof cover (WR4) reduced the losses on average by 34%. Insulation over the ceiling (WR5) reduced the losses by 57%. Low roof to attic emissivity (WR3) alone or combined with low solar absorptivity (WR9) reduced the losses by 40%. Combining ceiling insulation and low roof to attic emissivity (WR10) further reduced the losses to 69%. Attic ventilation generally caused an increase in heat losses but for WR5 conditions there were no alteration and for WR7 only 4% decrease in losses. The increase in heat losses was 10% for WR1, WR2 and WR6, 15% for WR8 and WR10, 35% for WR3 and WR9 and 74% for WR4.

Reducing the heat losses by the attic space caused the temperature of the under-side of ceiling to increase. This reached 2K above room air temperature during the night for low attic ventilation (WR10). The temperature of the air in the room did not change.

Effective resistances of the ventilated attic were calculated throughout the day. Values at the time of maximum ceiling heat loss (7h) were chosen as representative for winter design conditions and are presented in table 7.4.

Table 7.4 Effective thermal resistance of ventilated attics during the winter day.

	Attic Ventilation (ach)						
	0	1	7	13	33	65	130
	(m^2 K/W)						
WR1	0.21	0.21	0.20	0.20	0.19	0.18	0.18
WR2	0.21	0.21	0.20	0.20	0.19	0.18	0.18
WR3	0.75	0.73	0.67	0.62	0.56	0.52	0.49
WR4	0.22	0.20	0.17	0.15	0.13	0.12	0.12
WR5	0.31	0.31	0.31	0.30	0.30	0.30	0.30
WR6	0.21	0.21	0.20	0.20	0.19	0.18	0.18
WR7	0.21	0.21	0.21	0.21	0.21	0.22	0.22
WR8	0.22	0.21	0.20	0.19	0.18	0.17	0.17
WR9	0.74	0.72	0.67	0.62	0.56	0.52	0.49
WR10	1.04	1.01	0.95	0.90	0.84	0.80	0.79

7.6 DISCUSSION AND CONCLUSION

During a summer day the slope of the roof has relatively little influence on the ceiling heat flux and the effective attic resistances (ER). Doubling the wind convection coefficient (SR6) had a marked effect on the ceiling heat flux but did not changed the ER. The literature is not conclusive about this coefficient (see section 2.2.3). A better understanding of it is needed if more accurate estimations of the summer heat gained through roofs are to be made. Placing the insulation under the roof (SR4) is difficult in practice and, when there was ventilation, was not as good as placing it over the ceiling (SR5). As attics should be ventilated for moisture removal, insulation is better placed over the ceiling.

Reductions in peak summer ceiling heat flux caused by high attic ventilation rates varied from 10 to 35%. This compares well with the 30% decrease in ceiling heat flux measured by van Straaten (1957) and also observed in the test roof for groups of tests D, E and F. A slightly higher value of 40% was measured by Kiyohara et al. 1984). Comparative values were observed in the test roof for groups B and G of tests. These reductions are small when compared with the reductions predicted for a roof having a low solar absorptivity or one having a low emissivity. The predicted reductions in ceiling heat flux caused by painting the roof white was 57%. This value is between the 50% calculated by Reagan and Acklam (1979) and the 66% measured by Lamberts (1983). Aluminium foil placed under the roof reduced the ceiling heat flux by 75%. Similar values were measured by Oliveira (1984 - 77%), Lotz (1964 - 82%) and Lamberts (1983 - 86%). The reduction in ceiling heat flux caused by insulating the ceiling was 59%, very similar to the reduction predicted by painting the roof white.

From the above it can be concluded that the most relevant variables for reducing the heat flux through the ceiling during summer are

- solar absorptivity,
- roof emissivity,
- ceiling thermal resistance.

Table 7.5 summarizes the effective thermal resistances for various combinations of these variables with a range of attic ventilation.

Table 7.5 Effective thermal resistance of ventilated attics for summer design in naturally ventilated houses with various rates of attic ventilation.

Solar Absorb.	Roof Emiss.	Ceiling Resistance (m^2 K/W)	Effective Thermal Resistance (m^2 K/W)					
			Attic Ventilation (ach)					
			0	1	7	13	33	65
0.80	0.90	0.06	0.16	0.16	0.17	0.18	0.20	0.22
0.30	0.90	0.06	0.18	0.19	0.19	0.20	0.20	0.21
0.80	0.90	0.69	0.20	0.21	0.27	0.32	0.41	0.48
0.80	0.50	0.06	0.28	0.28	0.30	0.31	0.35	0.37
0.80	0.20	0.06	0.61	0.63	0.68	0.71	0.74	0.77
0.80	0.05	0.06	1.61	1.71	1.99	2.19	2.45	2.60
0.30	0.05	0.06	1.89	1.98	2.19	2.33	2.49	2.57
0.30	0.05	0.69	2.69	2.89	3.38	3.68	4.04	4.14

The summer ER for a solar absorptivity of 0.8, a roof emissivity of 0.9 and a ceiling resistance of 0.69 m^2 K/W are 0.20 m^2 K/W without ventilation and 0.41 m^2 K/W with 33 ach. The ER calculated from the test roof observations were of the same order: group D - 0.18 m^2 K/W without ventilation and 0.27 m^2 k/W with 31 ach; group E - 0.22 m^2 K/W with 2 ach and 0.41 m^2 K/W with 31 ach; and group F - 0.21 m^2 K/W without ventilation and 0.30 m^2 K/W with 31 ach. McQuiston reported similar values: 0.18 m^2 K/W without ventilation and 0.49 m^2 K/W with 36 ach. The values given by ASHRAE (based on the work of Joy 1958) are higher: 0.33 m^2 K/W without ventilation and 1.50 m^2 K/W with 33 ach. Robinson et al. (1954) also reported a similar value, 0.21 m^2 K/W, for measurement of the thermal resistance of a 90 mm plane air space without ventilation with high emissivity, a mean temperature of 10K and a temperature difference of 16.7K.

The simulated summer ER for a solar absorptivity of 0.8 , a roof emissivity of 0.05 and a ceiling resistance of 0.06 m^2 K/W are 1.61 m^2 K/W without ventilation and 2.45 m^2 K/W with 33 ach. Joy's results (ASHRAE 1985) of 1.14 m^2 K/W without ventilation and 2.11 m^2 K/W with 33 ach are close to this. The resistance of a 90mm unventilated air space with a low emissivity (0.05) from Robinson

et al. 1954), is also similar: 1.44 m^2 K/W. No direct comparison can be made with either the experimental results or the McQuiston values because of the different roof emissivity.

Simulation SR3 was recalculated with an emissivity of 0.13 (same as in the test roof) and the ER values obtained were 0.86 m^2 K/W without ventilation and 1.09 m^2 K/W with 33 ach. These values compare well with the ER calculated from the observations on the test roof: in group B, it was 0.70 m^2 K/W without ventilation and 1.06 m^2 K/W with 31 ach and, in group G, it was 0.80 m^2 K/W without ventilation 1.19 m^2 K/W with 31 ach. The simulated ER's are also close to McQuiston values of 0.69 m^2 K/W without ventilation and 1.69 m^2 K/W with 36 ach.

The summer ER's calculated are thus consistent with information contained in the literature and values derived from the observations on the test roof (chapter 5). They are therefore recommended as design values for naturally ventilated houses in Brazil.

Under winter conditions, the slope of the roof affected heat losses. A low pitched roof lost considerably more heat to the sky than a high pitched one. Nevertheless, ER's for the different slopes were very similar.

Attaching the insulation under the roof (WR4) was clearly disadvantageous when compared to placing it over the ceiling. Losses increased considerably with ventilation when the insulation was attached under the roof.

Attic ventilation increased the heat losses except for a roof slope of 10° (WR7), where ventilation was actually beneficial.

In winter, the variables that proved to be most relevant for minimizing heat losses were

- roof emissivity,
- ceiling thermal resistance.

Table 7.6 summarizes the effective thermal resistance for various combinations of these variables over a range of attic ventilations.

Table 7.6 Effective thermal resistance of ventilated attics for winter design in unheated houses with various rates of attic ventilation.

Roof Emissivity	Ceiling Resistance (m^2 K/W)	Effective Thermal Resistance (m^2 K/W)					
		Attic Ventilation (ach)					
		0	1	7	13	33	65
0.90	0.06	0.21	0.21	0.20	0.20	0.19	0.18
0.90	0.69	0.31	0.31	0.31	0.30	0.30	0.30
0.05	0.06	0.75	0.73	0.67	0.62	0.56	0.52
0.05	0.69	1.04	1.01	0.95	0.90	0.84	0.80

ER's for roofs under winter conditions having a high emissivity and a ceiling thermal resistance of 0.69 m^2 K/W are 0.31 m^2 K/W without ventilation and 0.30 m^2 K/W with 33 ach. The values calculated by McQuiston are 0.26 m^2 K/W without ventilation and 0.21 m^2 K/W with 2 ach. Differences of 19% and 43% respectively. Winter ER's for roof with a low emissivity were recalculated for an emissivity of 0.1 to allow comparison with McQuiston's results. The values that were obtained were 0.9 m^2 K/W without ventilation and 0.88 m^2 K/W with 1 ach. McQuiston's values are 0.77 m^2 K/W without ventilation and 0.51 m^2 K/W with 2 ach. His ER values for roofs without ventilation are similar to the ones obtained in this study; however contradictory to the present results, his values showed a greater reduction with ventilation. This is probably due to his calculations being done for a heated house, where losses become more pronounced as attic ventilation increases.

The ER's calculated for winter conditions are also consistent with the literature and are therefore recommended as design values for unheated houses in the south of Brazil.

During summer, roof with low emissivity facing the attic has reduced the ceiling heat flux more than ceiling insulation, but during winter the insulation gave better results.

The average attic ventilation flow rate during a typical summer day in Porto Alegre is estimated to vary from 2 ach to 9 ach depending on the type and size of openings and roof material (chapter 3). A ventilation flow rate of 10 ach reduced the ceiling heat flux in the standard house by 7%. This is a very small reduction compared to improvements that can be gained from low solar absorptivity, low

attic emissivity or ceiling insulation. In addition, attic ventilation is disadvantageous during winter. It is therefore suggested that attic ventilation be kept to the minimum necessary for moisture removal under winter conditions.

Winter discomfort is reduced by casual heat gains from such things as lights, cooking and by metabolic process of inhabitants. Conversely summer discomfort is enhanced by these.

During summer, air temperatures indoors become too hot. If the roof is not carefully designed, ceiling surface temperatures become still higher than air temperatures. High levels of thermal discomfort can be caused by low radiant temperature asymmetries from hot ceilings. Temperatures of the under-side of ceiling surface as high as the ones predicted in the standard house (SR1) are not acceptable and it is crucial that ceiling heat flux be reduced. Lowering the solar absorptivity of the roof reduces the temperature difference between under ceiling surface and ambient air (from 11K-SR1 to 2K-SR2). Even greater ceiling heat flux reduction, and consequently lower ceiling temperatures can be obtained by combining low solar absorptivity with low roof emissivity. Room ceiling temperature 3K less than room air temperature were obtained (SR10). This is due to the high thermal resistance of the attic and low temperature of the floor. It highlights the importance of considering the building as a whole for thermal design purposes.

CHAPTER 8 CONCLUSIONS

Standardizing the thermal performance requirements of low cost houses in Brazil is essential if the country is to safeguard the health and well-being of its inhabitants. The roof, being the most exposed element of the building, is of great interest and reliable thermal performance data is required by designers involved in low cost housing developments.

On site data is difficult to collect and so mathematical models played an important role in this work. The observations from the test roof gave an insight into the heat transfer process through ventilated attics and provided experimental validation of the mathematical models. It was shown that models considering only two surfaces (roof and ceiling) did not predict the ceiling heat flux with sufficient accuracy, due to the over simplification of the heat transfer process. The five surface models produced data that agreed with the observations. The seven surface models only slightly improved the accuracy and, due to uncertainties associated with the input data, the increase in accuracy was not enough to justify their additional complexity. The unsteady state model developed from the best steady state model was the most complex and included the response of the whole house to the heat transferred through the roof. This was very important and showed the influence the floor temperature has on keeping the indoor air temperature cool. Also, effective resistances of ventilated attics were obtained with this model and are suggested as design values. They allow simpler and more accurate calculation of the heat transfer through different roofs. Although they were calculated with Porto Alegre climatic data, the summer values are considered to be valid throughout Brazil.

Reducing summer ceiling heat flux lowered the internal air temperature below that of the outside air. The most important reduction was in the temperature of the ceiling surface. This affects the radiation component which is crucial in minimizing the thermal discomfort caused by the already high air temperatures.

The methods of reducing the heat transferred from the attic space to the living quarters that were studied involved using a low emissivity material in the attic (aluminium foil), painting the roof

white, insulating the ceiling and ventilating the attic. Comments on the use of each of these are given below.

Aluminium Foil

The main heat transfer mechanism through an attic is radiation. Lowering the emissivity of the roof or the ceiling is a very effective way of reducing the amount of heat transfered through the attic to the room below. Ceiling heat flux reductions of 75% were found by placing aluminium foil under an old asbestos cement roof.The low emissivity material is better placed on the under-side of the roof so as to minimize dust accumulation which is detrimental. In dusty areas, attic ventilation should be kept to a minimum. There is some controversy in the literature about the effects of time on the thermal performance of these radiation barriers and more research is needed. As this technique is extremely beneficial in reducing the ceiling heat flux, methods of keeping the emissivity low for long periods of time should be sought.

White Roof Surface

Reducing the solar absorptivity of external roof surfaces enhances the reflection of a large amount of energy coming from the sun. It also protects the roof material. Ceiling heat flux reductions of 57% were predicted by painting an old asbestos cement roof white. This technique has the potential to be an outstanding improvement in the north of Brazil where year round heat gain is a serious problem. It is nevertheless an improvement that needs periodical maintenance.

Ceiling Insulation

Placing insulation above the ceiling is the most usual way of reducing the heat flux through it. A 25mm quilt of glass fibre reduced the ceiling heat flux by 59%. This reduction was similar to the one obtained by painting the roof white. White coloured roofs however, are not effective in winter, whereas insulation is. Ceiling insulation is the most reliable solution for ceiling heat flux reductions, but the cost limits its application in low cost houses. Aluminium foil can also play a major role in ceiling insulation as a lining in sealed cavities.

Attic Ventilation

Ventilating the attic space was the least effective way of reducing ceiling heat flux. Contrary to intuitive reasoning, attic ventilation has a minor effect on the downward heat flux because the main form of heat transfer from roof to ceiling is by radiation. Predicted reductions to the ceiling heat flux caused by very high ventilation rates (130 ach) varied from 10% to 35% in simulations with the unsteady state model. Slightly higher values, 30% to 40%, were observed in the test roof with lower ventilation rates (31 ach).

Increasing attic ventilation usually means providing larger openings; these must be protected against driving rain and ingress of small animals. This generally implies extra cost. Due to the small reductions predicted in ceiling heat flux, it is better to save this expenditure and allocate it to the other improvements mentioned earlier. The main criterion governing the need for attic ventilation should be the avoidance of condensation.

Combined Solutions

Combining an insulated ceiling with aluminium foil under the roof and painting the roof white produced a very low ceiling heat flux. It is not necessary to have all these improvements in low cost houses, but at least one is needed to reduce thermal discomfort in the house during summer. The most effective is aluminium foil followed by white paint and ceiling insulation. The latter two being of similar benefit. Choosing among the three methods involves a cost analysis approach. Further research is needed to establish the long term deterioration and maintenance cost of these solutions.

Thermal Comfort

The physiological and psychological effects of an over-heated ceiling combined with a high air temperature are not well understood. Koenigsberger and Lynn (1965) suggested a maximum of 4.5 K for the difference between ceiling and air temperatures. The standard roof analysed in chapter 7 (old asbestos cement - attic - 10mm plaster board) produced a temperature difference of 11 K. This would be very uncomfortable. Any of the improvements studied, apart from attic ventilation, reduced the ceiling-air temperature

difference to below 2 K; well below the suggested limit of 4.5 K. Combining a white roof surface with aluminium foil and an insulated ceiling produced ceiling temperatures 3 K lower than the room air temperatures; a situation very much desired to allow radiative cooling of the body.

This work has contributed significantly to the theoretical and experimental understanding of heat transfer mechanisms through ventilated attics of Brazilian houses. The external surface heat balance including shortwave and longwave radiation, wind convection and evaporation, allied to an air permeable roof, is extremely difficult to be simulated in laboratory. Direct field observations are now required to test the assumptions made and the design data provided.

Suggestions for Further Work

- Field validation of the unsteady state model and verification of the wind convection coefficient relationship used.
- Field observations of effective attic thermal resistances and measurements of attic ventilation flow rates and attic air speeds.
- Effect of time on the thermal performance of aluminium foil in attics.
- Long term deterioration of white painted roof surfaces.
- Physiological and psychological effects of high ceiling temperature on persons subjected to high air temperatures (above comfort).
- Study of the natural evaporative cooling process in clay tiles envisaging its optimization in humid climates.
- Study of local materials for the development of cheap ceiling insulation.

REFERENCES

Ahmad, A.M. 1974. On Ceiling Heights and Human Thermal Comfort. *Overseas Building Notes* no. 155, Building Research Establishment, Watford, U.K.

Alamdari, F. and Hammond, G.P. 1983. Improved Data Correlations for Buoyancy-Driven Convection in Rooms. *BSER & T*, vol. 4, no. 3, pp. 106-12.

Anderson, B.R. 1980. The Assessment of U-Values for Insulated Roofs. *BSER & T*, vol. 1, no. 3, pp. 119-22.

Anderson, B.R. 1981. The Thermal Resistance of Air Spaces in Building Constructions. *Building and Environment*, vol. 16, no. 1, pp. 35-39.

Anderson, B.R. and Ward T.I. 1981. Measurements of Heat Loss Through an Insulated Roof. *BSER & T*, vol. 2, no. 2, pp. 65-72.

Aroztegui, J.M. 1981. Estudo das Temperaturas Internas de Tres Conjuntos Habitacionais COHAB-RS Construidos com Tecnologias Diferentes (Study of the Internal Temperatures of Three Housing Developments from COHAB-RS Built with Different Technologies). In *Proceedings of the Latin American Symposium: Rational Organization of Buildings Applied to Low Cost Housing*. October. Sao Paulo, Brazil, pp. 647-61.

Ashley, S.K. 1984. Basic Wind Pressure Difference Coefficient Data Set for Pitched or Flat Roof Rectangular Buildings. In 1984 Wind Pressure Workshop. Brussels. *AIC Technical Note 13.1*, Air Infiltration Centre, pp. 123-28.

ASHRAE. 1985. *Handbook - Fundamentals, SI Edition*. American Society of Heating, Refrigerating and Air-Conditioning Engineers. Atlanta, GA, U.S.A.

Azevedo, S. and Andrade, L.A.G. 1981. *Habitaçao e Poder* (Housing and Power). Zahar Editores, Rio de Janeiro, Brazil.

Beckett, H.E. 1935. New Equipment for the Investigation of Heat Transmission Through Roofs. *Journal IHVE*, vol. 3, pp. 530-33.

Berdahl, P. and Fromberg, R. 1982. The Thermal Radiance of Clear Skies. *Solar Energy*, vol. 29, no. 4, pp. 299-314.

Berdahl, P. and Martin, M. 1978. The Resource for Radiative Cooling. In *Proceedings of the Second National Passive Solar Conference, Passive Solar: State of the Art*. Philadelphia, Pennsylvania, U.S.A., pp. 684-86.

Berdahl, P. and Martin, M. 1984. Emissivity of Clear Skies. *Solar Energy*, vol. 32, no. 5, pp. 663-64.

Bliss, R.W. 1961. Atmospheric Radiation Near the Surface of the Ground: A Summary for Engineers. *Solar Energy*, vol. 5, no. 3, pp. 103-20.

Bogle, A., McMullan, J.T. and Morgan, R. 1984. An Experimental Examination of the Effects of Rainfall on the Heat Loss from a Red Brick Wall. *Energy Research*, vol. 8, pp. 1-18.

Boldrin, B., Scalabrin, G., Lazzarin, R. and Sovrano, M. 1978. Cooling of a Fluid by a Noturnal Radiator. In *Energy Conservation in Heating, Cooling and Ventilating Buildings*. ed. Hoogendoorn, C.J. and Afgan, N.H.. Washington, London, Hemosphere Publ. pp. 839-51.

British Standard Institution. 1973. *BS 874 - Methods for Determining Thermal Insulating Properties with Definition of Thermal Insulation Terms*.

British Standards Institution. 1981. *BS 1042- Measurement of Fluid Flow in Closed Conduits. Part 1: Pressure Differential Devices. Section 1.1: Orifice Plates, Nozzles and Venturi Tubes Inserted in Circular Cross-Sectional Conduits Running Full*.

Burch, D.M. and Harrje, D.T. 1985. A State-of-the-Art Research Assessment for Residential Attic Condensation. In *Conference on Moisture Problems in Residential Construction: Separating Myth from Reality*. October. Seatle, Washington, U.S.A.

Cheema, L.S., Castor, S.E. and Ribeiro, C.M.C. 1978. Refrigeraçao a Baixo Custo em Casas no Nordeste do Brasil (Low Cost Air-Conditioning in Houses on Northeast Brazil). In *Simposio Latino-Americano de Energia Solar*. Paraiba, Brazil, pp. 949-58.

Chrenko, F.A. 1953. Heated Ceilings and Comfort. *Journal IHVE*, vol. 20, pp. 375-96 and vol. 21, pp. 145-54.

CIBSE. 1986. *CIBSE Guide Volume A*. The Chartered Institution of Building Services Engineers. London.

Clarke, J.A. 1985. *Energy Simulation in Building Design*. Bristol, U.K., Adam Hilger LTD.

Cole, R.J. 1976a. The Longwave Radiation Environment Around Buildings. *Building and Environment*, vol. 11, pp. 3-13.

Cole, R.J. 1976b. The Longwave Radiation Incident Upon the External Surface of Buildings. *BSE*, vol. 44, Dec, pp. 195-206.

Cross, B.M. 1984. The Use of a Solar Reflective Coating to Reduce Cooling Loads in Buildings. In *Efficient Use of Energy in Buildings. Proceedings of UK-ISES*. ed. Gillett, N.B. and Morton, J., U.K., pp. 81-83.

Duffie, J. and Beckman, W. 1980. *Solar Engineering of Thermal Processes*. New York, John Willey & Sons.

Fairey, P.W. 1982. Effects of Infrared Radiation Barriers on the Effective Thermal Resistance of Building Envelopes. In Proceedings of Thermal Performance of the Exterior Envelope of Buildings II. *ASHRAE Special Publication 38*. U.S.A., pp. 859-75.

Fairey, P.W. and Bettencourt, W. 1981. "La Sucka" - A Wind Driven Ventilation Augmentation and Control Device. In *Passive Cooling*. Bowen, A., Clark, E. and Labs, K. US-ISES, pp. 196-200.

Fanger, P.O. 1986. Radiation and Discomfort. *ASHRAE Journal*, vol. 28, no. 2, pp. 33-34.

Fanger, P.O., Banhidi, L., Olesen, B.W. and Langkilde, G. 1980. Comfort Limits for Heated Ceilings. *Transactions ASHRAE*, vol. 86, no. 2, pp. 141-56.

Ferraro, R., Godoy, R. and Turrent, D. 1983. *Monitoring Solar Heating Systems- A Practical Handbook*. Oxford, Pergamon Press.

Flanders, S.N. 1985. Confidence in Heat Flux Transducer Measurements of Buildings. *Transactions ASHRAE*, vol. 91, no. 1B, pp. 515-31.

Fundaçao Joao Pinheiro. 1984. *Diagnostico Nacional da Industria da Construçao* (National Diagnostic of the Construction Industry). Volume 1. Belo Horizonte, Brazil.

Gids, W.F. 1984. Wind Pressure on Roof Vents. In 1984 Wind Pressure Workshop. Brussels. *AIC Technical Note 13.1*, Air Infiltration Centre, pp. 133.

Givoni, B. 1962. The Effect of Roof Construction Upon Indoor Temperature. In *International Bioclimatological Congress*, London. Pergamon Press.

Higgs, F.S. and Hand, J.W. 1978. Assessing the Viability of the Sky as Heat Sink for Passive Cooling in North Central Texas. In *Proceedings of the Second National Passive Solar Conference, Passive Solar: State of the Art*. Philadelphia, Pennsylvania, U.S.A.

Hoglund, B.I., Mitalas, G.P. and Stephenson, D.G. 1967. Surface Temperatures and Heat Fluxes for Flat Roofs. *Building Science*, vol. 2, pp. 29-36.

IHVE. 1970. *Guide Book A*. The Institution of Heating and Ventilating Engineers, London.

Incropera, F.P. and De Witt, D.P. 1981. *Fundamentals of Heat Transfer*. New York, John Willey & Sons.

IPT. 1979. *Desempenho Termico de Coberturas* (Thermal Performance of Roofs). Instituto de Pesquisas Tecnologicas, Sao Paulo, Brazil.

Ito, N., Kimura, K. and Oka, J. 1972. A Fiel Experiment Study on The Convective Heat Transfer Coefficient on Exterior Surface of a Building. *Transactions ASHRAE*, vol. 78,pp. 184-91.

Joy, F.A. 1958. Improving Attic Space Insulating Values. *Transactions ASHRAE*, vol. 64, pp. 251-66.

Kiyohara, E., Jabardo, J.M.S. and Affonso Jr., W. 1984. *Conforto Termico - Relatorio Final* (Thermal Comfort - Final Report).

Instituto de Pesquisas Tecnologicas do Estado de Sao Paulo (IPT), Relatorio no. 21326, Sao Paulo, Brazil.

Klucher, T.M. 1979. Evaluation of Models to Predict Insolation on Tilted Surfaces. *Solar Energy*, vol. 23, pp. 111-14.

Kneubuhl, F.K., Finger, G., Thiebaud, F., Zurcher, Ch., Sagelsdorff, R. and Frank, Th. 1981. Energy Saving by Reduction of Thermal Radiation from Building Envelopes. In *Building Energy Management*. ed. Fernandes, E.O., Woods, J.E. and Faist, A.P. Oxford, Pergamon Press.

Koenigsberger, O. and Lynn, R. 1965. Roofs in the Warm Humid Tropics. *Architectural Association Paper no. 1*, London.

Kreith, F. 1973. *Principles of Heat Transfer*. 3rd edition.New York, London, Harper and Row.

Kronvall, J. 1985. Ventilation Strategies for Crawl-Spaces, Attics, Etc. In *Ventilation Strategies and Measurement Techniques*. 6th AIC Conference, September 16-19. Netherlands.

Lamberts, R. 1983. *Desempenho Termico de Coberturas Leves com Atico: Bancada de Testes e Modelo Matematico* (Thermal Performance of Light Weight Roofs with Attic: Test Rig and Mathematical Model). MSc dissertation. Curso de Pos-Graduaçao em Engenharia Civil, UFRGS, Porto Alegre, Brazil.

Liddament, M.W. 1986. *Air Infiltration Calculation Techniques - An Applications Guide*. Air Infiltration and Ventilation Centre, Bracknell, U.K.

Liddament, M.W. and Allen, C. 1983. The Validation and Comparison of Mathematical Models of Air Infiltration. *AIC Technical Note 11*. Air Infiltration and Ventilation Centre, Bracknell, U.K.

Lotz, F.J. 1964. The Effect of Dust on the Efficacy of Reflective Metal Foil Used as Roof/Ceiling Insulation. *CSRI Research Report 212*, Pretoria, South Africa.

Loudon, A.G. 1963. Heat Transmission Through the Roofs of Buildings. *Journal IHVE*, vol. 31, pp. 273-298.

Lund, C.E. and Lander, R.M. 1961. Heat Transfer Through Mineral Wool Insulation in Combination with Reflective Surfaces. *ASHRAE Journal*, vol. 3, pp. 47-54, 98, 100, 102, 104.

Maricato, E. 1983. *Industria da Construçao e Politica Habitacional* (Construction Industry and Housing Policy). Doctorate Thesis. Faculdade de Arquitetura e Urbanismo, Universidade de Sao Paulo, Sao Paulo, Brazil.

Martin, M. and Berdahl, P. 1984a. Characteristics of Infrared Sky Radiation in the United States. *Solar Energy*, vol. 33, no. 3/4, pp. 321-36.

Martin, M. and Berdahl, P. 1984b. Summary of Results from the Spectral and Angular Sky Radiation Measurements Program. *Solar Energy*, vol. 33, no. 3/4, pp. 241-52.

McAdams, W.H. 1958. *Heat Transmission*. 3rd edition. Tokio, McGraw Hill.

McQuiston, F.C., Der, S.L. and Sandoval, S.B. 1984. Thermal Simulation of Attic and Ceiling Spaces. *Transactions ASHRAE*, vol. 90, no. 1A, pp. 139-63.

Mukhtar, Y.A. 1978. Roofs in Hot Dry Climates With Special Reference to Northern Sudan. *Overseas Building Notes no 182*, Building Research Establishment, Watford, U.K.

Mumaw, J.R. 1980. Thermal Research Facility - A Large Calibrated Hot Box for Horizontal Building Elements. In *Thermal Insulation Performance. ASTM STP 718*. ed McElroy, D.L. and Rye, R.P., U.S.A., pp. 195-207.

NAG. 1984. *Numerical Algorithms Group Fortran Library Manual*, Mark 11, vol. 1. Oxford.

Nayak, J.K., Srivastava, A., Singh, U. and Sodha, M.S. 1982. The Relative Performance of Different Approaches to the Passive Cooling of Roofs. *Building and Environment*, vol. 17, no. 2, pp. 145-61.

NBS. 1979. Summer Attic and Whole-House Ventilation. Proceedings of a Workshop. *NBS Special Publication 548*. U.S.A.

Oliveira, A.M.de. 1984. *Analise Experimental do Desempenho Termico de Verao do Telhado de Cimento-Amianto com Atico* (Experimental Analysis of Summer Thermal Performance of Asbestos Cement Roofs with Attic). MSc dissertation. Curso de Pos-Graduaçao em Engenharia Civil, UFRGS, Porto Alegre, Brazil.

Parmelee, G. and Aubele, W.W. 1952. Radiant Energy Emission of Atmosphere and Ground. *Transactions ASHVE*, no. 1442, pp. 85-106.

Peavy, B.A. 1979. A Model for Predicting the Thermal Performance of Ventilated Attics. In *Summer Attic and Whole-House Ventilation*. NBS SP 548. U.S.A. pp. 119-49.

Pitts, A.C. and Ward, I.C. 1983. *A Review of the Prediction and Investigation of Air Movement in Buildings*. BS69 Department of Building Science, University of Sheffield, U.K.

Pratt, A.W. and Daws, L.F. 1958. Some Observations of Heat Transmission in Winter Through Factory Roofs. *Journal IHVE*, vol. 26, pp. 73-9.

Reagan, J.A. and Acklam, D.M. 1979. Solar Reflectivity of Common Building Materials and its Influence on the Roof Heat Gain of Typical Southwestern U.S.A Residences. *Energy and Buildings*, vol. 2, pp. 237-48.

Robinson, H.E., Powlitch, F.J. and Dill, R.S. 1954. The Thermal Insulation Value of Airspaces. *Housing Research Paper no 32*, Housing and Home Finance Agency, U.S. Gov. Printing Office, U.S.A.

Rucker, J.L. and Mumaw, J.R. 1981. Calibration Procedures and Results for a Large Calibrated Hot Box. In *Thermal Performance of Exterior Envelope of Buildings. ASHRAE SP28.* U.S.A.

Sabuja, G.S. 1986. Heat Loss from Pitched Roofs. *BSER & T*, vol. 7, no. 4, pp. 146-52.

Sattler, M.A. 1986. *The Generation of Climatic Building Design Data From Meteorological Data With Particular Reference to Porto Alegre (30° 02'S; 51° 13'W), Brazil.* BS 80 Department of Building Science, University of Sheffield, U.K.

Sattler, M.A., Sharples, S. and Page, J.K. 1987. The Geometry of the Shading of Buildings by Various Tree Shapes. *Solar Energy*, vol. 38, no. 3, pp. 187-201.

Schubert, R.P. and Kennedy, B. 1981. The Testing of Full Scale Ventilator Cap Types to Determine Their Effect on Natural Ventilation. In *Passive Cooling.* ed Bowen, A., Clark, E. and Labs, K., US-ISES, pp. 201-5.

Sharples, S. 1984. Full-Scale Measurements of Convective Energy Losses from Exterior Building Surfaces. *Building and Environment*, vol. 19, no. 1, pp. 31-39.

Sodha, M.S., Bansal, N.K., Bansal, P.K., Kumar, A. and Malik, M.A.S. 1986. *Solar Passive Building, Science and Design.* Oxford, Pergamon Press.

Taylor, J.R. 1982. *An Introduction to Error Analysis.* U.S.A., Oxford University Press.

Tinker, J.A. 1984. *Aspects of Mix Proportioning and Moisture Content on the Thermal Conductivity of Lightweight Aggregate Concretes.* PhD Thesis, Department of Applied Acoustics, University of Salford, U.K.

Unsworth, M.H. and Monteith, J.L. 1975. Longwave Radiation at the Ground. I. Angular Distribution of Incoming Radiation. *Quart. J. R. Met. Soc.*, vol. 101, pp. 13-24.

Vahid, F. 1982. Theoretical Consideration for the Effect of Rainfall in the Mathematical Models for Simulation of the Thermal Behaviour in Houses. *BSER & T*, vol. 3, no. 1, pp. 30-34.

Valentin, J. 1981. Desempenho Termico: Coberturas de Fibro-Cimento (Thermal Performance: Asbestos Cement Roof). In *Proceedings of the Latin American Symposium: Rational Organization of Buildings Applied to Low Cost Housing.* October. Sao Paulo, Brazil, pp. 615-32.

Van Straaten, J.F. 1967. *Thermal Performance of Buildings.* London, Elsevier Publ. Comp.

Van Straaten, J.F., Roux, A.J.A. and Richards, S.J. 1957. The Effects of Attic Ventilation on The Indoor Thermal and Ventilation Conditions in Dwellings of Conventional Construction. *Bulletin no. 15*, National Building Institute, Pretoria, South Africa.

Whiteley, P. and Gardiner, D. 1981. Solar Reflectivite Paints. *Information Paper no. 26*, Building Research Establishment, Garston, U.K.

Wilkes, G.B., Hechler, F.G. and Queer, E.R. 1940. Thermal Test Coefficient of Aluminium Insulation for Buildings. *Transactions ASHVE*, vol. 46, pp. 109-24.

Wilkes, K.E. 1981. Modelling of Residential Attics. In *Thermal Performance of the Exterior Envelope of Buildings I. ASHRAE SP 28*. U.S.A., pp. 436-55.

Wilkes, K.E. 1982. Dynamic Thermal Performance of Walls and Ceilings/Attics. In *Thermal Performance of the Exterior Envelope of Buildings II. ASHRAE SP 38*. U.S.A., pp. 131-59.

Wilkes, K.E. and Rucker, J.L. 1983. Thermal Performance of Residential Attic Insulation. *Energy and Buildings*, vol. 5, pp. 263-77.

Wiren, B.G. 1984. Wind Pressure Distributions and Ventilation Rates for a Single-Family House as Influenced by Surrounding Buildings - A Wind Tunnel Study. In 1984 Wind Pressure Workshop. Brussels. *AIC Technical Note 13.1*, Air Infiltration and Ventilation Centre, pp. 75-101.

Yarbrough, D.W. 1983. *Assessment of Reflective Insulation for Residential and Comercial Application*. Oak Ridge National Laboratory (TM-8891), TN, U.S.A.

APPENDIX 1

Measuring the Thermal Conductivity of Plywood and Calibration of Heat Flux Meters

1 Plain Hot-Plate Apparatus

A plain hot-plate apparatus was used to measure the thermal conductivity of the plywood used for the ceiling in the test roof and also to calibrate the heat flux meters. It was designed to meet the specifications of British Standard 874 (1973) and amendment AMD 3006 (1979). The main part of the equipment is described in detail elsewhere (Tinker 1984). An improved data logging system was added which interfaced data acquisition to data analysis. The logger used was a MFI 1000 series (CIL-Electronics Ltd) with 24 channels linked via a RS 232 communication port to an IBM XT micro computer where the data analysis was carried out. The equipment is shown in figure A1.1.

The apparatus was calibrated for edge heat loss using 40 mm glass fibre samples. The temperature difference between the hot and cold plates was varied from 6 to 26 K. Measured thermal conductivities were compared with those obtained on the same samples in a guarded hot-plate apparatus at a British Calibration Service approved laboratory. The heat loss at various temperature differences was determined. The overall measurement error ($\Delta\lambda$), including random and systematic errors, was estimated to be $\pm$ 3%.

2 Thermal Conductivity of the Plywood

The ceiling of the test roof was constructed from a sheet of 18 mm plywood. Two samples, 300 mm x 300 mm, were cut from it and their thermal conductivity measured in the plain hot-plate apparatus. The samples had a mean dry density of 630 kg/m^3 and an equilibrium moisture content of 4.9% by volume. Their measured thermal conductivity was 0.13 W/m K. This compares well with 0.14 W/m K given by CIBSE (1986).

3 Calibration of the Heat Flux Meters

Heat flux meters (HFMs) produce a voltage proportional to the heat flux passing through them. To obtain the heat flux rate, the

Figure A1.1 Plain hot plate apparatus, data logging system and micro computer used for data analysis.

voltage is multiplied by a constant that is generally supplied by the manufacturer.

The HFMs were a disturbance in the environment where they should measure the heat flux. The measurement desired was the heat flux through the ceiling (plywood), but what was actually being measured was the heat flux through a sandwich of plywood-sensor-plywood. As the thermal conductivity of the sensor (0.2 to 0.3 W/m K) was different from that of the plywood (0.13 W/m K), the measured heat flux was higher than the undisturbed ceiling heat flux through the plywood. Thus, a conversion factor to the HFMs constants was necessary. The HFMs were calibrated embedded in the same square pieces 300 mm by 300 mm of plywood that were used during the roof experiment (see chapter 6).

3.1 Conversion Factor

To determine the conversion factor, two HFMs were placed in the plain hot-plate apparatus, one on each side of the hot-plate, as for a normal measurement of thermal conductivity (figure A1.2).

The heat flux rate (q/S) through the plywood is given by

$$q/s = \Delta t.\lambda/l \qquad (A1.1)$$

where

Δt - the temperature difference across the plywood, K
λ - thermal conductivity, W/m K
l - thickness, m

To determine the converted sensor's constant the q/S value was divided by its emf reading. Tests were carried out with temperature differences across the samples of 5, 10 and 15 K. No important variation of the constant was found over this range.

The constants determined for the three sensors are presented in table A1.1 and compared with the values supplied by the manufacturer for homogeneous heat flux.

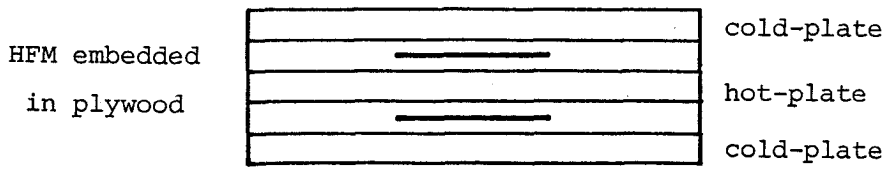

Figure A1.2 Plain hot-plate apparatus with HFM embedded in plywood for non-homogeneous heat flux calibration.

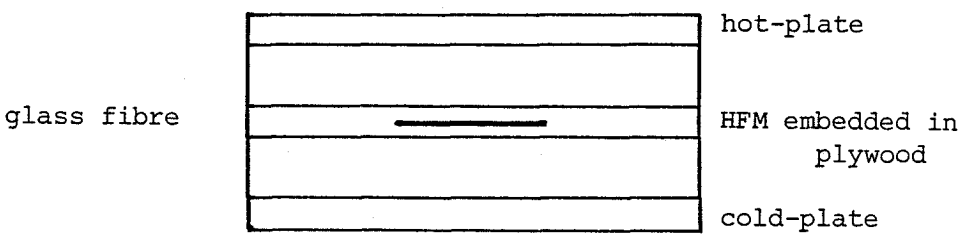

Figure A1.3 Plain hot-plate apparatus with HFM embedded in plywood and glass fibre samples for homogeneous heat flux calibration.

Table A1.1 Constants for the three HFMs.

	A Manufacturer (W/m^2 mV)	B Measured (W/m^2 mV)	B/A Conversion Factor
HFM1	5.30	4.62	0.87
HFM2	5.30	4.78	0.90
HFM3	5.30	4.66	0.88

A theoretical conversion factor was also calculated according to Flanders (1985). As the precise thermal conductivity of the sensor was not known, a range varying from 0.90 to 0.94 was found. Therefore, the conversion factors found in these measurements for sensors HFM1 and HFM3 were considered slightly too low and it was decided to check the manufacturers constant for homogeneous heat flux.

3.2 Check of the Manufacturer's Constants

To generate an homogeneous heat flux through the embedded sensor, it was placed between two 40 mm slabs of glass fibre. The sandwiched HFM was then located between the hot and one of the cold plates in the thermal conductivity apparatus (figure A1.3). The difference between the heat flux through the sensor and through the plywood was estimated to be only about 0.4%. Analysis of the first results showed the importance of carrying out the experiments with the plywood at ambient temperature to minimize edge losses, so that measurements were only made when this condition was satisfied. The heat flux rate through the glass fibre was calculated from the temperature difference across it, its thickness and its thermal conductivity (measured in a guarded hot-plate). The constants applicable to the individual HFM were then obtained by dividing this value by the emf given by the sensors. These are presented and compared with manufacturer's values in table A1.2. The differences range from 3.7 to 6.0%

Table A1.2 Measured and manufacturer's supplied constants for the three HFMs under homogeneous heat flux.

	Measured ($W/m^2.mV$)	Manufacturer	Δ%
HFM1	5.03	5.30	5.4
HFM2	5.11	5.30	3.7
HFM3	5.00	5.30	6.0

Comparing the non-homogeneous heat flux constants with the homogeneous ones (table A1.3), the conversion factors now fall within the calculated range mentioned above (section 3.1).

Table A1.3 Constants for homogeneous and non-homogeneous heat flux and conversion factors.

	A Homogeneous ($W/m^2.mV$)	B Non-homogeneous	B/A Conversion Factor
HFM1	5.03	4.62	0.92
HFM2	5.11	4.78	0.94
HFM3	5.00	4.66	0.93

The non-homogeneous heat flux constants were used to calculate the ceiling heat flux during the roof experiment. The overall experimental error is estimated to be ± 5%.

The large differences between the manufacturer's constants and these obtained in this calibration highlight the importance of calibrating heat flux sensors for the specific use as pointed out by Flanders (1985).

APPENDIX 2

Solar Absorptivity and Longwave Emissivity of Materials Used in Roofs

Table A2.1 shows the values of the solar absorptivity and longwave emissivity of the materials most commonly used in the roofs of low cost Brazilian houses.

Table A2.1 Solar absorptivity and longwave emissivity of materials used in roofs.

Surface	Conditions	Solar Absorptivity	Longwave Emissivity	Reference *
Aluminium sheet	new	0.10-0.25	0.10-0.25	(2)
	oxidized	0.30-0.50	0.20-0.50	(2)
Galvanized sheet	new	0.20-0.30	0.13-0.23	(2)/(1)/(3)
	oxidized	0.30-0.50	0.20-0.40	(2)
	rusty	0.60-0.85	0.70-0.90	(2)
Asbestos cement sheet	6 months	0.61	0.96	(3)/(1)
	12 months	0.71	0.96	(3)/(1)
	6 years	0.83	0.96	(3)/(1)
Clay tiles	cream	0.30-0.50	0.85-0.95	(2)
	red	0.65-0.80	0.85-0.95	(2)
Concrete		0.45-0.65	0.85-0.95	(2)
Wood		---	0.80-0.95	(5)
Aluminium foil	new	0.05-0.10	0.03-0.05	(2)/(3)
	90% area covered with dust	---	0.90	(4)
Paints				
aluminium		0.40-0.55	0.40-0.55	(2)
white		0.20-0.30	0.85-0.90	(2)
cream		0.30-0.50	0.85-0.90	(2)
black		0.85-0.95	0.85-0.95	(2)

* References

(1) Anderson, B. 1977. Solar Energy: *Fundamentals in Building Design*. New York, McGraw-Hill Book Comp.

(2) Evans, M. 1980. *Housing Climate and Comfort*. London, The Architectural Press Ltd.

(3) Gurbareff, G.G., Janssen, J.E. and Torborg, R.H. 1966. *Thermal Radiation Properties Survey*. Honeywell Research Center, Minneapolis, Minnesota, U.S.A.

(4) Lotz, F.J. 1964. The Effect of Dust on the Efficacy of Reflective Foil Used as Roof/Ceiling Insulation. *CSIR-Research Report 212*. Pretoria, South Africa.

(5) Sparrow, E.M. and Cess, R.D. 1970. *Radiation Heat Transfer*.